DYNAMIC ANALYSIS OF DEEPWATER MULTI-SEGMENT MOORING LINES USING MODAL SUPERPOSITION

A Thesis

by

SHIJIN TANG

Submitted to the Office of Graduate and Professional Studies of
Texas A&M University
in partial fulfillment of the requirements for the degree of

MASTER OF SCIENCE

Chair of Committee,	Richard S. Mercier
Committee Members,	Hamn-Ching Chen
	Zhizhang Xie
Head of Department,	Sharath Girimaji

May 2017

Major Subject: Ocean Engineering

ABSTRACT

This thesis starts from the construction of a mathematical model of the multi-segment mooring line, based on the work-energy variational method. The equations of motion in both Cartesian and Lagrange local coordinate systems are derived. Meanwhile, with the catenary theory applied, the static equilibrium configuration of the multi-segment mooring line is determined. Furthermore, Galerkin's finite element method is used to generate mass, stiffness and damping coefficient matrices of a single mooring line. The coefficient matrices in the Lagrange local coordinate system are shown to be diagonal, which means the motions in the three directions of this coordinate system are uncoupled. With this information, the eigenvalue problem is solved to obtain the natural frequencies and associated mode shapes of a mooring line in both coordinate systems. By approximating the mooring line as a linear system, the modal superposition approach allows computationally efficient modeling of dynamics in the frequency domain, including estimation of extreme value statistics using Rice's theory for Gaussian processes. The accuracy of the modal superposition approach is demonstrated through comparison with results from nonlinear time domain simulations using OrcaFlex. This approximate

modeling approach is useful for optimizing the design of a mooring system in the preliminary phases of design.

ACKNOWLEDGEMENTS

I would like to thank my advisor, Dr. Richard S. Mercier, for giving me the opportunity to carry out research under his supervision. He inspired me what an excellent researcher should be. His guidance, trust and encouragement enabled me to complete a thesis that I can be proud of in years to come. Besides the research, he has turned my life philosophy into sublime, always chasing challenges and making unique contributions.

I thank Dr. Hamn-Ching Chen and Dr. Zhizhang Xie serving in my advisory committee. Their assistance to me constructing the mathematical model and understanding the computational procedure is appreciated.

I thank the generosity of Bechtel, American Bureau of Shipping and Ocean Engineering Scholarship Committee of Texas A&M University for awarding me their scholarships. I am deeply appreciative of their financial support.

I thank my friends, colleagues, the department faculty and staff for making my time at Texas A&M University a wonderful experience.

CONTRIBUTORS AND FUNDING SOURCES

Contributors

This work was supported by a thesis committee consisting of Professor Richard S. Mercier and Hamn-Ching Chen of the Department of Civil Engineering and Professor Zhizhang Xie of the Department of Mathematics.

The validation data sets for Chapter 5 were initially used by Professor W. M. Henghold and Professor M. S. Triantafyllou. Their work were published in 1976 in an article listed in the Computers & Structures and in 1984 in an article listed in The Quarterly Journal of Mechanics and Applied Mathematics, respectively. This thesis also utilized a commercial mooring analysis software called OrcaFlex to validate the results. The data analyzed for Chapter 7 was provided by Professor Richard S. Mercier. The analyses depicted in Chapter 3 were partially conducted by Professor S. Chucheepsakul and were published in 2002 in an article listed in the Ocean Engineering.

All other work conducted for the thesis was completed by the student, under the advisement of Professor Richard S. Mercier of the Department of Civil Engineering.

Funding Sources

There are no outside funding contributions to acknowledge related to the research and compilation of this document. However, the Ocean Engineering Scholarships provided by Bechtel and American Bureau of Shipping supported the student to finish the graduate program and were acknowledged.

TABLE OF CONTENTS

Page

Page

LIST OF FIGURES

Page

Page

Page

LIST OF TABLES

Page

Page

1. INTRODUCTION

As a kind of station keeping system, mooring systems are widely used in the offshore industry for floating structures to maintain their positions and thus to operate safely. Due to environmental disturbances, the structures are allowed to move within certain allowable offset limits. As a consequence, the mooring systems produce corresponding restoring forces or moments to keep the floating structures over specified locations. Different types of mooring systems are designed considering the types of floating structures, the water depth and the environmental conditions.

The external environmental forces on floating structures include wave and wind forces, etc. Obviously, those forces will lead to motion of the floating structures. Since the top end of the mooring line is attached to the structure, it will be in motion as well. Meanwhile, the bottom end is usually treated as a fixed point. Inevitably, the mooring line will vibrate to some degree. Hence, designers of mooring systems should pay sufficient attention to the dynamics of mooring lines.

Vibrations of a mooring line can lead to large fluctuations of mooring line top tension, while the mooring line top tension is a critical point of the mooring system design. It

should be considered carefully to guarantee that allowable tension levels are not exceeded. Therefore, in order to develop a fast design tool for the mooring system design, an investigation of the vibration of a single mooring line is needed.

Since a mooring line is a kind of continuous system, the study of the dynamics of a mooring line is considered to be challenging. Due to its own submerged weight, the static equilibrium configuration of a mooring line is highly non-linear. Meanwhile, with external forces applied, the mooring line is easily displaced from the static equilibrium configuration. The axial stress and strain are not distributed uniformly along the mooring line. Accordingly, a more complicated model than a single degree of freedom system is needed to study the dynamics of a mooring line.

Rather than one- or two-dimensional dynamic analysis, three-dimensional study is necessary to fully understand the dynamics of a mooring line. Since the excitation forces cannot always be in the plane of the static equilibrium configuration, vibration in the swinging direction can be generated.

In contrast to a cable in air, the dynamics of a mooring line is influenced significantly by the surrounding water. The water has two different effects on the motion of a mooring line. One is hydrostatic pressure; the other is hydrodynamic force. The hydrodynamic force on a slender body like a mooring line can be easily modeled using Morison's equation. It includes the added mass effect and hydrodynamic damping effect. The

hydrodynamic lift effect is neglected in this thesis, consistent with standard design practice for mooring lines. The added mass effect can be considered as the surrounding water being in motion together with the mooring line. Meanwhile, with hydrodynamic damping effect considered, the resonant frequencies of the mooring line will shift from the undamped values and a set of corresponding modal harmonic response functions can be developed to model the dynamics in the frequency domain.

To study the vibration of mooring lines, an approach called modal analysis may be applied. This method is equivalent to solving an eigenvalue problem, which contains physical information of the mooring line, to obtain a set of natural frequencies and associated mode shapes. The results are helpful to understand the dynamics of the mooring line and conduct the subsequent analyses.

Multi-segment mooring lines are extensively used to moor offshore drilling and production platforms in deep water. The line usually consists of both steel and fiber material. Steel is in the form of wire rope or chain, which is also the main component of traditional lines. The total weight of the all-steel mooring system increases dramatically as the water depth increases, as well as the manufacturing cost. As a result, it produces a large downward pull on the floating structure, decreasing the payload capacity and increasing the required buoyancy. Therefore, the all-steel mooring design is economically inefficient in deep water.

Fiber ropes have several advantages over steel for deep-water mooring systems, including weight savings, durability and reduced platform offset. Since the top and bottom parts of the mooring line are exposed to winching operations and friction with the seabed respectively, steel is a better material for these parts. Accordingly, multi-segment chain-polyester-chain mooring lines are suitable in deep water. The experiences using them in the Gulf of Mexico, offshore Brazil and elsewhere have been favorable.

Another consequence considering deep water depth is the large hydrostatic pressure applied on the bottom portion of the mooring line. Since the axial extensibility is considered in this thesis, the hydrostatic pressure squeezes the mooring line and thus increases the axial strain energy, which is known as Poisson's effect. In deep water, large hydrostatic pressure contributes to the axial strain significantly. Therefore, this thesis will consider Poisson's effect and estimate its degree of influence.

Based on the catenary solution of cables, the work-energy variational method and the finite element method, this thesis develops three sets of codes: the first is to calculate the static equilibrium configuration of the mooring line; the second uses this information to obtain corresponding coefficient matrices and conducts modal analysis; the last performs extreme value analysis and estimates needed statistical properties of the mooring line top tension. The outcomes are sets of natural frequencies, associated mode shapes for the vibration of the mooring line and extremes of the mooring line top tension. With a

presented time series of the vessel surge motion, the time series of mooring line top tension or any other response of the mooring line can be obtained by modal superposition. Extreme value analysis of the time series of mooring line top tension can be conducted. Several cases will be analyzed and the results will be compared with time domain simulations using OrcaFlex, a commercial mooring analysis software.

With the approach presented in this thesis, the dynamic mooring line top tension can be estimated accurately and quickly for the preliminary design of offshore floating systems based on limited information. During the preliminary design process, the overall system configuration and technical requirements are defined. Hull structures and risers are initially designed to satisfy general requirements, such as payload, air gap, offset limits, etc. Based on the buoyancy and payload capacity of these designs, the vertical mooring top tension can be estimated in order to size the mooring system. The design of the mooring line is influenced by variations in design parameters (vessel offset limits, anchor radius, length and diameter of segments, etc.). Simulations are required in order to estimate the extreme mooring line top tension as one aspect of determining the suitability of a design.

Furthermore, the designs of hull structures, mooring systems and other components are coupled. Therefore, initial designs of different parts need to be adjusted several times in an iterative procedure in order to optimize the performance of the entire system. This

optimization process is an evolving route of ascendant helix requiring a set of loops, where design of the entire system is improved more and more. Accordingly, the estimation of extreme mooring line top tension needs to be conducted for different mooring system designs a large number of times. It can be inefficient if a single estimation is time-consuming.

This thesis is intended to develop an approach to improve this preliminary design process by accelerating the estimation of the extreme mooring line top tension. The approach that is going to be presented is capable of computing the extreme mooring line top tension in seconds, along with other useful information such as the time series of top tension. In contrast, current commercial mooring system software OrcaFlex takes hours to run a time domain simulation, then the data needs to be processed outside the software to estimate the extremes. Meanwhile, the present approach maintains sufficient accuracy compared with OrcaFlex. In conclusion, the present approach can improve the efficiency of the preliminary design of offshore floating systems significantly.

2. REVIEW OF LITERATURE

The mooring line, as a kind of cable structure, has attracted the attention of many researchers. Correct solutions had been given for linear vibrations of uniform cables in air by 1820. In the first half century of 1900s, some solutions for the vibrations considering symmetric and asymmetric modes of the in-plane vibration were put forward. However, these theories assumed inextensible cables.

Irvine (1981) presented the catenary theory for cable structures, which is useful to calculate the static equilibrium configuration of a mooring line. Irvine also addressed a linear theory of free vibration of a suspended flat-sag cable, considering material stretching. Triantafyllou (1984) developed a general asymptotic solution to the linear vibration of a taut inclined cable. Hybrid mode of the in-plane vibration was produced, which was a mixture of symmetric and antisymmetric shapes, with a significant effect on the dynamic tension. His study laid a foundation for some commonly used mooring design tools in the frequency domain.

Vassalos (1996) put forward that because of hydrodynamic forces, the dynamics of mooring lines is quite different from that of the cable structures in air, mainly because of the hydrodynamic drag force. Triantafyllou (1984) also implemented the hydrodynamic

added mass effect for marine cables. Morison (1949) developed an equation used to model the hydrodynamic added mass and drag forces on an underwater slender body, well known as Morison's equation.

The governing equation of the dynamics of a mooring line is a differential equation. Since the mooring line is a continuous system and the configuration is highly non-linear, the analytical solution is difficult to obtain. To solve this differential equation numerically, the finite element method is a powerful tool. As a kind of finite element method, Galerkin's weak form formulation is suitable to solve the equations of motion of cable structures. This method was well expressed by Reddy (2006).

Garrett (1982) implemented the finite element method to conduct dynamic analysis of inextensible slender rods, allowing large deflections. His study includes the bending stiffness; thus the primary variables of the finite element method include the displacements and the derivative of the displacements with respect to local coordinates. Since the two primary variables are continuous along the entire structure, his approach worked for both uniform cables and beams. However, it cannot deal with multi-segment mooring lines with discontinuous derivatives of the displacements at the boundaries of segments.

Henohold and Russell (1976) conducted a modal analysis of single-span cable structures using the finite element method. Sets of natural frequencies for several examples were obtained for small oscillations about the non-linear static equilibrium

position. Their study concerned large elastic deflections and the principle of virtual work was applied. The class of elements used in their study retained all geometric nonlinearities.

Chucheepsakul and Srinil (2002) used the variational method, which is equivalent to the principle of virtual work, to investigate the free vibrations of three-dimensional extensible marine cables. The equations of motion were derived using the variational method and solved numerically following Garrett's finite element method. Similarly, only a uniform marine cable was considered in their study. Meanwhile, hydrodynamic damping is not included. With modal analysis, their study presented and discussed results of the natural frequencies for coupled in-plane motion, associated mode shapes and the dynamic tension.

3. FORMULATION OF THE EQUATIONS OF MOTION

3.1 Variation of the axial strain of the mooring line

In the Cartesian coordinates, for an element of the mooring line with unstretched arc-length ds_0 at the static equilibrium state, its stretched arc-length is

$$ds = \sqrt{x'^2 + y'^2 + z'^2}\, ds_0 \tag{1}$$

in which x', y' and z' represent the derivatives of x, y and z with respect to the local curvilinear coordinate along the unstretched mooring line s_0. The static equilibrium state is the state where all parts of the mooring line are in static equilibrium.

Based on the definition of Lagrangian strain, another form of the stretched arc-length ds of the element at the static equilibrium state is

$$ds = (1+\varepsilon) ds_0 \tag{2}$$

where ε is the axial strain at the static equilibrium state. From Eqs. (1) and (2), let $s' = \sqrt{x'^2 + y'^2 + z'^2}$, then the axial strain of the element is as

$$\varepsilon = s' - 1 \tag{3}$$

The displaced state denotes an arbitrary configuration of the mooring line while the mooring line is in motion. Similarly, at the displaced state, with the displacements ξ, η and ζ in the Cartesian coordinates, the stretched arc-length is given by

$$d\bar{s} = \sqrt{(x'+\xi')^2 + (y'+\eta')^2 + (z'+\zeta')^2}\, ds_0 \tag{4}$$

$$d\bar{s} = (1+\bar{\varepsilon})ds_0 \tag{5}$$

Combining Eqs. (4) and (5), the axial strain at the displaced state can be written as

$$\bar{\varepsilon} = \sqrt{(x'+\xi')^2 + (y'+\eta')^2 + (z'+\zeta')^2} - 1 \tag{6}$$

The variational form of Eq. (6) is

$$\delta\bar{\varepsilon} = \frac{(x'+\xi')\delta\xi' + (y'+\eta')\delta\eta' + (z'+\zeta')\delta\zeta'}{\sqrt{(x'+\xi')^2 + (y'+\eta')^2 + (z'+\zeta')^2}} \tag{7}$$

3.2 Strain energy due to the axial deformation

Two actions contribute to the strain energy due to the axial deformation. One is pulling on the mooring line due to the axial tension; the other is squeezing of the mooring line due to the hydrodynamic pressure (Sparks (1984)). So the total strain energy can be represented as

$$U = U_T + U_P \tag{8}$$

where U_T and U_P represent the energy due to the axial tension and squeezing of the mooring line by the hydrostatic pressure, respectively.

Both contributions can be expressed in the form of the axial strain as below.

$$\varepsilon = \frac{\sigma}{E} - 2\nu\frac{\sigma_P}{E} \tag{9}$$

In Eq. (9), E is Young's modulus and ν is Poisson's ratio; the first term denotes the axial strain due to the axial tension and the second term is due to squeezing of the mooring line by the circumferential stress and radial stress, which are both equal to the

hydrostatic pressure, expressed by the Lamé's Equations. According to Lamé's Equations, the circumferential stress σ_c and radial stress σ_r for a thick cylinder are given as

$$\sigma_c = \frac{P_I R_I^2 - P_O R_O^2}{R_O^2 - R_I^2} + \frac{\left(P_I - P_O\right) R_O^2 R_I^2}{\left(R_O^2 - R_I^2\right) R^2} \tag{10}$$

$$\sigma_r = \frac{P_I R_I^2 - P_O R_O^2}{R_O^2 - R_I^2} - \frac{\left(P_I - P_O\right) R_O^2 R_I^2}{\left(R_O^2 - R_I^2\right) R^2} \tag{11}$$

In Eqs. (10) and (11), R represents the radius; subscript I and O denote the inner and outer surface of the hollow cylinder, respectively. For a solid cylinder as in the present case ($R_I = 0$), the circumferential stress σ_c and radial stress σ_r are equal to the outer pressure σ_P.

The hydrostatic pressure is given as $\sigma_P = -P = -\rho_w g(Z_H - z)$, where ρ_w is the density of the surrounding fluid and Z_H is the vertical coordinate of the sea surface.

For a mooring line, the strain energy due to the axial deformation U is given as

$$U = \frac{1}{2}\int_V \sigma\varepsilon dV \tag{12}$$

In Eq. (12), $dV = Ads$, A is the cross-section area of the mooring line, ds is the arc-length of the element at the static equilibrium state and σ is the corresponding axial stress. In the case of elastic deformation, the axial stress σ is obtained from Eq. (13) as

$$\sigma = E(\varepsilon + 2\nu\frac{\sigma_P}{E}) \tag{13}$$

Therefore, another form of Eq. (12) is given as

$$U = \frac{1}{2}\int_V E\varepsilon^2 dV - \int_V \nu\sigma\frac{P}{E}dV = \frac{1}{2}\int_0^{S_t} EA\varepsilon^2 ds - \int_0^{S_t} \nu\rho_w g(\mathrm{Z}_H - z)A\varepsilon ds \tag{14}$$

With an unstretched element of the mooring line, the volume is $dV_0 = A_0 ds_0$, where ds_0 is the unstretched arc-length of the element, while A_0 is the unstretched cross-section area. For the case at the displaced state, it is obvious that $d\bar{V} = \bar{A} d\bar{s}$. Assuming that the volume of one element doesn't change while stretching the mooring line, then

$$d\bar{V} = dV_0 = A_0 ds_0 \tag{15}$$

Meanwhile, at the displaced state, the strain energy due to the axial deformation is given as

$$\bar{U} = \frac{1}{2}\int_0^{S_{t_0}} EA_0 \bar{\varepsilon}^2 ds_0 - \int_0^{S_{t_0}} \nu\rho_w g(\mathrm{Z}_H - z) A_0 \bar{\varepsilon} ds_0 \tag{16}$$

where S_{t_0} is the total unstretched arc-length. Combining Eqs. (2), (3), (6) and (7), the variation of Eq. (16) is

$$\delta\bar{U} = \int_0^{S_{t_0}} \left\{ \left[T_a + T_b \left(1 - \frac{1}{\sqrt{1+2\lambda}}\right) \right] \left[\frac{(x'+\xi')\delta\xi' + (\mathrm{y}'+\eta')\delta\eta' + (z'+\zeta')\delta\zeta'}{s'} \right] \right\} ds_0 \tag{17}$$

in which

$$\lambda = \frac{x'\xi' + \mathrm{y}'\eta' + z'\zeta' + \frac{1}{2}(\xi'^2 + \eta'^2 + \zeta'^2)}{s'^2} \tag{18}$$

$$T_a = EA_0\varepsilon - \nu\rho_w g A_0 (\mathrm{Z}_H - z) \tag{19}$$

$$T_b = EA_0 + \nu\rho_w g A_0 (\mathrm{Z}_H - z) \tag{20}$$

By neglecting small quantities of higher order terms, Eq. (18) reduces to

$$\lambda = \frac{x'\xi' + \mathrm{y}'\eta' + z'\zeta'}{s'^2} \tag{21}$$

Using the binomial approximation $\frac{1}{\sqrt{1+2\lambda}} \cong 1-\lambda$ and neglecting higher order terms, Eq. (17) becomes

$$\delta\bar{U} = \int_0^{S_{t_0}} \left\{ \begin{array}{l} \left[\frac{T_a}{s'}(x'+\xi') + \frac{T_b}{s'^3}(x'^2\xi' + x'\,\mathrm{y}'\,\eta' + x'z'\zeta') \right]\delta\xi' \\ + \left[\frac{T_a}{s'}(\mathrm{y}'+\eta') + \frac{T_b}{s'^3}(x'\,\mathrm{y}'\,\xi' + \mathrm{y}'^2\,\eta' + \mathrm{y}'\,z'\zeta') \right]\delta\eta' \\ + \left[\frac{T_a}{s'}(z'+\zeta') + \frac{T_b}{s'^3}(x'z'\xi' + \mathrm{y}'\,z'\eta' + z'^2\zeta') \right]\delta\zeta' \end{array} \right\} ds_0 \qquad (22)$$

3.3 Virtual work done by the external forces

The virtual work done by the effective weight of the submerged mooring line is

$$\delta W_e = -\int_0^{S_{t_0}} w_e \delta\zeta \, ds_0 \qquad (23)$$

where w_e is the unit wet weight of the unstretched mooring line.

The virtual work done by the inertia force is

$$\delta W_i = -\int_0^{S_{t_0}} \bar{m}(\ddot{\xi}\delta\xi + \ddot{\eta}\delta\eta + \ddot{\zeta}\delta\zeta) ds_0 \qquad (24)$$

where $\bar{m} = \frac{w_c}{g}$ represents the mass per unit unstretched length of the mooring line and w_c is the unit weight of the unstretched mooring line in air.

The virtual work done by the hydrodynamic forces is

$$\delta W_h = \int_0^{S_{t_0}} (F_x\delta\xi + F_y\delta\eta + F_z\delta\zeta) ds_0 \qquad (25)$$

where F_x, F_y and F_z are hydrodynamic forces components per unit stretched length in the *x*, *y* and *z* direction, respectively. Meanwhile, the hydrodynamic forces on a mooring

line can be modeled using Morison's equation in Lagrange local coordinates *p-q-r* (see Section 3.7 for the orientation of the Lagrange local coordinates). These hydrodynamic forces can be expressed as

$$F_p = -\frac{1}{2}\rho_w D_0 C_{DT} \left|\dot{\bar{p}}\right| \dot{\bar{p}} - \rho_w A_0 C_A \ddot{\bar{p}} \tag{26}$$

$$F_q = -\frac{1}{2}\rho_w D_0 C_{DN} \left|\dot{\bar{q}}\right| \dot{\bar{q}} - \rho_w A_0 C_A \ddot{\bar{q}} \tag{27}$$

$$F_r = -\frac{1}{2}\rho_w D_0 C_{DN} \left|\dot{\bar{r}}\right| \dot{\bar{r}} - \rho_w A_0 C_A \ddot{\bar{r}} \tag{28}$$

in which, $\dot{\bar{p}}$, $\dot{\bar{q}}$, $\dot{\bar{r}}$ and $\ddot{\bar{p}}$, $\ddot{\bar{q}}$, $\ddot{\bar{r}}$ are the relative velocities and accelerations of the mooring line and surrounding fluid in Lagrange local coordinates. C_{DT}, C_{DN} and C_A are the tangential drag, normal drag and added mass coefficient, respectively. Meanwhile, the corresponding forces F_x, F_y and F_z can be obtained easily using a transform matrix between the Lagrange local and Cartesian coordinates.

In reality, the mooring line will experience hydrodynamic lift forces as well as drag forces. The direction of the lift force is perpendicular to the direction of the relative motion of mooring line and surrounding fluid. This will result in coupling between the normal and bi-normal motions in Lagrange local coordinates and the in-plane and swinging motions in Cartesian coordinates. The directions of motions and coordinate systems mentioned here are introduced in Section 3.7. In this thesis, the lift effect is neglected, consistent with standard design practice for mooring lines.

3.4 Euler-Poisson equations

The virtual work-energy of the mooring line system can be expressed as

$$\delta\Pi = \delta U - \delta W_e - \delta W_i - \delta W_h \tag{29}$$

Substituting Eqs. (22) to (25) into Eq. (29); then integrating by parts from lower boundary zero to upper boundary S_{t_0} and considering the virtual displacements equal to zero at boundaries, Eq. (29) becomes

$$\delta\Pi = \int_0^{S_{t_0}} \left\{ \begin{array}{l} \left\{ -\left[\frac{T_a}{s'}(x'+\xi') + \frac{T_b}{s'^3}(x'^2\xi' + x'y'\eta' + x'z'\zeta') \right]' + \bar{m}\ddot{\xi} - F_x \right\} \delta\xi \\ + \left\{ -\left[\frac{T_a}{s'}(y'+\eta') + \frac{T_b}{s'^3}(x'y'\xi' + y'^2\eta' + y'z'\zeta') \right]' + \bar{m}\ddot{\eta} - F_y \right\} \delta\eta \\ + \left\{ -\left[\frac{T_a}{s'}(z'+\zeta') + \frac{T_b}{s'^3}(x'z'\xi' + y'z'\eta' + z'^2\zeta') \right]' + \bar{m}\ddot{\zeta} - \left(F_y - w_e\right) \right\} \delta\zeta \end{array} \right\} ds_0 \tag{30}$$

The Euler-Poisson equations associated with the virtual displacements are given respectively as

$$\left[\frac{T_a}{s'}(x'+\xi') + \frac{T_b}{s'^3}(x'^2\xi' + x'y'\eta' + x'z'\zeta') \right]' - \bar{m}\ddot{\xi} = -F_x \tag{31}$$

$$\left[\frac{T_a}{s'}(y'+\eta') + \frac{T_b}{s'^3}(x'y'\xi' + y'^2\eta' + y'z'\zeta') \right]' - \bar{m}\ddot{\eta} = -F_y \tag{32}$$

$$\left[\frac{T_a}{s'}(z'+\zeta') + \frac{T_b}{s'^3}(x'z'\xi' + y'z'\eta' + z'^2\zeta') \right]' - \bar{m}\ddot{\zeta} = -\left(F_z - w_e\right) \tag{33}$$

3.5 Static equilibrium conditions

By substituting the static equilibrium conditions as below

$$\xi = \eta = \zeta = \xi' = \eta' = \zeta' = \xi'' = \eta'' = \zeta'' = \dot{\xi} = \dot{\eta} = \dot{\zeta} = \ddot{\xi} = \ddot{\eta} = \ddot{\zeta} = 0 \tag{34}$$

and with the hydrodynamic forces set equal to zero, Eqs. (31) to (33) become

$$\left(\frac{T_a}{s'}x'\right)' = \left(\frac{T_a}{s'}y'\right)' = \left(\frac{T_a}{s'}z'\right)' - w_e = 0 \tag{35}$$

This Eq. (35) defines the static equilibrium configuration of the mooring line.

3.6 Coupled equations of motion

Combining with Eq. (35), Eqs. (31) to (33) yield the coupled equations of motion as below, with $\bar{m}_{ax}$, $\bar{m}_{ay}$ and $\bar{m}_{az}$ representing the unit added mass for each direction.

$$\frac{T_a}{s'}\xi'' + \frac{T_b}{s'^3}(x'^2\xi'' + x'y'\eta'' + x'z'\zeta'') - \bar{m}\ddot{\xi} = -F_{dx} + \bar{m}_{ax}\ddot{\xi} \tag{36}$$

$$\frac{T_a}{s'}\eta'' + \frac{T_b}{s'^3}(x'y'\xi'' + y'^2\eta'' + y'z'\zeta'') - \bar{m}\ddot{\eta} = -F_{dy} + \bar{m}_{ay}\ddot{\eta} \tag{37}$$

$$\frac{T_a}{s'}\zeta'' + \frac{T_b}{s'^3}(x'z'\xi'' + y'z'\eta'' + z'^2\zeta'') - \bar{m}\ddot{\zeta} = -F_{dz} + \bar{m}_{az}\ddot{\zeta} \tag{38}$$

Eqs. (36), (37) and (38) can be rearranged in the form of a matrix system of equations as

$$[M]\{\ddot{\Delta}\} + [C]\{\dot{\Delta}\} + [A]\{\Delta''\} = 0 \tag{39}$$

where $\Delta=[\xi,\eta,\zeta]^T$. The coefficient matrices are

$$[M]=\begin{bmatrix} \bar{m}+\bar{m}_{ax} & 0 & 0 \\ 0 & \bar{m}+\bar{m}_{ay} & 0 \\ 0 & 0 & \bar{m}+\bar{m}_{az} \end{bmatrix} \tag{40}$$

$$[A]=-\begin{bmatrix} \frac{T_a}{s'}+\frac{T_b x'^2}{s'^3} & \frac{T_b x'y'}{s'^3} & \frac{T_b x'z'}{s'^3} \\ \frac{T_b x'y'}{s'^3} & \frac{T_a}{s'}+\frac{T_b y'^2}{s'^3} & \frac{T_b y'z'}{s'^3} \\ \frac{T_b x'z'}{s'^3} & \frac{T_b y'z'}{s'^3} & \frac{T_a}{s'}+\frac{T_b z'^2}{s'^3} \end{bmatrix} \tag{41}$$

Matrix $[C]$ contains the nonlinear drag components of the hydrodynamic forces. The linearization for these terms needs to be done. Assuming the linearization matrix is $[L]$, and the transform matrix from Cartesian coordinates to Lagrange local coordinates is $[T]$, $[C]$ can be given as

$$[C]=\frac{1}{2}\rho_w D[T]\cdot[L]\cdot\begin{bmatrix} C_{DT} & 0 & 0 \\ 0 & C_{DN} & 0 \\ 0 & 0 & C_{DN} \end{bmatrix}[T]^{-1} \tag{42}$$

where *D* is the diameter of the mooring line. The form of the linearization matrix $[L]$ is addressed in Section 3.9.

Since the static equilibrium configuration of the suspended portion of a mooring line is lying in one plane, by choosing a proper orientation of the Cartesian coordinate system then y' can be zero for all parts of the mooring line. Therefore, in Cartesian coordinates the out-of-plane or swinging motion is uncoupled from the in-plane motion.

3.7 Transform between global and local coordinates

Figure 1 shows both the Cartesian coordinates *x*-*y*-*z* and Lagrange local coordinates represented by 3 orthogonal vectors *p*-*q*-*r*, which are tangential, bi-normal and normal vector of the mooring line, respectively. The tangential and bi-normal unit vectors lie on the plane of the mooring line, while the normal unit vector is perpendicular to that plane.

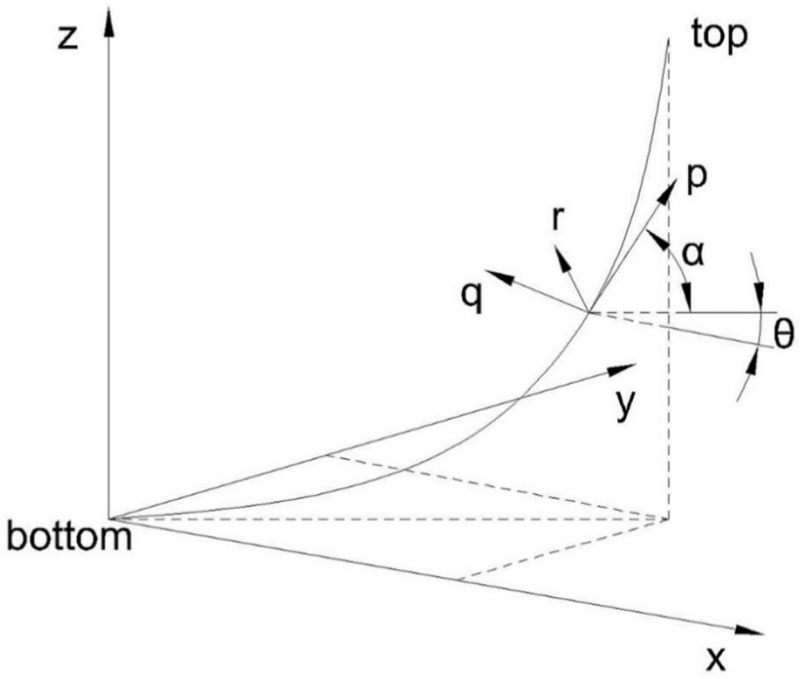

Figure 1. Global and local coordinates of a mooring line

Transformation between the two coordinate systems can be achieved with a transform matrix, according to

$$\begin{Bmatrix} \xi \\ \eta \\ \zeta \end{Bmatrix} = [T] \cdot \begin{Bmatrix} p \\ q \\ r \end{Bmatrix} \tag{43}$$

As defined in Figure 1, θ is the angle between the x axis and the plane of the mooring line p-q and α is the angle between the tangential unit vector p and the x-y plane. Accordingly, the transform matrix is given as

$$[T] = \begin{bmatrix} \cos\alpha\cos\theta & -\sin\theta & -\sin\alpha\cos\theta \\ \cos\alpha\sin\theta & \cos\theta & -\sin\alpha\sin\theta \\ \sin\alpha & 0 & \cos\alpha \end{bmatrix} \tag{44}$$

where $\theta = \tan^{-1}(y'/x')$ and $\alpha = \tan^{-1}(z'/(x'^2 + y'^2)^{0.5})$.

The transform matrix is an orthogonal matrix since its inverse is equal to its transpose.

3.8 Equations of motion in Lagrange local coordinates

The matrix form of the equations of motion in Lagrange local coordinates is given as

$$[M_l]\{\ddot{\Delta}_l\} + [C_l]\{\dot{\Delta}_l\} + [A_l]\{\Delta_l''\} = 0 \tag{45}$$

where $\Delta_l = [p, q, r]^T$ and the coefficient matrices are given as

$$[M_l] = [T]^T [M][T] = \begin{bmatrix} \bar{m} & 0 & 0 \\ 0 & \bar{m} + \rho_w A_0 C_A & 0 \\ 0 & 0 & \bar{m} + \rho_w A_0 C_A \end{bmatrix} \tag{46}$$

$$[C_l] = [T]^T [C][T] = \frac{1}{2}\rho_w D_0 [L] \cdot \begin{bmatrix} C_{DT} & 0 & 0 \\ 0 & C_{DN} & 0 \\ 0 & 0 & C_{DN} \end{bmatrix} \tag{47}$$

$$[A_l] = [T]^T [A][T] = -\begin{bmatrix} \frac{(T_a + T_b)}{s'} & 0 & 0 \\ 0 & \frac{T_a}{s'} & 0 \\ 0 & 0 & \frac{T_a}{s'} \end{bmatrix} \tag{48}$$

It is surprisingly found that the coefficient matrices in Lagrange local coordinates are all diagonal; thus the motions in the three directions of the Lagrange local coordinates are actually uncoupled. Combining the virtual work-energy expressions of the mooring line at both the displaced and the static equilibrium state will eliminate the work done by the submerged weight. Moreover, the submerged weight is the only force which is not in the primary directions of the Lagrange local coordinates. This result is significantly important since the vibration of each direction can be analyzed individually. Additionally, the coefficients for normal and bi-normal directions are the same. Therefore, two individual equations of motion can be given as follows; one is for the tangential direction and the other is for the normal and bi-normal direction.

$$\bar{m}\ddot{p} + \frac{1}{2}\rho_w D_0 L_p C_{DT} \dot{p} - EA_0 p'' = 0 \tag{49}$$

$$\left(\bar{m} + \rho_w A_0 C_A\right)\ddot{q} + \frac{1}{2}\rho_w D_0 L_q C_{DN} \dot{q} - \frac{T_a}{s'} q'' = 0 \tag{50}$$

where L_p and L_q represent linearization factors in Morison's equation for tangential and bi-normal directions, respectively.

Notice that the equation of motion for the tangential direction is independent of Poisson's ratio, while the equations for the normal and bi-normal direction are not. Since the multi-segment mooring line is widely used in deep water, where hydrostatic pressure

can be extremely high, the influence of the hydrostatic pressure is considered in the form of Poisson's effect. It is necessary to investigate how and to which extent this effect influences the dynamics of the mooring line.

3.9 Linearization of Morison's drag with prescribed top motion spectra

As illustrated by Eq. (27), the Morison' drag force can be modeled as

$$F_q = -\frac{1}{2}\rho_w D_0 C_{DN} \left|\dot{\bar{q}}\right| \dot{\bar{q}} \tag{51}$$

which is for the bi-normal direction in Lagrange local coordinates. This drag force is non-linear. In order to implement the drag force in modal analysis in the frequency domain, it is necessary to linearize this force term. The linearized drag force term can be expressed as

$$F_q = -\frac{1}{2}\rho_w D_0 C_{DN} L_q \dot{q} \tag{52}$$

However, the drag force is applied on the entire mooring line; and the velocities of the different parts of the mooring line vary when the mooring line is in motion. Meanwhile, the velocities of all parts of the mooring line are periodic in time, which vary from zero to the corresponding amplitude. The linearization factor L_q has the dimension of velocity. The only given information in this thesis related to the velocity is the surge motion power spectrum of the vessel $S_{xx}(f)$. This spectrum will be provided in the subsequent analysis. Therefore, the linearization factor L_q should be dependent on this spectrum. In order to obtain the surge velocity spectrum of the vessel $S_{\dot{x}\dot{x}}(f)$, the following relationship is used:

$$S_{\dot{x}\dot{x}}(f) = f^2 S_{xx}(f) \tag{53}$$

where f is the cyclic frequency.

Therefore, the zeroth spectral moment of the surge velocity spectrum $m_{0\dot{x}}$ is given as

$$m_{0\dot{x}} = \int_0^{+\infty} S_{\dot{x}\dot{x}}(f)\,df = \int_0^{+\infty} f^2 S_{xx}(f)\,df = m_{2x} \tag{54}$$

Since the direction of the surge velocity v_x is horizontal, this velocity must be resolved in three directions in Lagrange local coordinates.

The transformation of the velocities in two coordinate systems can be conducted using

$$\begin{Bmatrix} v_p \\ v_q \\ v_r \end{Bmatrix} = \left[T_T\right]^T \cdot \begin{Bmatrix} v_x \\ v_y \\ v_z \end{Bmatrix} \tag{55}$$

where v_p, v_q and v_r are the resolved velocities in tangential, bi-normal and normal direction, respectively. The subscript *x*, *y*, *z* represent the Cartesian global coordinate system of the vessel, which is different from the Cartesian coordinate system utilized to diagonalize the coefficient matrices for a single mooring line in Section 3.6. For instance, in this Cartesian global coordinate system, *x* denotes the surge direction of the vessel. The transform matrix $[T]$ is generated based on this Cartesian global coordinate system. The subscript *T* denotes the top node of the mooring line, because the transform matrix used here requires the angle information at the top node.

With this transform matrix, the square root of the zeroth spectral moment of the surge velocity spectrum in these three directions can be written as

$$\begin{Bmatrix} \sqrt{m_{0\dot{p}}} \\ \sqrt{m_{0\dot{q}}} \\ \sqrt{m_{0\dot{r}}} \end{Bmatrix} = \left[T_T\right]^T \cdot \begin{Bmatrix} \sqrt{m_{0\dot{x}}} \\ 0 \\ 0 \end{Bmatrix} \tag{56}$$

The linearization factor L_q for the bi-normal direction is assumed to have the form:

$$L_q = C_{Lq}\sqrt{m_{0\dot{q}}} \tag{57}$$

The coefficient C_{Lq} should have the scale of one. Because the velocities of most parts of the mooring line are smaller than the velocity of the top node; and the velocity of every node of the mooring line varies from zero to the corresponding amplitude, it is reasonable to select a small value for this coefficient C_{Lq}. Meanwhile, the linearization factors in the other two directions have the same form. In addition, the damping effect in the tangential direction usually is recognized to be the result of structural damping of the material (i.e. the contribution from the fluid shear stresses is assumed to be negligible). The coefficients in all three Lagrangian local directions C_{Lp}, C_{Lq} and C_{Lr} are set as

$$C_{Lp} = C_{Lq} = C_{Lr} = \frac{\sqrt{2}}{4} \tag{58}$$

This selection of coefficient is actually a multiplication of one $\sqrt{2}$ factor and two $\frac{1}{2}$ factors. The $\sqrt{2}$ factor is needed since the significant surge velocity amplitude

$A_{\dot{x}S} = \sqrt{2}\sqrt{m_{0\dot{x}}}$. The first $\frac{1}{2}$ factor is used to average the velocity amplitudes of all nodes of the mooring line with the velocity amplitude of the top node specified. The second $\frac{1}{2}$ factor is introduced for averaging of the velocity of each node in a periodic cycle with the velocity amplitude specified.

3.10 Static catenary solution for a multi-segment mooring line

In order to prepare the coefficient matrices in the equations of motion for subsequent modal analysis, the catenary theory of cable structures (Irvine (1981)) is used to obtain the static equilibrium configuration of a multi-segment mooring line. The static equilibrium configuration is lying in one plane. The catenary equations are given as

$$x(s_0) = \frac{H_A s_0}{EA_0} + \frac{H_A}{w_e}\left[\sinh^{-1}\left(\frac{w_e s_0 + V_A}{H_A}\right) - \sinh^{-1}\left(\frac{V_A}{H_A}\right)\right] \tag{59}$$

$$z(s_0) = \frac{s_0}{EA_0}\left(\frac{w_e s_0}{2} + V_A\right) + \frac{1}{w_e}\left[\sqrt{H_A^2 + (w_e s_0 + V_A)^2} - \sqrt{H_A^2 + V_A^2}\right] \tag{60}$$

where subscript *A* denotes the bottom of the suspended span of the mooring line segment, H_A is the horizontal component of tension in the span; and V_A is the vertical component of tension at the bottom of the span. In the case where a portion of the mooring line is lying on the seabed, the seabed friction is neglected and V_A is set to be zero at the touchdown point.

The multi-segment mooring line consists of several line segments. Different segments can have different line properties, such as material density, Young's modulus, Poisson's ratio, length, cross-section area and so on. Multi-segment mooring lines with different line properties are widely used in deep water, such as the chain-polyester-chain mooring line, which is referred as CPC line for short. The multi-segment mooring line will lead to discontinuity of the slope of the static equilibrium configuration at the boundaries between segments. Furthermore, this method allows addition of external forces at the boundaries between segments, such as clumped weight or the buoyancy of buoys.

In order to obtain the static equilibrium configuration of the multi-segment mooring line, the Newton-Raphson method is implemented to perform the numerical iteration solving Eqs. (59) and (60). Meanwhile, the extensibility of the mooring line is considered. With water depth, line properties, vertical mooring line top tension or anchor radius specified, the code will calculate where the touchdown point is in case a portion of the mooring line is lying on the seabed. Additionally, the code can ignore the seabed if needed. The outputs are top and bottom tension of each segment, stretched length of each segment and anchor radius if unknown. A sample input file of this code is listed in Table 1.

Table 1. A sample input file of the catenary solution code

Number of segments:	3		
Property	Bottom segment	Middle segment	Top segment
Length, *m*	300	400	300
E, *Pa*	2000000	1000000	2000000
A, m^2	1	1	1
Wet weight, *N/m*	1	1	1
Clumped weight, *N*	0	0	0
Poisson's ratio	0.5	0.5	0.5
Bottom coordinates, *m*	(800, 0, 0)		
Top coordinates, *m*	(0, 0, 500)		

Based on this information, the complete static equilibrium configuration can be easily obtained using the catenary equations. Table 2 lists a sample output file.

Table 2. A sample output file of the catenary solution code

Number of segments:	3	Horizontal force, *N*:	544.352
Property	Bottom segment	Middle segment	Top segment
Horizontal span, *m*	187.198	325.054	178.547
Vertical span, *m*	32.488	226.679	240.833
Unstretched length, *m*	190.800	400.000	300.000
Length, *m*	190.905	400.271	300.276
Bottom vertical force, *N*	0.000	190.800	590.800
Top vertical force, *N*	190.800	590.800	890.800

The corresponding plot for the static equilibrium configuration of a multi-segment mooring line is given as Figure 2. This mooring line has a portion lying on the seabed. The result produced by OrcaFlex is also plotted in this figure. Both configurations are in good agreement.

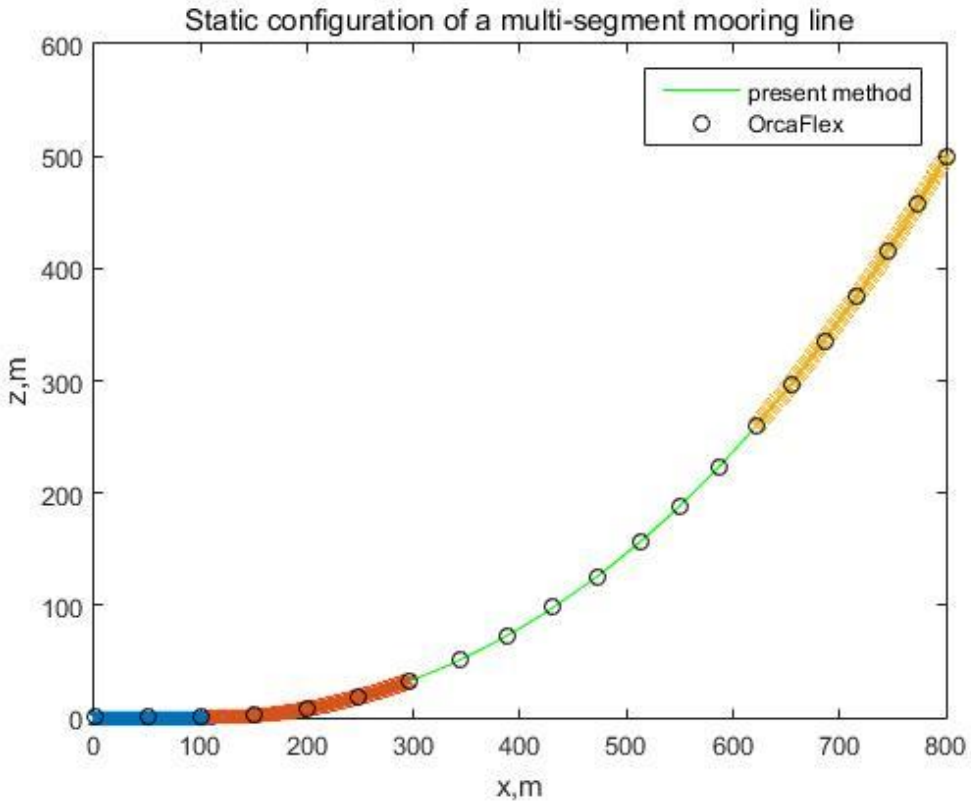

Figure 2. Example static equilibrium configuration of a mooring line

4. FINITE ELEMENT FORMULATION OF THE MOORING LINE

4.1 Weak form of the equations of motion

Galerkin's method is used to construct the finite element model of the mooring line. The procedures are described by Reddy (2006). By multiplying both sides of the equation of motion by the weighting function w_i and integrating, the weak form for semi-discretization of the governing equation Eq. (39) in Cartesian coordinates is given as

$$0 = \int_{s_{0a}}^{s_{0b}} \left(w_i \left[M\right]\left\{\ddot{\Delta}\right\} + w_i \left[C\right]\left\{\dot{\Delta}\right\} - \frac{\partial w_i}{\partial s_0}\left[A\right]\left\{\Delta'\right\} \right) ds_0 - w_{i(s_{0a})} Q_1 - w_{i(s_{0b})} Q_2 \qquad (61)$$

where s_{0a} and s_{0b} represent the vertical coordinates of two ends of one element, Q_1 and Q_2 are the external forces applied on two ends, which are

$$\begin{aligned} Q_1 &= \left(\left[A\right]\left\{\Delta'\right\}\right)_{s_{0a}} \\ Q_2 &= \left(-\left[A\right]\left\{\Delta'\right\}\right)_{s_{0b}} \end{aligned} \qquad (62)$$

4.2 Finite element approximation of the mooring line

A Lagrange quadratic approximation of the solution within a finite element of the mooring line is used. Some previous work used Hermite cubic shape functions (Chen (2002) and Chucheepsakul (2002)), which means that the primary variables in their approaches are displacements and the first derivatives of displacements with respect to a specific coordinate. However, according to the principles of the finite element method, the

primary variables should be continuous across the boundaries of elements (Reddy (2006)). In the case of multi-segment mooring lines, the first derivatives of displacements are not continuous across the boundaries of segments. So Lagrange quadratic shape functions are chosen for this formulation, instead of Hermite cubic ones. The approximation of the solution is assumed to be of the form

$$\Delta_l(s_0,t) \approx \Delta_{lh}(s_0,t) = \sum_{j=1}^{3} \left\{ S_j(t) \right\} \varphi_j(\bar{s}_0) \tag{63}$$

where $S_j(t)$ represents the displacements at the nodes. $\bar{s}_0$ is the local curvilinear coordinate along the mooring line in one element, varying from 0 to *h*. The Lagrange quadratic shape functions are given as follows, with *h* as the unstretched arc-length of one element:

$$\begin{aligned} \varphi_1(\bar{s}_0) &= 1 - 3\frac{\bar{s}_0}{h} + 2\left(\frac{\bar{s}_0}{h}\right)^2 \\ \varphi_2(\bar{s}_0) &= 4\frac{\bar{s}_0}{h}\left(1 - \frac{\bar{s}_0}{h}\right) \\ \varphi_3(\bar{s}_0) &= \frac{\bar{s}_0}{h}\left(2\frac{\bar{s}_0}{h} - 1\right) \end{aligned} \tag{64}$$

To clarify, $S_j(t)$ are as below, where subscript 1, 2 and 3 represent the three nodes of one quadratic element

$$\begin{aligned} \left\{ S_1(t) \right\} &= [x_1, y_1, z_1]^T \\ \left\{ S_2(t) \right\} &= [x_2, y_2, z_2]^T \\ \left\{ S_3(t) \right\} &= [x_3, y_3, z_3]^T \end{aligned} \tag{65}$$

Since the coefficient matrices are varying along the local curvilinear coordinate s_0, the same quadratic shape functions are applied for these matrices, Eq. (66) shows the

approximation for $[M]$, similar to that for $[C]$ and $[A]$. $[M_k]$ is the value of $[M]$ at the corresponding node *k* of one quadratic element.

$$[M] \approx [M_h] = \sum_{k=1}^{3} [M_k] \varphi_k(\overline{s}_0) \tag{66}$$

4.3 Finite element model of the mooring line

By applying the approximations to the weak form of the governing equation, the finite element model for one quadratic element is obtained as

$$\left[P^e\right]\left\{\ddot{S}^e\right\} + \left[H^e\right]\left\{\dot{S}^e\right\} + \left[K^e\right]\left\{S^e\right\} = \left\{R^e\right\} \tag{67}$$

where the element coefficient matrices are defined as

$$\left[P_{ij}^e\right] = \sum_{k=1}^{3} [M_k^e] \int_0^h \varphi_i^e \varphi_j^e \varphi_k^e d\overline{s}_0 \tag{68}$$

$$\left[H_{ij}^e\right] = \sum_{k=1}^{3} [C_k^e] \int_0^h \varphi_i^e \varphi_j^e \varphi_k^e d\overline{s}_0 \tag{69}$$

$$\left[K_{ij}^e\right] = -\sum_{k=1}^{3} [\mathrm{A}_k^e] \int_0^h \frac{\partial \varphi_i^e}{\partial \overline{s}_0} \frac{\partial \varphi_j^e}{\partial \overline{s}_0} \varphi_k^e d\overline{s}_0 \tag{70}$$

$$\left\{R_i^e\right\} = \varphi_i^e\left(s_{0a}\right) Q_1^e + \varphi_i^e\left(s_{0b}\right) Q_2^e \tag{71}$$

And the discretized values of the displacements at nodes $S^e(t)$ are given as

$$\left\{S^e(t)\right\} = [x_1^e, y_1^e, z_1^e, x_2^e, y_2^e, z_2^e, x_3^e, y_3^e, z_3^e]^T \tag{72}$$

The values of these coefficient matrices depend on the coordinate values of three discrete element nodes based on the static equilibrium configuration of the mooring line. Furthermore, in order to prepare the condensed coefficient matrices for the whole mooring

line consisting of a large number of elements, a complete set of elements are assembled and boundary conditions at the two ends are imposed. Additionally, in order to maintain high numerical accuracy for the case of multi-segment mooring lines, the element sizes for segments should be allowed to be different. The sequence of elements is arranged from anchor point or touchdown point to fairlead.

As for the boundary conditions, although the top end is in motion, it is actually connected to the vessel. The motion of the top node is identical to the vessel surge motion. In this thesis, the vessel surge motion is specified and relatively small. The top end of the mooring line is treated as fixed. The bottom end is anchored on the seabed. Therefore, the components of the first and the last nodes in the displacement vector both equal to zero. Consequently, the condensed coefficient matrices are obtained by deleting the corresponding rows and columns.

In addition, since the equations of motion in Lagrange local coordinates are uncoupled in three directions, it is easy to form the finite element model for each direction individually using the preceding approach. The condensed coefficient matrices in each direction in Lagrange local coordinates are prepared for the subsequent modal analyses.

5. MODAL ANALYSIS OF THE MOORING LINE

The modal analysis of the mooring line is equivalent to solving the eigenvalue problem for the matrix system of equations and finding the corresponding eigenvalues and eigenvectors, which are natural frequencies and mode shapes for the dynamic system, respectively. For the free vibrations, it is assumed that the form of the displacement solution is periodic in time at the natural frequency of vibration. The configuration of the mooring line at a natural frequency is called the associated mode shape. The general procedure for the modal analysis of a mooring line in Cartesian coordinates involves solving an eigenvalue problem in two uncoupled directions of Cartesian coordinates (in-plane and swinging). Following the same procedure, the modal analysis can be conducted in each direction in Lagrange local coordinates, in other words, the eigenvalue problem in each of the three uncoupled directions of Lagrange local coordinates (tangential, bi-normal and normal) is solved. The corresponding coefficient matrices in the normal and bi-normal directions are the same, while the coefficient matrices in the tangential direction are different from those in the other two directions. Accordingly, two sets of natural frequencies and associated mode shapes in the Lagrange local coordinate system and another two sets in the Cartesian coordinate system are the outcomes of modal analysis.

5.1 Modal analysis of a mooring line without damping effect

In this case, the damping term of Eq. (67) vanishes. The harmonic displacement in Cartesian coordinates is assumed to have the form:

$$\{S^e\} = e^{i\omega t}\{S^e_{am}\} \tag{73}$$

where ω denotes the frequency of natural vibration of the system. Substituting Eqs. (68), (70) and (73), assembling all elements of the mooring line system and applying the boundary conditions at the top and bottom ends, Eq. (67) becomes

$$\left(-\omega^2[P]+[K]\right)\{S_{am}\} = 0 \tag{74}$$

So the eigenvalue problem without damping involves solving the characteristic equation

$$\left|-\omega^2[P]+[K]\right| = 0 \tag{75}$$

where $|\ |$ represents the determinant of the matrix inside.

A sample set of natural frequencies for the vibration without damping in the swinging direction in Cartesian coordinates is given in Table 3. The associated mode shapes are shown in Figure 3.

Table 3. Natural frequencies in swinging direction for a CPC mooring line

Mode	1	2	3	4	5	6
Natural frequency, *Hz*	0.01845	0.05549	0.08138	0.12080	0.16884	0.20826

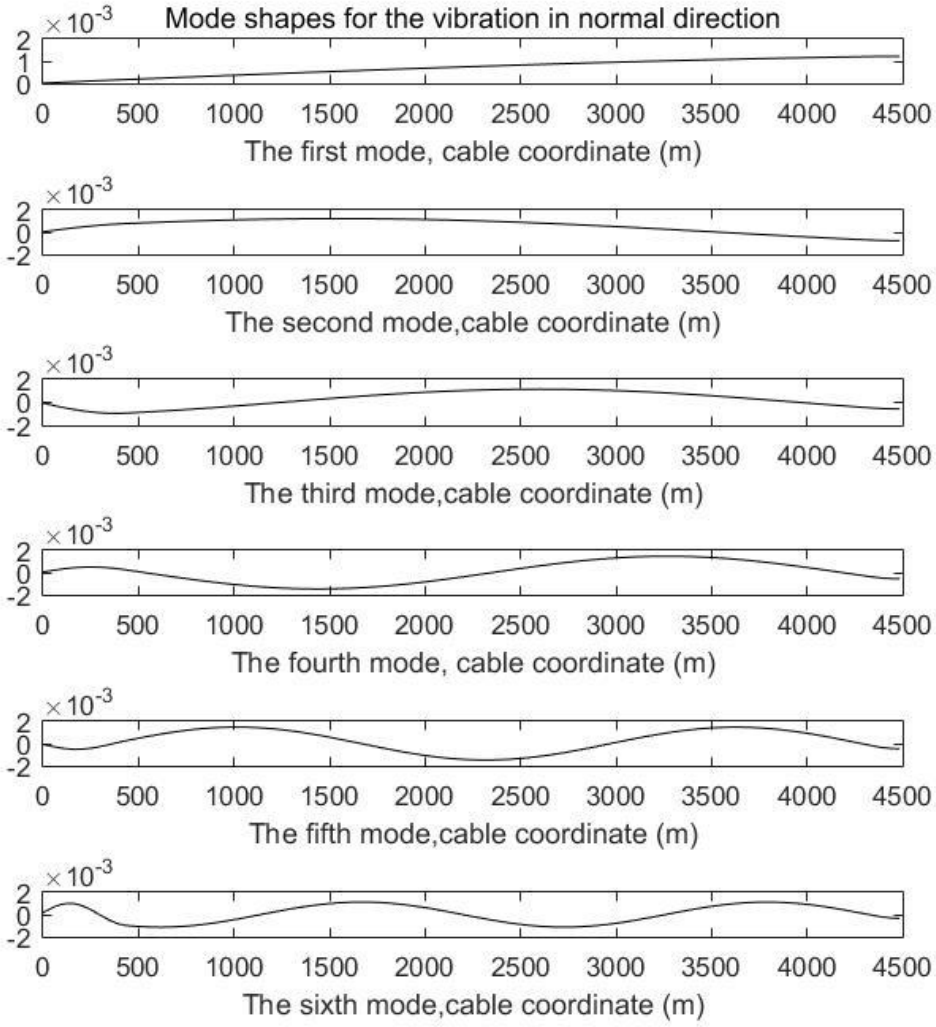

Figure 3. The first six mode shapes for the vibration in swinging direction

5.2 Modal analysis of a mooring line with damping effect

In the case with damping, the general solution for displacement has the form

$$\{S^e\} = e^{\lambda t}\{S^e_{am}\} \tag{76}$$

Following the same procedure as for the case without damping, the corresponding equation for the eigenvalue problem of the entire mooring line system can be generated with assembled mass, stiffness and damping matrices using the finite element method, which is represented as

$$\left(\lambda^2[P] + \lambda[H] + [K]\right)\{S_{am}\} = 0 \tag{77}$$

The eigenvalue problem with damping is formed by setting

$$\left|\lambda^2[P] + \lambda[H] + [K]\right| = 0 \tag{78}$$

In order to solve Eq. (77), define a displacement vector as

$$\{X\} = \begin{Bmatrix} S_{am} \\ \lambda S_{am} \end{Bmatrix} \tag{79}$$

Eq. (77) can be rewritten as

$$\lambda\{X\} = \begin{bmatrix} [0] & [I] \\ -[P]^{-1}\cdot[K] & -[P]^{-1}\cdot[H] \end{bmatrix}\{X\} \tag{80}$$

where $[I]$ represents the identity matrix with the same size as $[K]$. By solving Eq. (80), complex values of λ are obtained. The imaginary parts of them are the corresponding natural frequencies in the case with damping.

5.3 Validation of present method with previous work

Three cases from previous work are analyzed using the present method. The first is case (i), a cable in air by Henghold (1976); the second is case (ii), a marine cable surrounded by water by Triantafyllou (1984); the last one is case (iii), a multi-segment

mooring line analyzed using OrcaFlex. The information of the first two cases is shown in Table 4. The information of the last case is given in Table 8, without the damping effect considered.

Table 4. Information about the properties of two cables

Case	(i), Henghold	(ii), Triantafyllou
Water depth, *m*	500	130
Anchor radius, *m*	800	303.15
Length, *m*	1000	330
E, Pa	1e6	1.5e11
A, m^2	1	7.07e-4
Wet weight, *N/m*	1	47.6
C_A	0	0.128
Fluid density, kg/m^3	0	1000

The static equilibrium configuration plot for case (i) is shown as Figure 4 (a), while that for (ii) is shown as Figure 4 (b). For case (iii), the static equilibrium configuration is plotted in Figure 10.

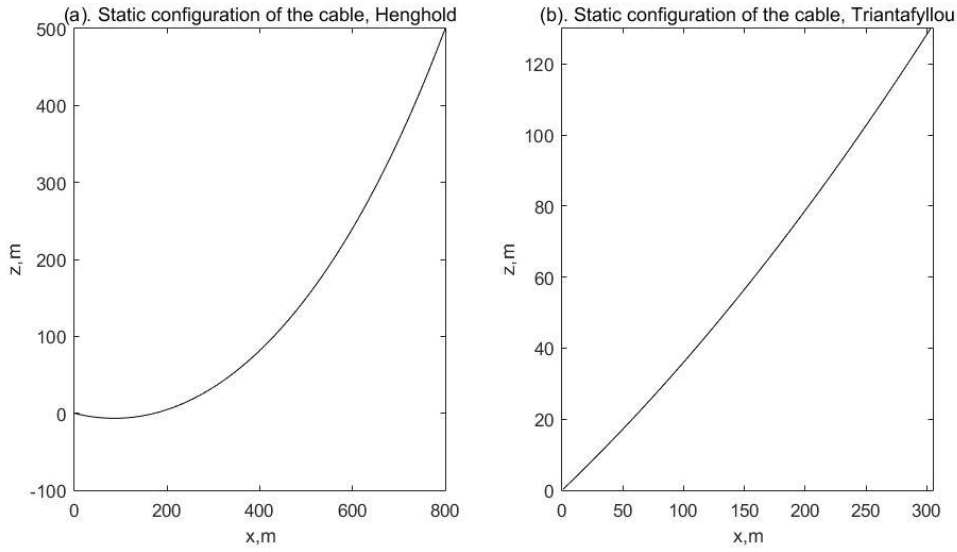

Figure 4. Static equilibrium configuration of the cable for two cases

The solution for the non-dimensional natural frequencies in the in-plane and swinging directions is given by Henghold (1976) for case (i). The cable in this case is uniform. Eight finite elements are used for his solution. The non-dimensional natural frequency $\bar{\omega}$ is defined by

$$\bar{\omega} = \frac{\omega}{\sqrt{g/L}} \tag{81}$$

For case (ii), Triantafyllou (1984) and Irvine (1981) provide their solutions for the in-plane direction. Therefore, the code for modal analysis in Cartesian coordinates is exercised to obtain corresponding natural frequencies for both cases (i) and (ii). Two hundred finite elements are used for both analyses. The solution for case (i) is given in Table 5 and the results for case (ii) are shown in Table 6. For case (iii), natural frequencies in both in-plane and swinging directions are listed in Table 7. The agreement with the

published results is within 10% in all cases, with some cases showing consistently better agreement than others. For example, for case (iii) the agreement in the in-plane natural frequencies is within 0.06% for all seven modes. Based on these results, the approach developed herein is deemed to yield sufficient accuracy in applications, especially for multi-segment mooring lines that are widely used in deep water.

Table 5. Comparison of non-dimensional natural frequencies for case (i)

	In-plane direction		Swinging direction	
Mode	Present method	Henghold	Present method	Henghold
1	4.804	4.878	2.712	2.715
2	7.478	7.755	5.359	5.425

Table 6. Comparison of in-plane natural frequencies for case (ii)

	In-plane natural frequencies, *rad/s*		
Mode	Present method	Irvine	Triantafyllou
1	2.27	2.17	2.15
2	2.33	2.20	2.21
3	3.58	3.39	3.38
4	4.64	4.39	4.37
5	5.81	5.51	5.48

Table 7. Comparison of the natural frequencies for case (iii)

	In-plane frequencies, *rad/s*		Swinging frequencies, *rad/s*	
Mode	Present method	OrcaFlex	Present method	OrcaFlex
1	0.3342	0.3341	0.2987	0.3289
2	0.5408	0.5405	0.4875	0.5383
3	0.7936	0.7931	0.7219	0.7926
4	1.1173	1.1179	1.0228	1.1166
5	1.3959	1.3964	1.2816	1.3948
6	1.5633	1.5660	1.4376	1.5620
7	1.7684	1.7680	1.6393	1.7671

5.4 Surge motion power spectrum of the vessel

After conducting the modal analysis, sets of natural frequencies and corresponding mode shapes for each direction are obtained. For each set of natural frequencies, only the lowest ones lying in the frequency range of vessel motion will be used for the subsequent analyses. The largest range of dynamic forces on the vessel imparted by the mooring system is in the surge direction. Therefore, for the subsequent analyses, the vessel motion

in the surge direction is prescribed and the motion in the other five degrees of freedom is constrained to zero. Note that this is a practical approximation, not a limitation inherent to the methodology. It would be a simple matter to superimpose the top tension fluctuations associated with any or all of the other five degrees of freedom while the associated spectra were specified.

The surge displacements of the vessel are synthesized from prescribed spectra. For example, for a chain-polyester-chain (CPC) mooring line, the spectral density for surge motion of the vessel usually concentrates on the band from 0 to 0.2 *Hz*. A spectrum for the surge motion of the vessel used in this thesis consists of the superposition of two individual spectra. One is the spectrum associated with surge motions at the same frequencies as the waves. The other is the spectrum associated with the slow drift surge motion of the vessel. For convenience and simplicity, both spectra are modeled analytically using the JONSWAP spectral form. The JONSWAP spectrum is a three-parameter spectrum; and it is developed and used to model wave elevation. However, this spectrum may be used to approximately model either the wave frequency surge motion or slow drift surge motion of a moored vessel in deep water. The analytical form of the JONSWAP spectrum is

$$S_{xx}(f) = \alpha X_s^2 \frac{f^{-5}}{f_p^{-4}} \exp\left(-\frac{5}{4}\left(\frac{f}{f_p}\right)^{-4}\right) \gamma^{\exp\left(-\frac{(f-f_p)^2}{2\tau^2 f_p^2}\right)} \tag{82}$$

where:

$$\alpha = \frac{1}{\left(1.555 + 0.2596\gamma - 0.02231\gamma^2 + 0.001142\gamma^3\right)^2}$$

$$\tau = 0.07,\ f \le f_p$$
$$\tau = 0.09,\ f > f_p$$

X_S is the significant value of process X (i.e. surge motion in this case)

f_p is the frequency associated with the maximum spectral density

γ is the spectral peakedness parameter

These spectral parameters depend on the environmental conditions and the properties of the mooring line.

5.5 Modal superposition of the top tension of the mooring line

With a specified spectrum of vessel surge motion, corresponding time series realizations of the surge motion can be synthesized using a random phase ϕ_i for each discretized frequency. For the superposed surge motion spectra, with the frequency interval Δf, the displacement amplitude $Amp(f)$ at each discretized frequency can be obtained as

$$Amp(f) = \sqrt{2 S_{xx}(f) \Delta f} \tag{83}$$

With the amplitude calculated by Eq. (83), the time series of the surge motion is synthesized according to

$$X(t) = \sum_{i=1}^{n} Amp(f_i) e^{i(2\pi f_i t + \phi_i)} \tag{84}$$

A sample time series realization of the surge motion is shown in Figure 5 (a).

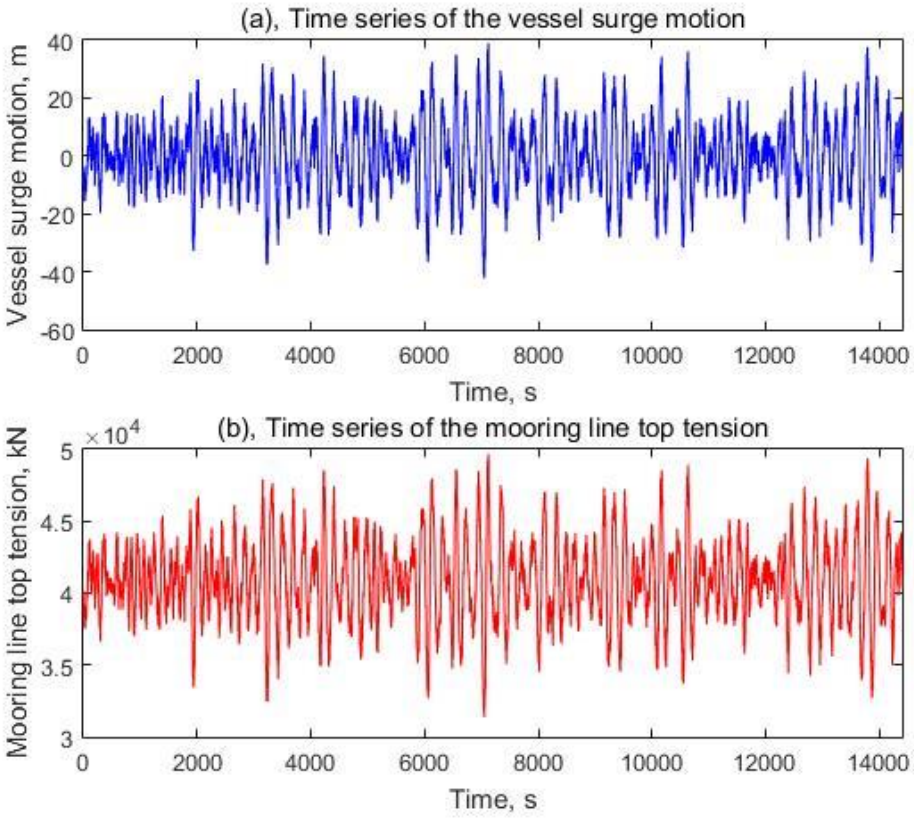

Figure 5. Time series of the vessel surge motion and mooring line top tension

For each static equilibrium configuration of the mooring line with a specified offset from the original positon, a set of additional offsets are selected. The corresponding mooring line top tensions are calculated using the catenary solution. The linear rate of change of top tension per unit change of surge offset, denoted as k_{surge}, can be easily obtained as the slope of the linear fit of the mooring line top tension versus surge offset curve, as shown in Figure 6.

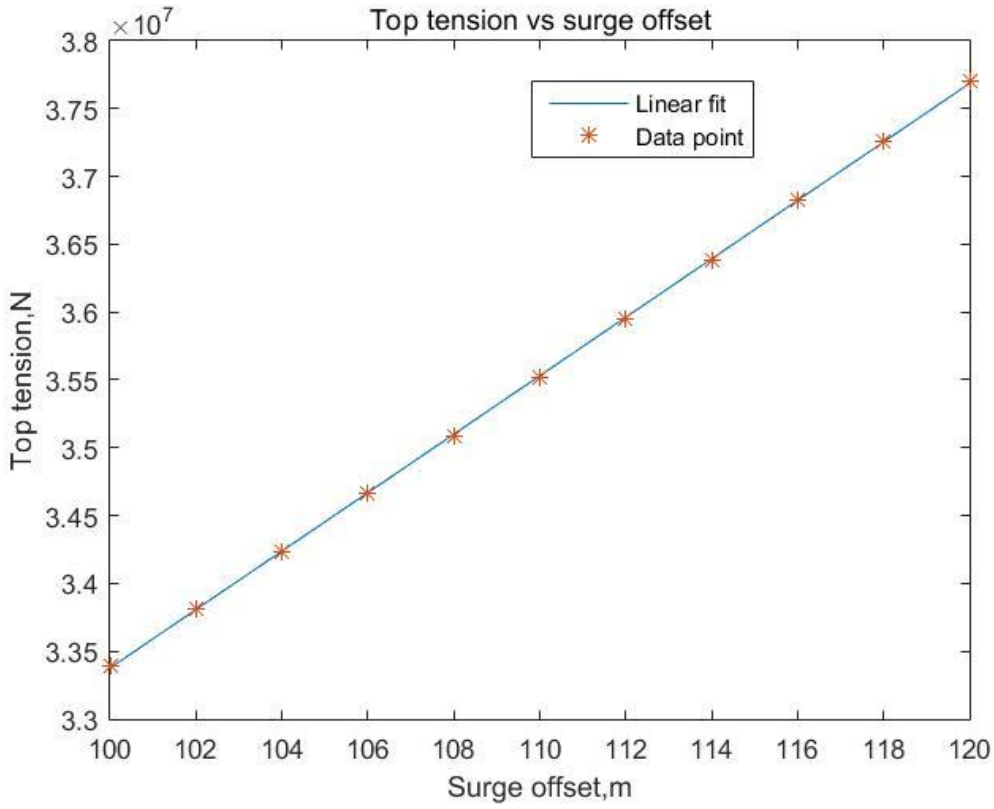

Figure 6. The linear regression of mooring line top tension and surge offset

The mooring line top tension $T_{top}(t)$ is assumed to be linearly related to the surge motion $X(t)$ according to

$$T_{top}(t) = k_{surge} X(t) + \bar{T}_{top} \tag{85}$$

where $\bar{T}_{top}$ is the mooring line top tension at the static equilibrium state. Meanwhile, the Fourier transform of the time series of top surge motion $\chi(f)$ is given as

$$\chi(f) = \int_{-\infty}^{+\infty} X(t) e^{-i(2\pi ft)} dt \tag{86}$$

In order to obtain the Fourier transform of time series of mooring line top tension fluctuation $\psi(f)$, the Fourier transform of the time series of mooring line top surge motion $\chi(f)$ is multiplied by a summation of harmonic response functions $H_i(f)$ for individual modes, which is equivalent to convolution of a time series and impulse response functions in time domain. This process can be represented as

$$\psi(f) = k \sum_{i=1}^{n_f} W_i H_i(f) \chi(f) \tag{87}$$

where n_f is the number of natural frequencies considered in this case.

The harmonic response function for each mode can be estimated with the corresponding natural frequency and an assumed damping ratio. The harmonic response function $H_i(f)$ for mode *i* is that for a viscously damped, linear single degree of freedom oscillator, namely

$$H_i(f) = \frac{1}{\left[1-(f/f_{ni})^2\right] + i\left[2\zeta_{di}(f/f_{ni})\right]} \tag{88}$$

where f_{ni} is the natural frequency for mode *i* and ζ_{di} is the damping ratio for mode *i*.

Meanwhile, W_i is the weighting factor for each mode. Since $H_i(0) = 1$ for all the modes and the top of the mooring line can be modeled as a linear spring while the frequency equals zero, W_i should have the following property:

$$\sum_{i=1}^{n_f} W_i = 1 \tag{89}$$

In this thesis, uniformly distributed weighting factors are used for all modes.

The result of the multiplication Eq. (87) is the Fourier transform of the time series of mooring line top tension fluctuation $\psi(f)$. The inverse Fourier transform can be conducted to obtain the corresponding time series of the mooring line top tension fluctuation $T_{top}(t)$ as

$$T_{top}(t) = \int_{-\infty}^{+\infty} \psi(f) e^{i(2\pi ft)} df \tag{90}$$

This time series of the mooring line top tension is shown in Figure 5 (b). Meanwhile, the spectrum of mooring line top tension $S_{TT}(f)$ is estimated using

$$S_{TT}(f) = \frac{1}{2\Delta f} \psi(f) \psi^*(f) \tag{91}$$

where superscript * denotes the complex conjugate of the corresponding complex number.

This spectrum of the mooring line top tension is compared with that from fully nonlinear time domain simulations performed using OrcaFlex. The damping ratios ζ_{di} for the individual modes need to be tuned to fit this spectrum with that derived from the OrcaFlex simulation.

6. EXTREME VALUE ANALYSIS OF MOORING LINE TOP TENSION

6.1 Local maxima distribution using Rice's theory

The time series of vessel surge motion can be modeled as an ergodic Gaussian process with zero mean. Associated with the harmonic response functions and modal superposition, the superposed time series for mooring line top tension fluctuation must represent a Gaussian process with zero mean as well because the superposition of a limited number of Gaussian processes is still Gaussian. Furthermore, the extremes (individual local maxima) of the general stationary Gaussian random process with zero mean are described by the Rice distribution (Broch (1963)). The probability density function of the Rice distribution is given as

$$f\left(x_r\right)=\frac{\varepsilon}{\sqrt{2\pi m_0}}e^{-\frac{x_r^2}{2m_0\varepsilon^2}}+\frac{\sqrt{1-\varepsilon^2}}{m_0}x_r e^{-\frac{x_r^2}{2m_0}}\left(\frac{1}{2}+\frac{1}{2}erf\left(\frac{x_r\sqrt{1-\varepsilon}}{\varepsilon\sqrt{2m_0}}\right)\right) \qquad (92)$$

Related parameters m_0 and ε are calculated based on the spectral moments of the original Gaussian process; and *erf* is so the called error function. The bandwidth parameter ε can be calculated using

$$\varepsilon=\sqrt{1-\frac{m_2^2}{m_0 m_4}} \qquad (93)$$

in which m_0, m_2 and m_4 are spectral moments of the Gaussian process, which are defined by the following integral:

$$m_n = \int_0^{+\infty} f^n S_{xx}(f) df \tag{94}$$

The error function *erf* is given as

$$erf(x) = \frac{2}{\sqrt{\pi}} \int_0^x e^{-t^2} dt \tag{95}$$

Accordingly, the local extreme values derived from the time series of the mooring line top tension using the present method may be represented by the Rice distribution. The Rice distribution for the extreme values of the mooring line top tension can be obtained based on the spectral moments of the original Gaussian process. In addition, this mooring line top tension needs to be adjusted to have a zero mean in order to fit the original Rice distribution. After the fit, it can be adjusted back to be actual mean value, which is the situation shown in the subsequent plots in this chapter. In order to verify this distribution fitting procedure, a popular approach for distribution fitting named maximum likelihood estimation (MLE) is used. The extremes of the time series of the mooring line top tension are obtained, then fitted with the Rice distribution using maximum likelihood estimation. The probability distribution function (PDF) plots for a multi-segment mooring line using both distribution fitting approaches are shown in Figure 7. This figure shows that the result

of the spectral moment fit approach is in accordance with that of maximum likelihood estimation, as expected.

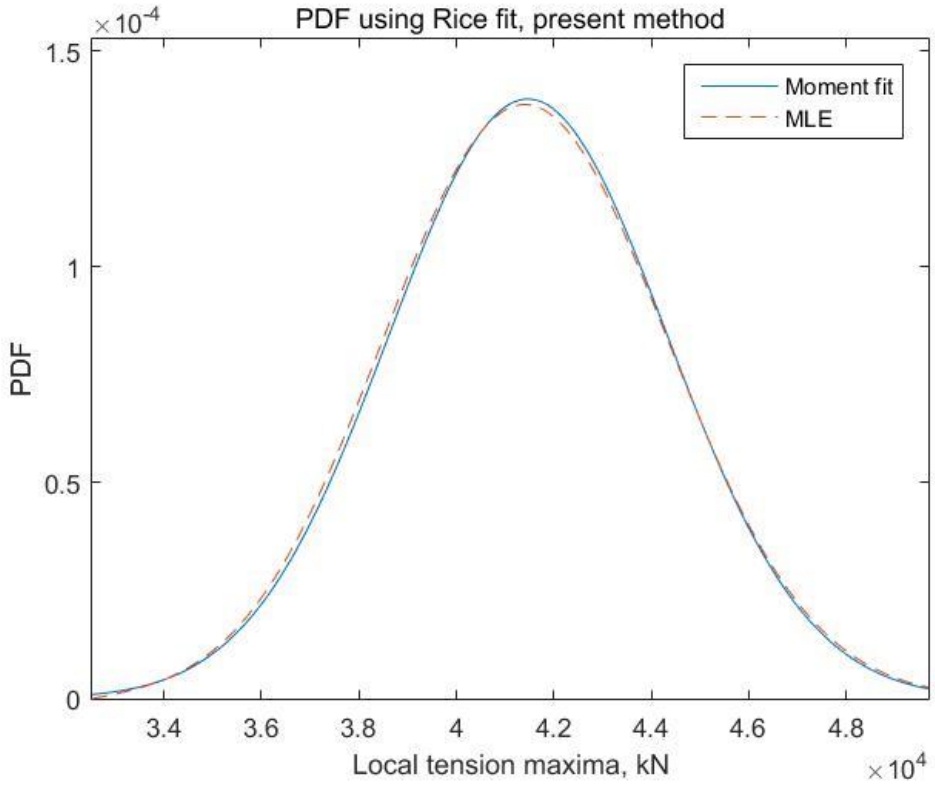

Figure 7. PDF of Rice distribution, using moment fit and MLE

Moreover, this distribution fitting procedure is conducted again with results from OrcaFlex simulations. Both outcomes will be compared to estimate the conformity of the present method and OrcaFlex simulation. Examples of cumulative distribution function (CDF) plots of the original data and the fitted Rice distribution using both the present

method and OrcaFlex are shown in Figure 8. The figure illustrates that the Rice distribution fits the original data very well, whether it is derived from OrcaFlex simulation or with the present method.

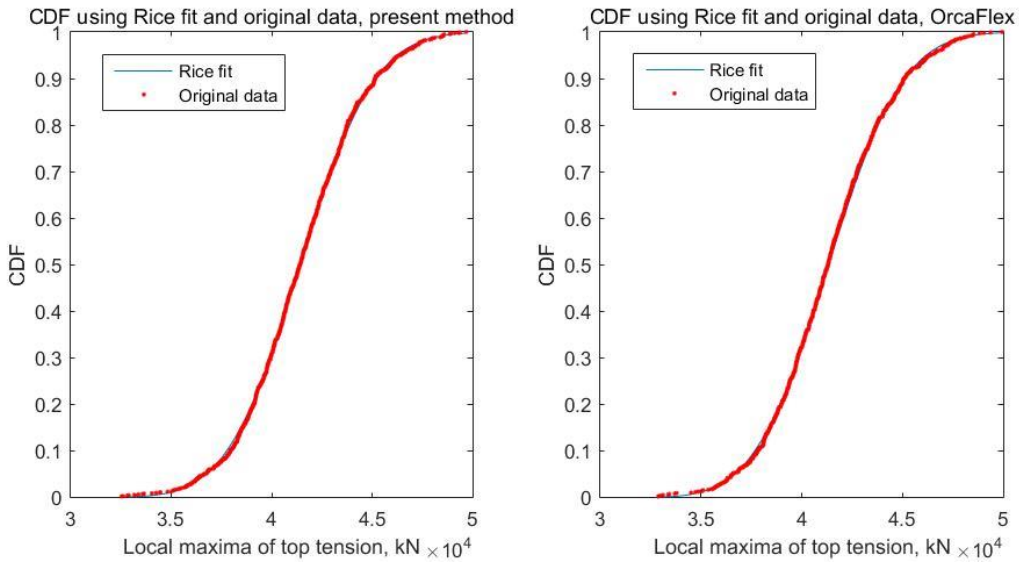

Figure 8. CDF of fitted Rice distribution using present method and OrcaFlex

6.2 Distribution of maximum among *N* local maxima

As described by Karimirad (2014), the "design wave" method is useful as a simple and preliminary check for the structural integrity of an offshore structure subjected to wave loads. A similar approach can be implemented in the present method in order to estimate the largest maximum among *N* local maxima of the mooring line top tension.

During a time simulation, $x_{\max 1}$, $x_{\max 2}$,…, $x_{\max N}$ denote N local maxima; the maximum among N maxima is denoted by x_M. It is assumed that all the local maxima are Gaussian distributed and independent. The probability of x_M being less than a certain value is given as

$$P\left(x_r > x_M\right) = P\left(x_r > x_{\max 1}\right) \cdot P\left(x_r > x_{\max 1}\right) \cdot \ldots \cdot P\left(x_r > x_{\max N}\right) \tag{96}$$

The cumulative distribution and probability density of the maximum among N maxima is written as follows

$$F_M\left(x_r\right) = \left[F\left(x_r\right)\right]^N \tag{97}$$

$$f_M\left(x_r\right) = N\left[F\left(x_r\right)\right]^{N-1} f\left(x_r\right) \tag{98}$$

where $F\left(x_r\right)$ represents the CDF of the Rice distribution.

The expectation of the maximum among N local maxima is given as

$$E\left(x_M\right) = \int_{-\infty}^{+\infty} x_r f_M\left(x_r\right) dx_r \tag{99}$$

If a stochastic Gaussian process is narrow-banded, its local maxima are Rayleigh distributed. The expected value of the largest maximum for this process can be calculated by

$$E\left(x_r\right) = \sqrt{m_0}\left(\sqrt{2\ln N} + \frac{0.57722}{\sqrt{2\ln N}} + O\left(\left(\ln N\right)^{-1.5}\right)\right) \tag{100}$$

In addition, the maximum of a broad-banded Gaussian process is Gaussian distributed. The expected value of the largest maximum of a general Gaussian process is smaller than that of a narrow-banded process and larger than that of a broad-banded process.

For a general Gaussian process, the expected time period between two contiguous local maxima can be determined as

$$E\left(t_{peak}\right)=\sqrt{\frac{m_2}{m_4}} \tag{101}$$

Given a time simulation, $E\left(t_{peak}\right)$ can be computed first with spectral moments of this process; then the number of local maxima *N* is calculated using the simulation duration divided by $E\left(t_{peak}\right)$. Furthermore, the expected largest maximum mooring line top tension T_M can be estimated for design purposes.

In addition, according to Naess and Moan (2012), in the design process of mooring lines, a quantity of particular interest for top tension is $T_p\left(t\right)$, which with probability *P* is not exceeded during time duration *t*. This quantity can be represented as

$$F_{M(t)}\left(T_P\right)=P \tag{102}$$

Combining with Eq. (97) and (101), Eq. (102) can be solved numerically for $T_P\left(t\right)$ with a given reasonable value of probability *P*.

7. CASE STUDY OF A MULTI-SEGMENT MOORING LINE

7.1 Properties of a lumped multi-segment mooring line

The study case developed herein is a lumped multi-segment mooring line. The original system is a semi-submersible with a mooring system using chain-polyester-chain line for a 2200 m water depth. The mooring system consists of four groups with four mooring lines each, for a total of sixteen mooring lines. In order to simplify the original case, a group of four mooring lines is lumped together to a single line, which is four times the cross-section area, axial stiffness, submerged weight, and top tension of the original mooring line. Figure 9 shows the static equilibrium configuration of the simplified mooring system. The initial anchor radius for each line at the static equilibrium state is 3953 m. In this case, three different segments are used. The line properties for all segments are list in Table 8.

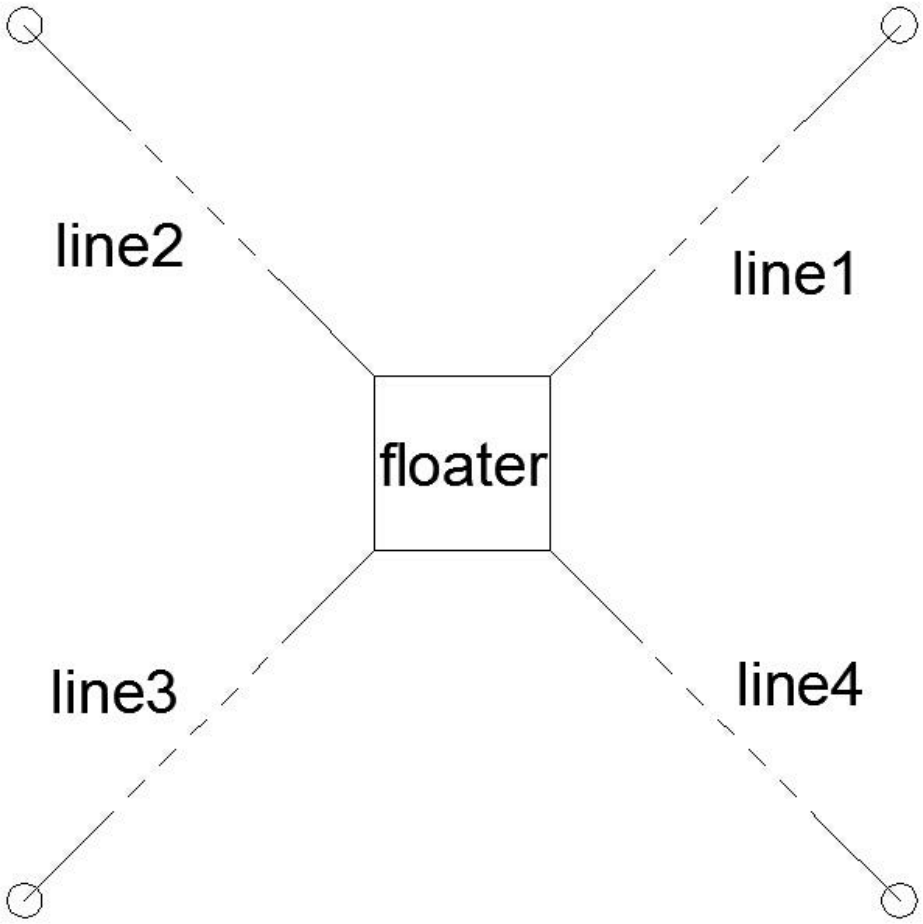

Figure 9. Configuration of the simplified mooring system

Table 8. Segment properties of a multi-segment mooring line

Segment property	Bottom chain	Polyester	Top chain
Length, *m*	450	3900	150
E, *Pa*	34156142431	11385428140	34156142431
A, m^2	0.26970259	0.14053051	0.26970259
Wet weight, *N/m*	18592	502.4	18592
C_A and C_D	Various	Various	Various

The static equilibrium configuration of this lumped multi-segment mooring line is shown in Figure 10.

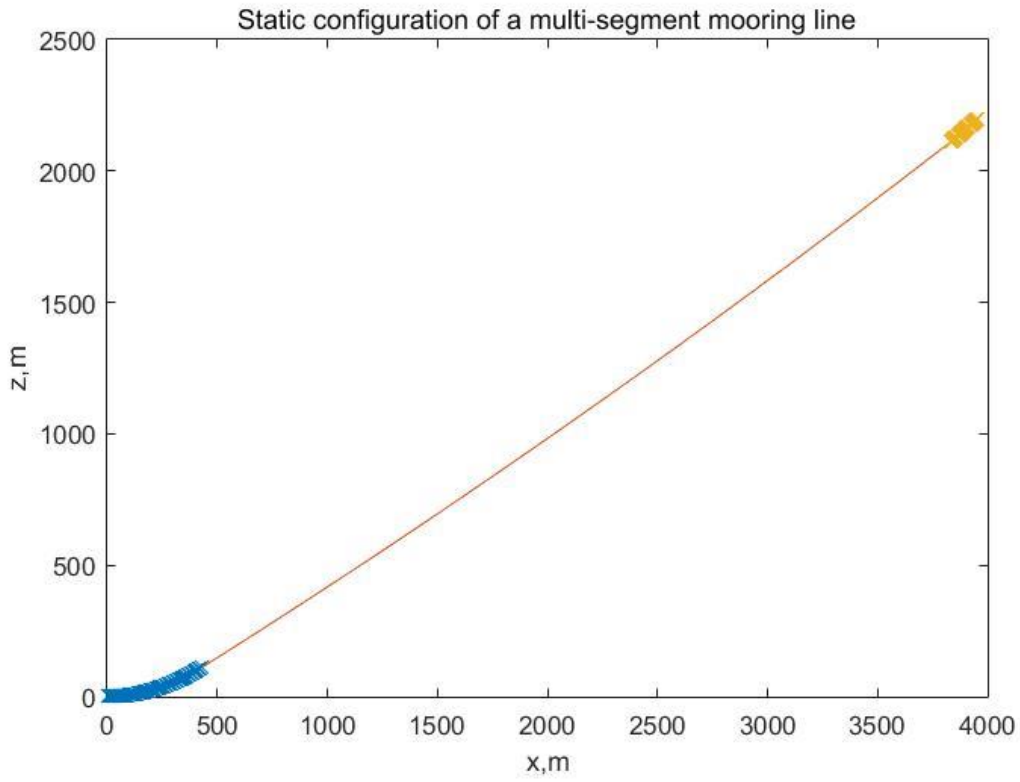

Figure 10. Static equilibrium configuration of a multi-segment mooring line

For this mooring line, a total of 151 elements are used. Uniform element size is adopted for each segment. In order to obtain a numerically stable solution, the element size for different segments must be similar.

7.2 Surrounding environmental conditions of the mooring line

Four cases with different surrounding environments are considered for the multi-segment mooring line. Descriptions of these cases are presented as follows.

1) Air

In this case, the mooring line is vibrating in air. Buoyancy, added mass effect and hydrodynamic damping are neglected. Although it is not a realistic situation for mooring lines, this case is still needed in order to compare the results with the submerged cases. In addition, it is a typical case in previous research related to cable structures. Additionally, the static equilibrium configuration of the mooring line in this case is more slack than those in the following cases.

2) Water with buoyancy

The buoyancy of the mooring line produced by the water is included in this case. The hydrodynamic forces, such as added mass effect and damping effect due to the motion of the mooring line are not considered.

3) Water with buoyancy and added mass effect

In this case, the added mass effect is introduced besides the buoyancy. The added mass effect can be modeled using Morison's equation. The force is proportional to the relative acceleration of the mooring line and surrounding fluid. The added mass coefficient in this research is set to be one; but can be adjusted to another value if needed.

4) Water with buoyancy, added mass and damping effect

The hydrodynamic damping effect is considered in this case; buoyancy and added mass effect are also included. The damping effect is modeled using Morison's equation at

first; then linearized following the linearization procedure proposed in Section 3.9. A range of damping coefficient values is applied in order to investigate the effect of hydrodynamic damping.

7.3 Poisson's effect of the material of a mooring line

Commonly used values of Poisson's ratio are 0.3 for steel and 0.4 for polyester. Eqs. (49) and (50) show that the Poisson's effect should be included in the normal and bi-normal directions in Lagrange local coordinates, but not in the tangential direction. In order to investigate the effect of hydrostatic pressure on the vibration of multi-segment mooring lines in deep water, cases with reasonable Poisson's ratio or zero Poisson's ratio are analyzed.

7.4 Surge offset and motion spectrum of the top of the mooring line

The offshore vessels often experience surge offset due to directional wave field and slow drift effects. Therefore, each vessel surge motion spectrum has an associated surge offset range. This surge offset is usually given as a percentage of the water depth. For the multi-segment mooring line considered, the values of the JONSWAP spectral parameters X_S, $T_p = 1/f_p$ and γ are provided in Table 9 for a vessel surge motion spectrum, while

the wind force is fluctuating. The associated surge offset range is also included. The return period for this surge motion spectrum is 100 years.

Table 9. Parameters of surge power spectrum used for the mooring line

Spectral parameter		X_S, m		T_P, s		γ	
Return period	Surge offset	Wave	Slow drift	Wave	Slow drift	Wave	Slow drift
100 years	4%-6%	9.14	50	15.5	188.68	1.0	3.3

Based on the main characteristics of the surge motion spectra given in Table 9, the surge spectrum with 100-year return period is plotted as Figure 11.

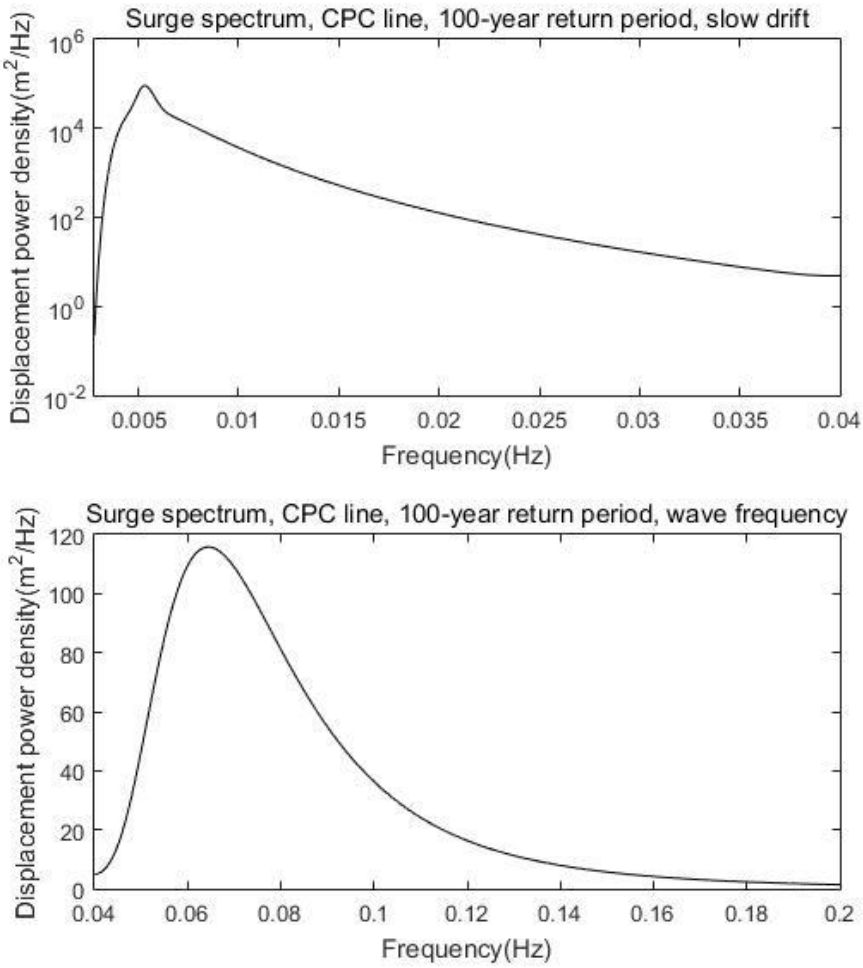

Figure 11. Surge motion power spectrum with 100-yr return period

This vessel surge motion spectrum with 100-year return period is used for the subsequent modal analysis. Five percent is chosen as the associated vessel surge offset. The corresponding static equilibrium configuration of this mooring line is shown in Figure 12.

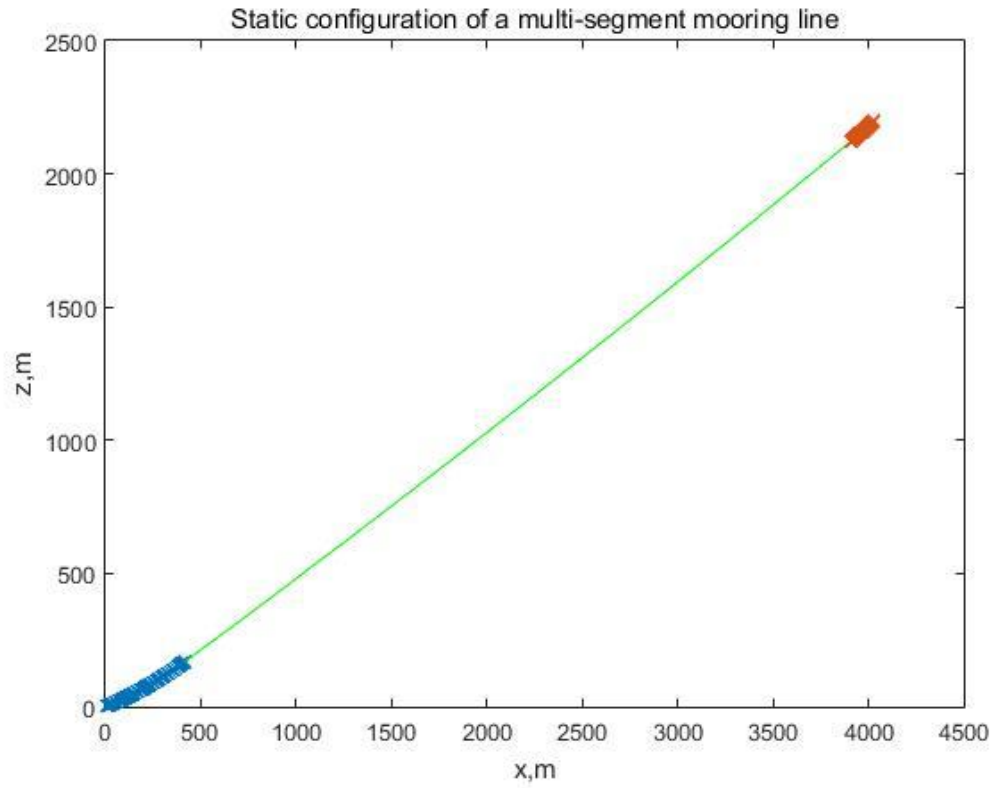

Figure 12. Static equilibrium configuration of a multi-segment mooring line with 5% offset

7.5 Results of the modal analysis of the mooring line

7.5.1 Results of the cases without damping effect

The natural periods of the first eight modes for this multi-segment mooring line in case (1), (2) and (3) using Lagrange local coordinate system are listed in Table 10. The corresponding first three mode shapes are shown in Figure 13 for case (1), Figure 14 for case (2) and Figure 15 for case (3). Meanwhile, Table 11 shows results in Cartesian

coordinate system; and Figure 16, Figure 17 and Figure 18 display the corresponding mode shapes for case (1), case (2) and case (3), respectively. The Poisson's ratios are set to be reasonable values according to the material for all cases. Only cases without damping involved are presented in this section. The surge motion spectrum with 100-year return period is used. The corresponding mean surge offset for all the cases is five percent of the water depth. The anchor radius of this mooring line during this 100-year event is calculated to be 4031.53 m.

Table 10. The first eight natural periods for the mooring line in Lagrange local coordinates

Direction	Case	Natural periods of the first eight modes, *s*							
		1	2	3	4	5	6	7	8
Tangential	1)	2.800	1.411	0.980	0.829	0.673	0.546	0.458	0.395
	2)	2.801	1.412	0.980	0.829	0.673	0.546	0.458	0.395
	3)	2.801	1.412	0.980	0.829	0.673	0.546	0.458	0.395
Normal and bi-normal	1)	20.612	12.667	8.529	6.036	4.846	4.334	3.811	3.275
	2)	21.752	13.362	8.980	6.360	5.113	4.573	4.019	3.450
	3)	27.983	15.772	11.241	8.126	6.344	5.363	4.817	4.281

Table 11. The first eight natural periods for the mooring line in Cartesian coordinates

Direction	Case	Natural periods of the first eight modes, *s*							
		1	2	3	4	5	6	7	8
In-plane	1)	18.565	12.641	8.522	6.051	4.860	4.353	3.814	3.278
	2)	21.055	13.233	8.964	6.371	5.123	4.590	4.022	3.453
	3)	24.610	14.580	10.258	7.372	5.788	5.030	4.498	3.939
Swinging	1)	20.612	12.667	8.529	6.036	4.846	4.334	3.811	3.275
	2)	21.752	13.362	8.980	6.360	5.113	4.573	4.019	3.450
	3)	27.983	15.772	11.241	8.126	6.344	5.363	4.817	4.281

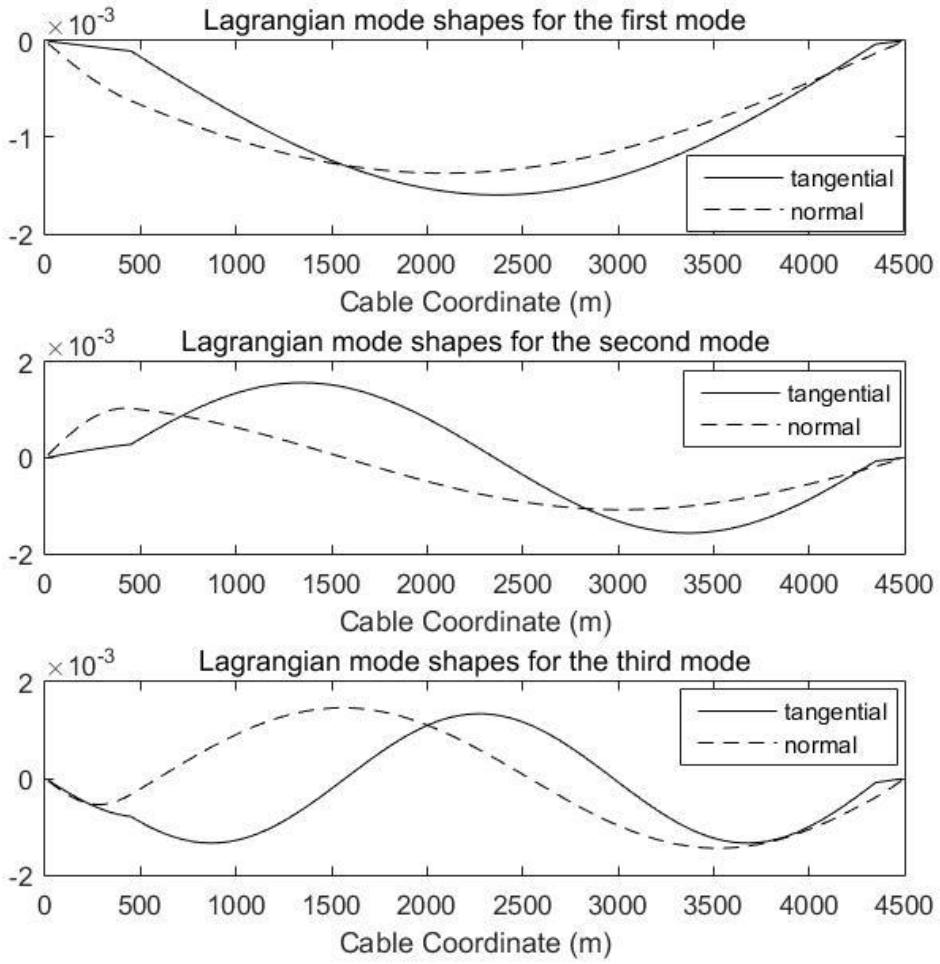

Figure 13. The first three mode shapes for case (1) in Lagrange local coordinates

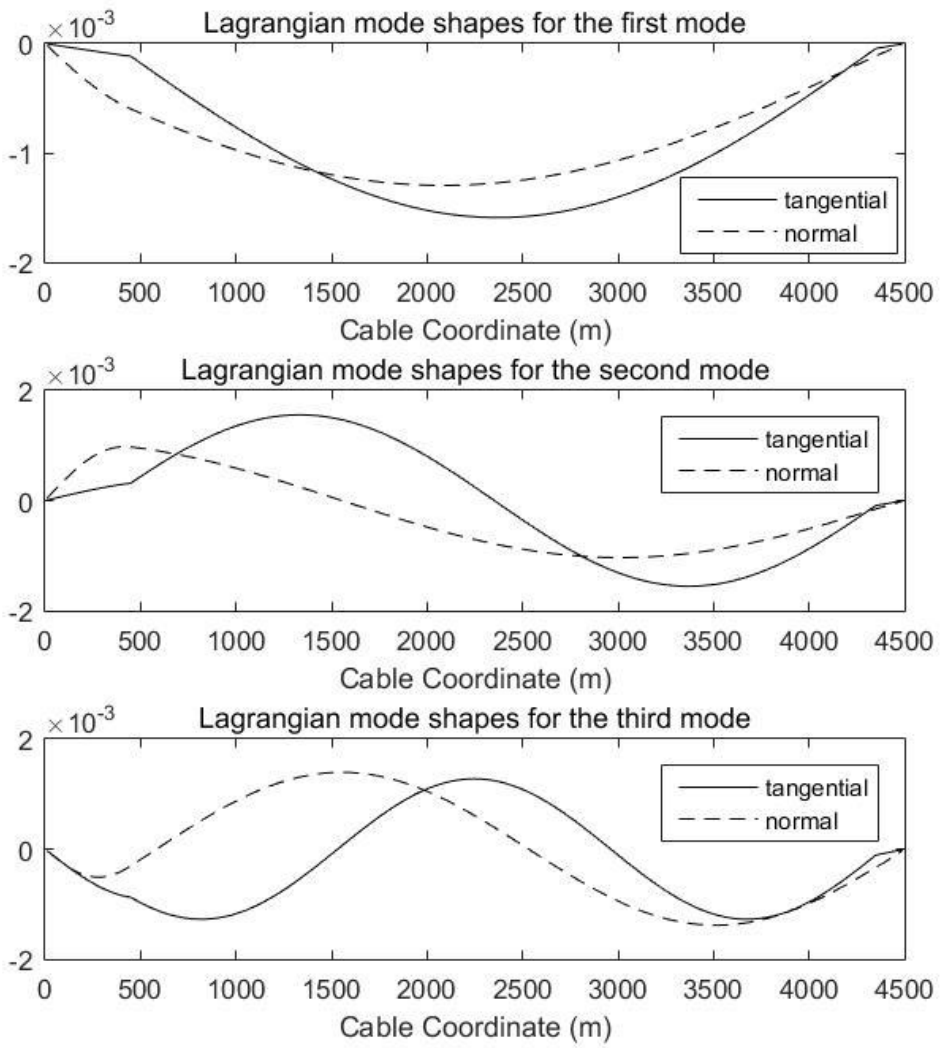

Figure 14. The first three mode shapes for case (2) in Lagrange local coordinates

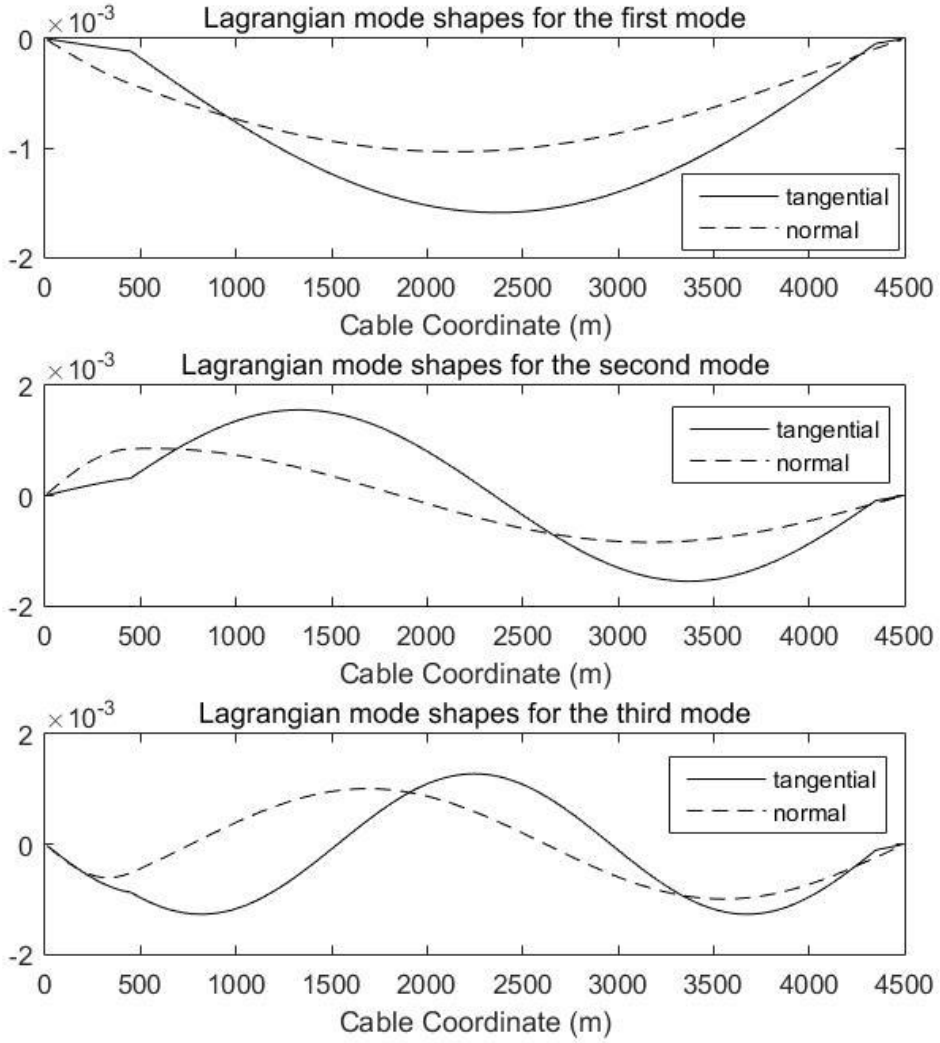

Figure 15. The first three mode shapes for case (3) in Lagrange local coordinates

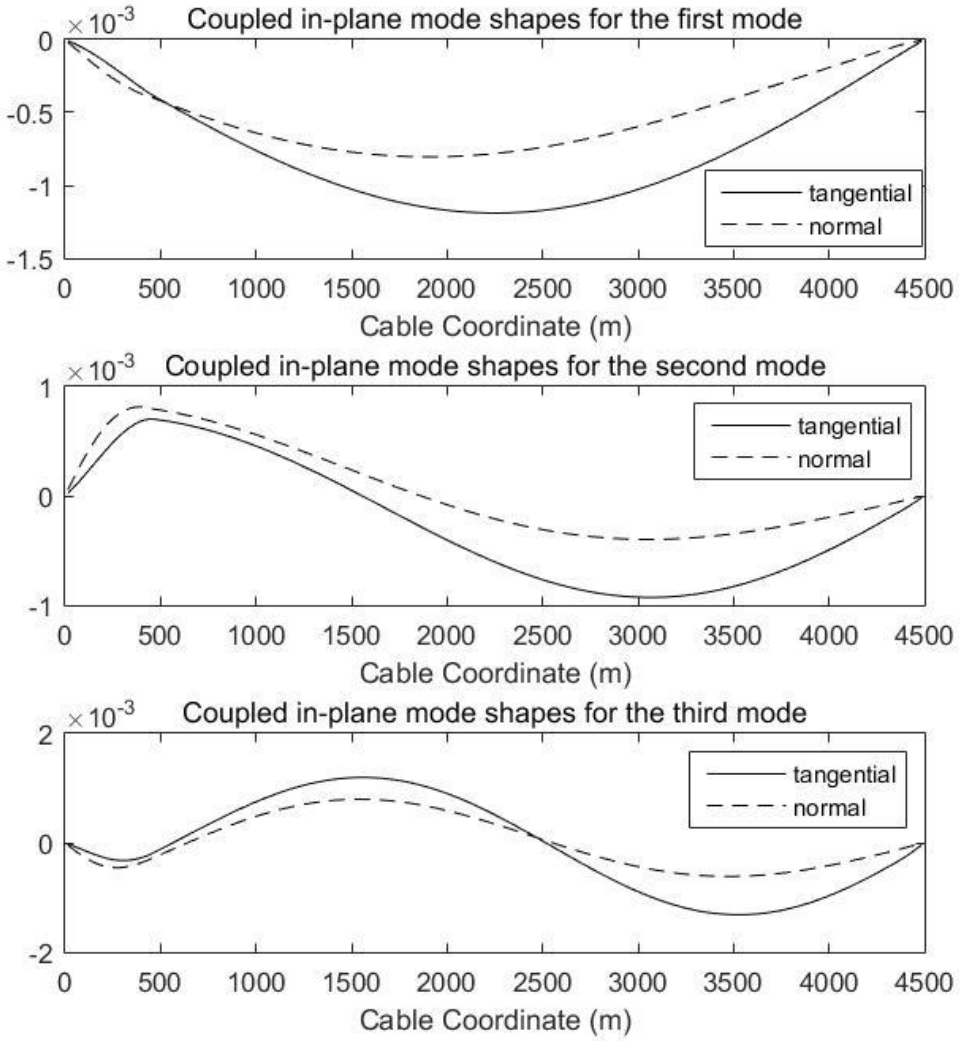

Figure 16. The first three in-plane mode shapes for case (1) in Cartesian global coordinates

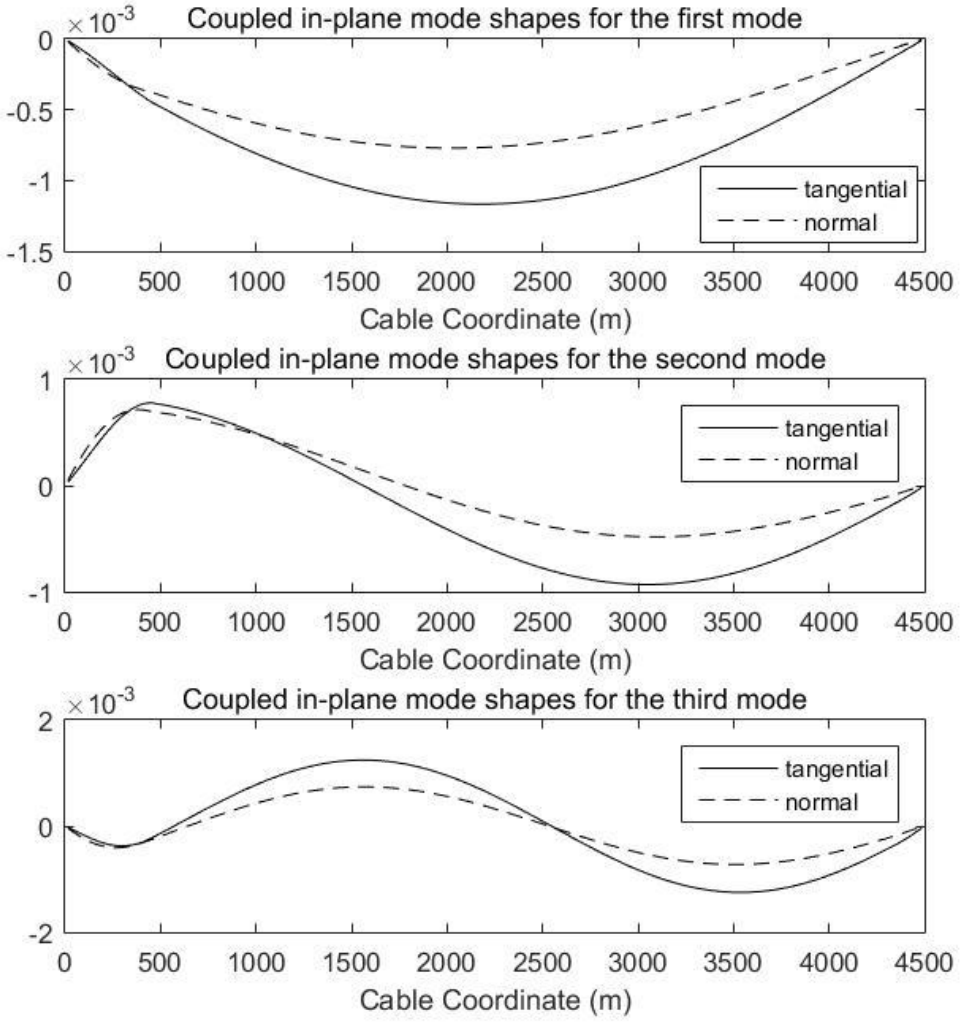

Figure 17. The first three in-plane mode shapes for case (2) in Cartesian global coordinates

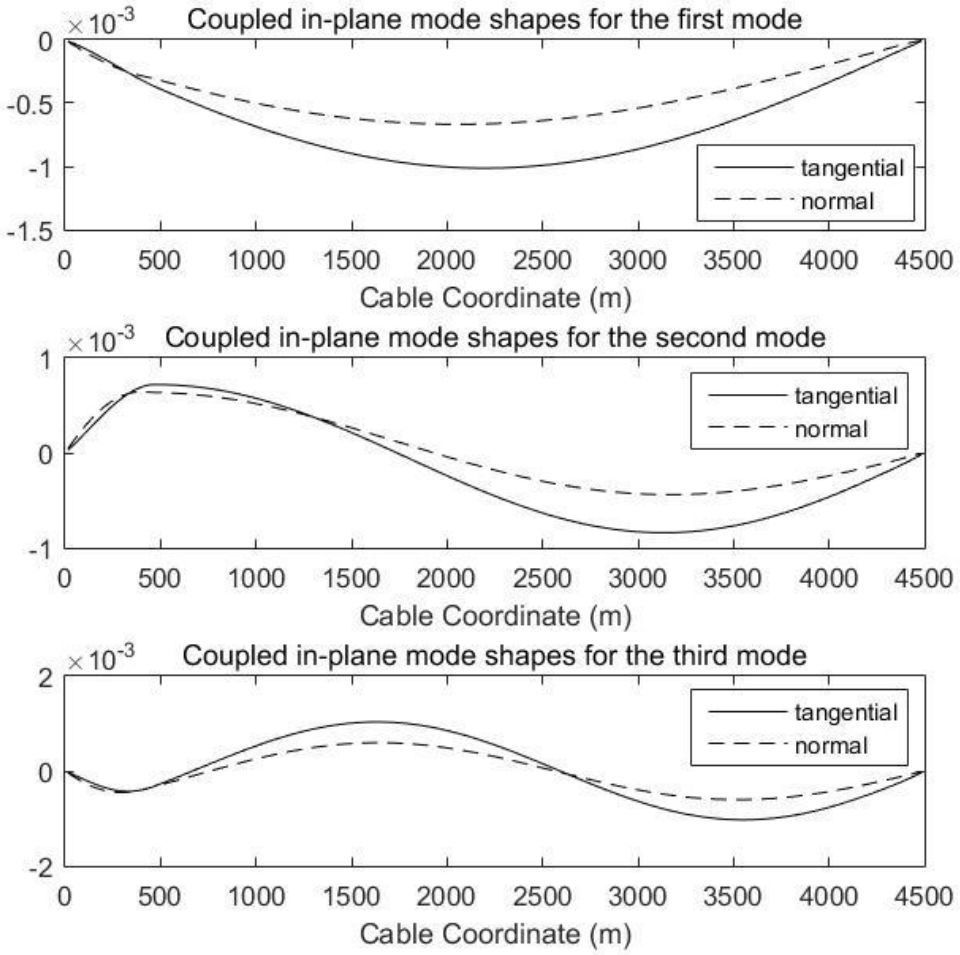

Figure 18. The first three in-plane mode shapes for case (3) in Cartesian global coordinates

In Lagrange local coordinates, the natural periods and mode shapes in the tangential direction of each mode are almost identical for the three cases. Therefore, the buoyancy and added mass effect have a trivial influence on the tangential vibration. At the same

time, the natural periods for vibrations in the tangential direction are far smaller than those for normal and bi-normal vibrations, which is easy to understand since the tangential direction is much stiffer than the normal and bi-normal direction. On the other hand, in the normal and bi-normal direction, the natural periods of modes in case (2) are slightly larger than those in case (1). Meanwhile, the natural periods in case (3) are larger than those in case (2) by a relatively larger amount. Although the initial static equilibrium configuration of the mooring line in case (1) is different from that in case (2) and (3), the buoyancy effect increases the natural periods in the normal direction only by a small amount. In contrast, the added mass effect will increase the natural periods in the normal direction more significantly. Furthermore, the plots of mode shapes show that the discontinuities of the slopes are associated with the chain/polyester rope segment boundaries of the mooring line. In Cartesian coordinates, similar conclusions for both in-plane and swinging direction are drawn as those that arise for the normal direction in Lagrange local coordinates. Moreover, the natural periods in the swinging direction are slightly larger than those in the in-plane direction.

7.5.2 Results of the cases considering damping effect

The linearization approach of hydrodynamic damping is proposed in Section 3.9. The magnitude of the linearized damping depends on the root mean square value of the

mooring line top surge motion spectrum and the hydrodynamic drag damping coefficient C_D. The five-percent surge offset has an associated top surge motion spectrum with 100-year return period. The cases are analyzed only in Lagrange local coordinates. A set of different damping coefficient values in both tangential and normal direction C_D are used. The natural periods of the cases with these different drag damping coefficients are listed in Table 12.

Table 12. The first eight natural periods for the damped mooring line in Lagrange local coordinates

Direction	C_D	Natural periods of the first eight modes, *s*							
		1	2	3	4	5	6	7	8
Tangential	7	2.997	1.433	0.976	0.836	0.677	0.548	0.459	0.395
	5	2.896	1.422	0.978	0.833	0.675	0.547	0.458	0.395
	1	2.805	1.412	0.980	0.829	0.673	0.546	0.458	0.395
	0.5	2.802	1.412	0.980	0.829	0.673	0.546	0.458	0.395
	0.1	2.801	1.412	0.980	0.829	0.673	0.546	0.458	0.395
Normal and bi-normal	7	N/A	17.310	13.135	8.910	6.572	5.306	4.920	4.385
	5	79.836	15.923	12.455	8.491	6.449	5.326	4.878	4.335
	1	28.442	15.789	11.282	8.140	6.348	5.362	4.819	4.283
	0.5	28.095	15.776	11.251	8.130	6.345	5.363	4.818	4.281
	0.1	27.988	15.772	11.241	8.126	6.344	5.363	4.817	4.281

Figure 19 and Figure 20 show the natural periods of the first eight modes in tangential and normal direction with various damping coefficients.

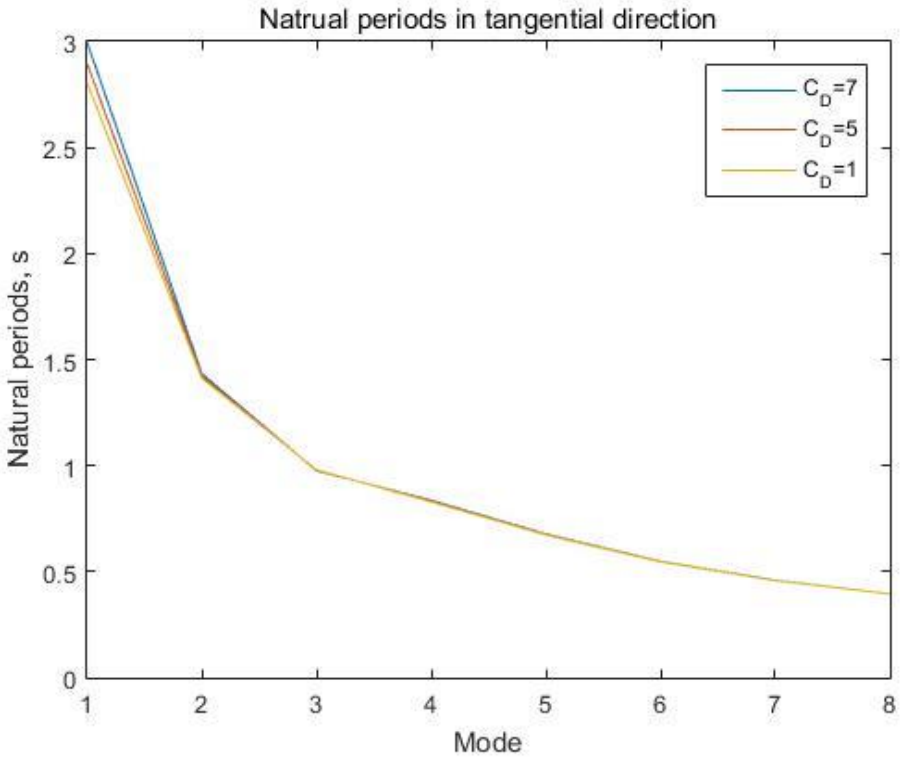

Figure 19. The first eight natural periods in tangential direction for the damped mooring line

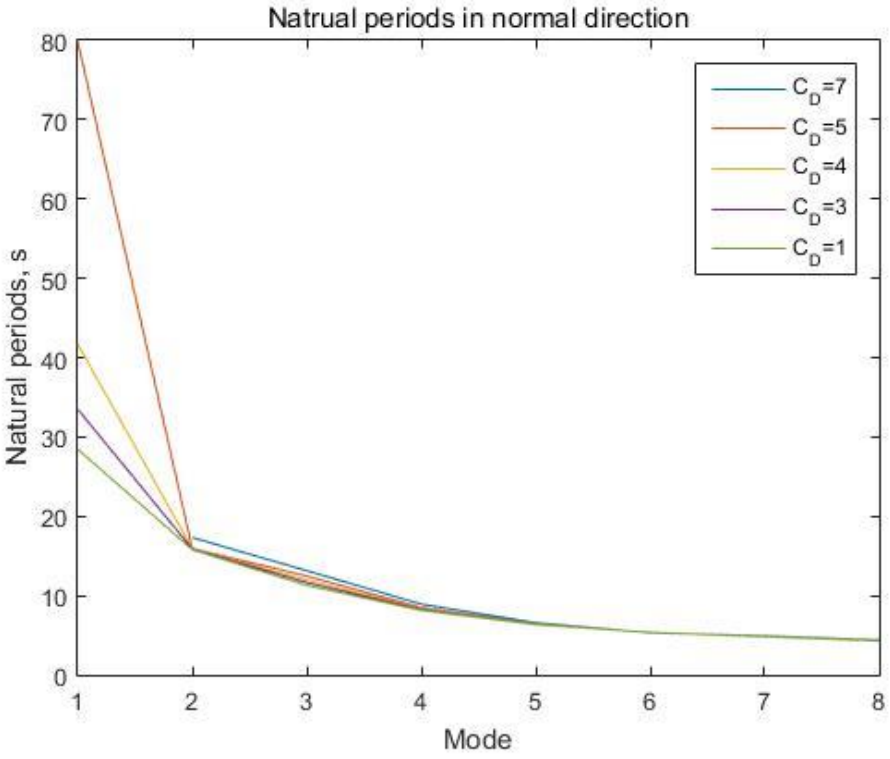

Figure 20. The first eight natural periods in normal direction for the damped mooring line

The mode shapes in Lagrange local coordinates while damping coefficient C_D equals to one are given in Figure 21.

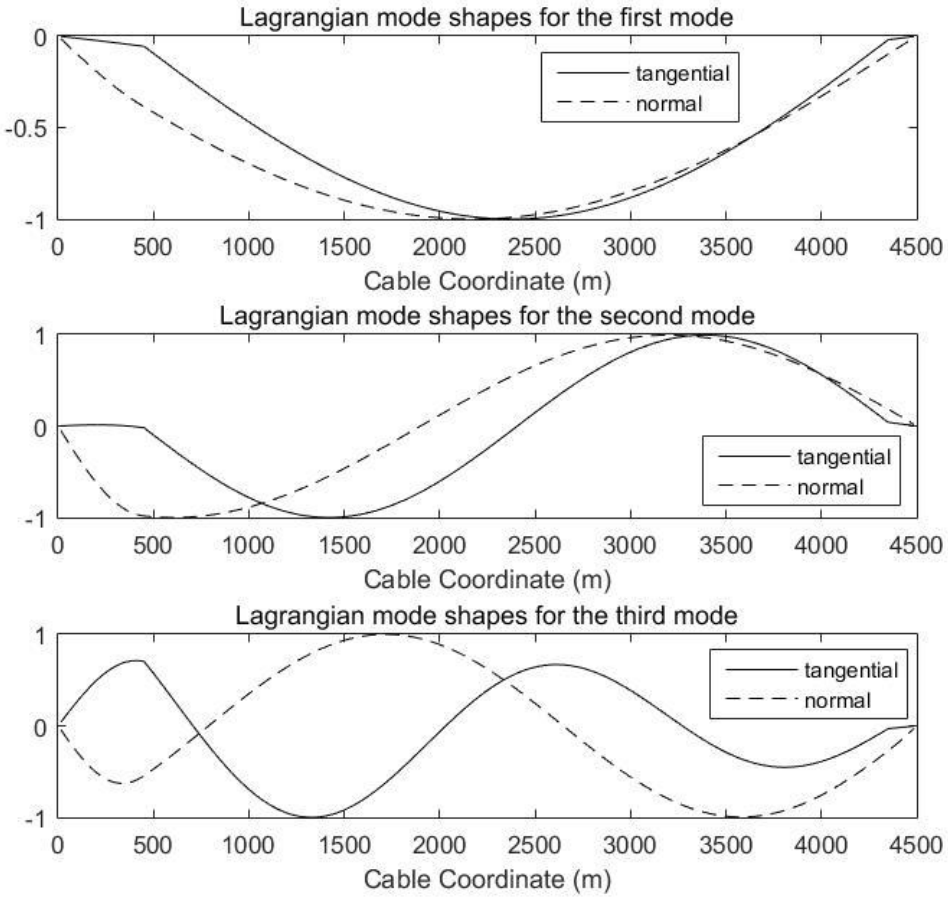

Figure 21. The first three mode shapes for the damped mooring line in Lagrange local coordinates

For the damped cases, as the drag damping coefficient increases, the natural periods of each mode in Lagrange local coordinates will increase. Meanwhile, as the drag damping coefficient varies, only the natural periods of the several lowest modes in the normal direction will change significantly. Even with a relatively large damping ratio, the natural

periods of other modes are almost identical to those for the undamped case. Furthermore, the slopes of the mode shape plots are discontinuous at the segment boundaries of the mooring line, as expected. Additionally, in the normal and bi-normal direction in Lagrange local coordinates, if the drag damping ratio is sufficiently large, several lowest modes will vanish.

7.5.3 Results of the cases considering Poisson's effect

Furthermore, in order to estimate the Poisson's effect on the dynamics of the mooring line, case (5) modified from case (3) is used. Poisson's ratio in case (5) equals zero for all segments; case (3) uses 0.3 for the top and bottom chain segments and 0.4 for the middle polyester segment. The results are listed in Table 13 and Table 14.

Table 13. The first eight natural periods for the mooring line in Lagrange local coordinates

Direction	Case	Natural periods of the first eight modes, *s*							
		1	2	3	4	5	6	7	8
Tangential	3)	2.801	1.412	0.980	0.829	0.673	0.546	0.458	0.395
	5)	2.801	1.412	0.980	0.829	0.673	0.546	0.458	0.395
Normal and bi-normal	3)	27.983	15.772	11.241	8.126	6.344	5.363	4.817	4.281
	5)	27.663	15.533	11.116	8.054	6.286	5.299	4.757	4.243

Table 14. The first eight natural periods for the mooring line in Cartesian coordinates

Direction	Case	Natural periods of the first eight modes, *s*							
		1	2	3	4	5	6	7	8
In-plane	3)	24.610	14.580	10.258	7.372	5.788	5.030	4.498	3.939
	5)	24.348	14.358	10.151	7.307	5.731	4.960	4.452	3.907
Swinging	3)	27.983	15.772	11.241	8.126	6.344	5.363	4.817	4.281
	5)	27.663	15.533	11.116	8.054	6.286	5.299	4.757	4.243

Table 13 and Table 14 illustrate that Poisson's effect slightly increases the natural periods in the normal direction in Lagrange local coordinates and the swinging direction in Cartesian coordinates. Meanwhile, it will not affect the tangential direction in Lagrange local coordinates, since the equation of motion in the tangential direction Eq. (49) does not include Poisson's ratio. Furthermore, in the in-plane direction in Cartesian coordinates, the natural periods of all modes in the case considering Poisson's effect are slightly larger than those in the case with zero Poisson's ratio. The reason is that the motion in the in-plane direction in Cartesian coordinates results from the coupling of the motion in both tangential and normal direction in Lagrange local coordinates. The coupled motion

in the in-plane direction is affected by the motion in the normal direction, on which the Poisson's effect has influence.

7.6 Estimation of mooring line top tension using modal superposition

For the following analyses, the results of modal analysis in Lagrange local coordinates are used. The vessel surge motion spectra used in this section concentrate mostly on the frequency range from 0 to 0.2 *Hz*. Only the first several natural frequencies in the normal or bi-normal direction lie in this range; and all natural frequencies in the tangential direction do not. The associated surge offset is from four percent to six percent, which is a significant quantity from a design perspective. The surge offset of offshore structures is limited in order to perform the intended function in a safe way. A severe environment event will lead to a relatively large surge offset that results in an increase of the mean of the dynamic mooring line top tension. Accordingly, the extreme values of the mooring line will increase, which is of interest in this thesis. For each surge offset, the slope of top tension versus surge offset and the sag can be obtained. The sag is defined as a ratio of the maximum vertical deviation D_v between the static configuration and the chord over the unstretched length of the mooring line L_0, which is as

$$sag = \frac{D_v}{L_0} \tag{103}$$

where the related variables are shown in Figure 22.

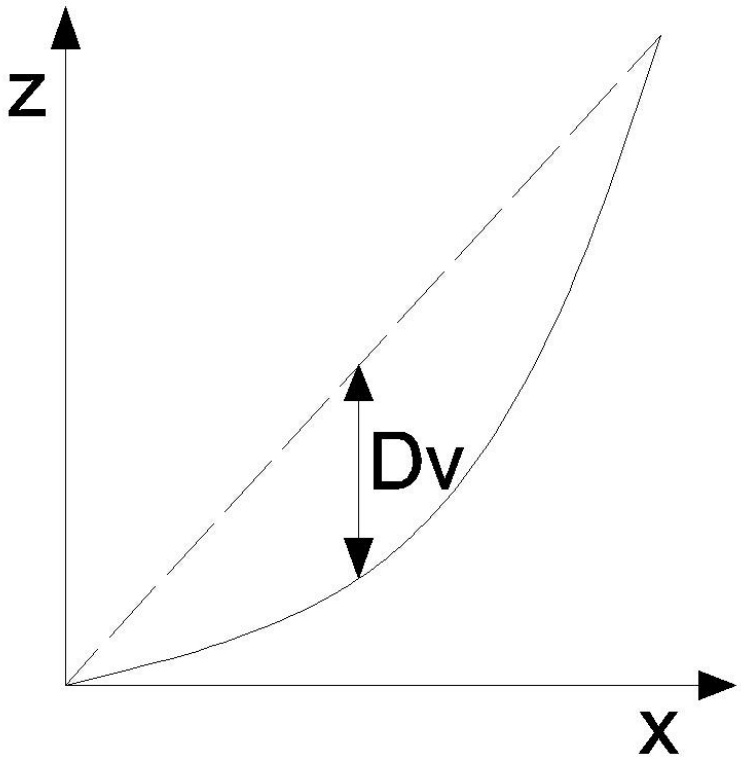

Figure 22. The configuration of a typical mooring line

For each case with specified surge offset and vessel surge motion spectrum, the spectrum of the mooring line top tension can be obtained using frequency domain analysis mentioned in Section 5.5. Furthermore, in order to fit the spectrum of top tension with OrcaFlex simulation, the damping ratio for each normal vibration mode is tuned.

7.6.1 Estimation of mooring line top tension with different surge offsets

A set of cases with surge offset from four percent to six percent with half-percent interval are selected for the analyses. Table 15 lists other variables of these cases. The error is defined as the difference between zeroth spectral moments of the mooring line top tension spectra obtained using the present method relative to that obtained using OrcaFlex.

Table 15. Variables of a set of mooring line cases with different surge offset

C_A:	1		C_D:	1	
Poisson's ratio:		0.3 for top and bottom chain; 0.4 for polyester			
Case	Surge offset, *%*	Slope, *N/m*	Sag, *1e-2*	Damping ratio	Error, *%*
(a)	4	213838.53	1.649	0.40	1.3689
(b)	4.5	220733.18	1.536	0.45	1.3883
(c)	5	226518.26	1.435	0.50	1.3458
(d)	5.5	231354.96	1.345	0.55	1.3230
(e)	6	235424.98	1.264	0.60	1.3198

As Figure 23 illustrates, the relationship between damping ratio and the sag of the mooring line is quite linear in the surge offset range four to six percent.

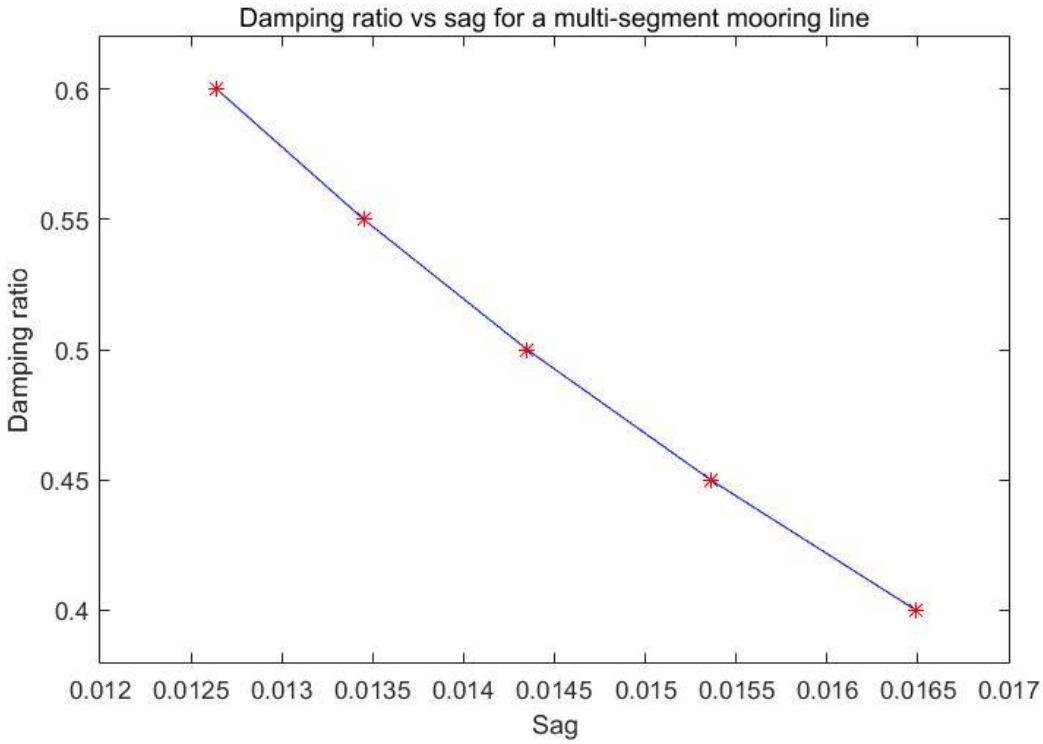

Figure 23. Damping ratio vs sag for a multi-segment mooring line

The first seven natural frequencies in the normal direction considered in these cases are shown in Table 16, where underlined natural frequencies represent the modes lying in the frequency range of interest.

Table 16. First seven natural frequencies of a mooring line in normal direction

Case	First seven natural frequencies in normal direction, *Hz*						
	1	2	3	4	5	6	7
(a)	0.0332	0.0590	0.0829	0.1149	0.1472	0.1739	0.1936
(b)	0.0344	0.0612	0.0859	0.1190	0.1524	0.1802	0.2006
(c)	0.0356	0.0634	0.0889	0.1230	0.1576	0.1865	0.2076
(d)	0.0368	0.0655	0.0918	0.1270	0.1627	0.1926	0.2144
(e)	0.0379	0.0676	0.0947	0.1309	0.1677	0.1987	0.2212

Mooring line top tension spectra with four to six percent offset with a half-percent interval using the present method and OrcaFlex are shown in Figure 24 to Figure 28. The damping ratios for considered modes of each case are uniform and listed in Table 15. As illustrated by Figure 24 to Figure 28, the spectra produced by both procedures are in good agreement.

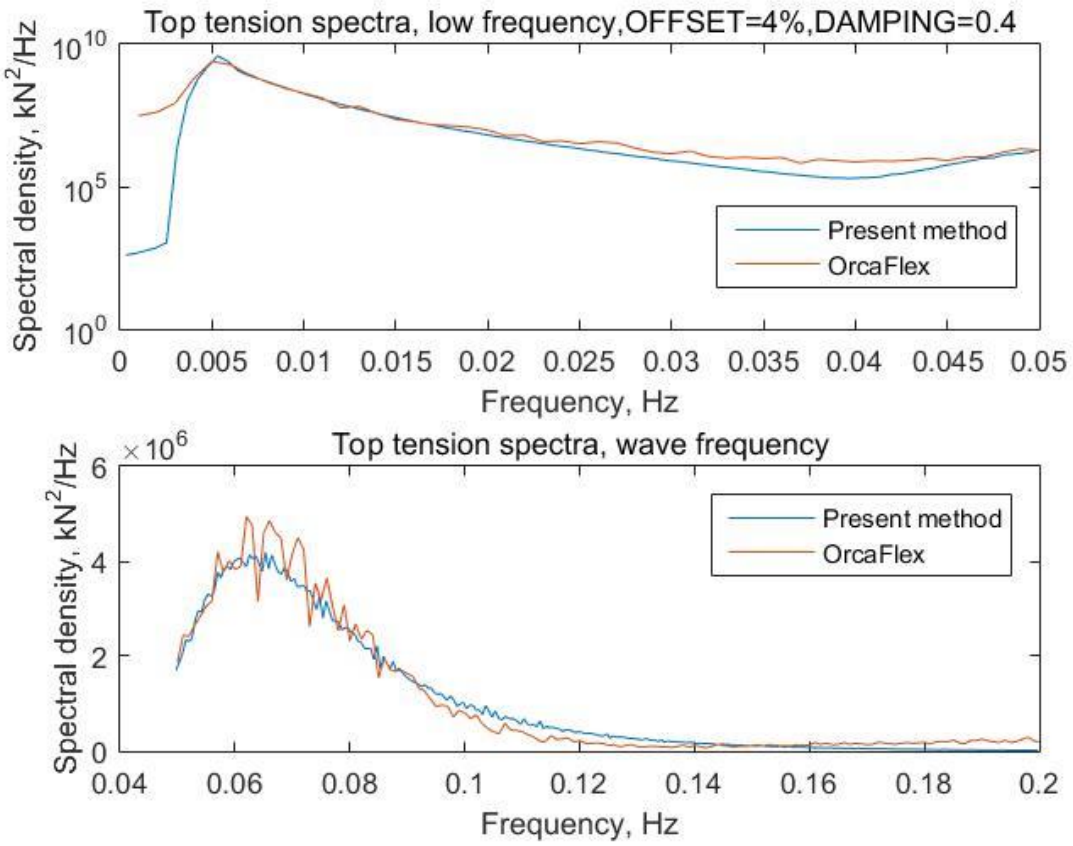

Figure 24. Spectra of the mooring line top tension for case (a)

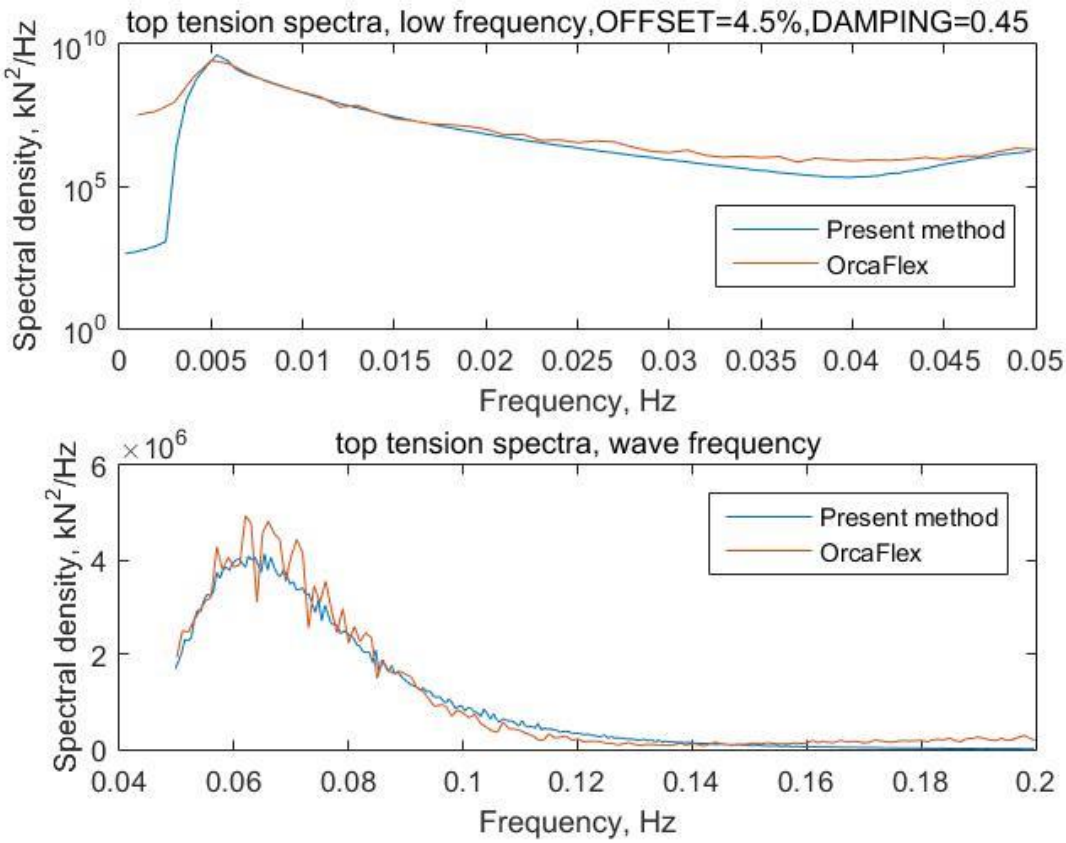

Figure 25. Spectra of the mooring line top tension for case (b)

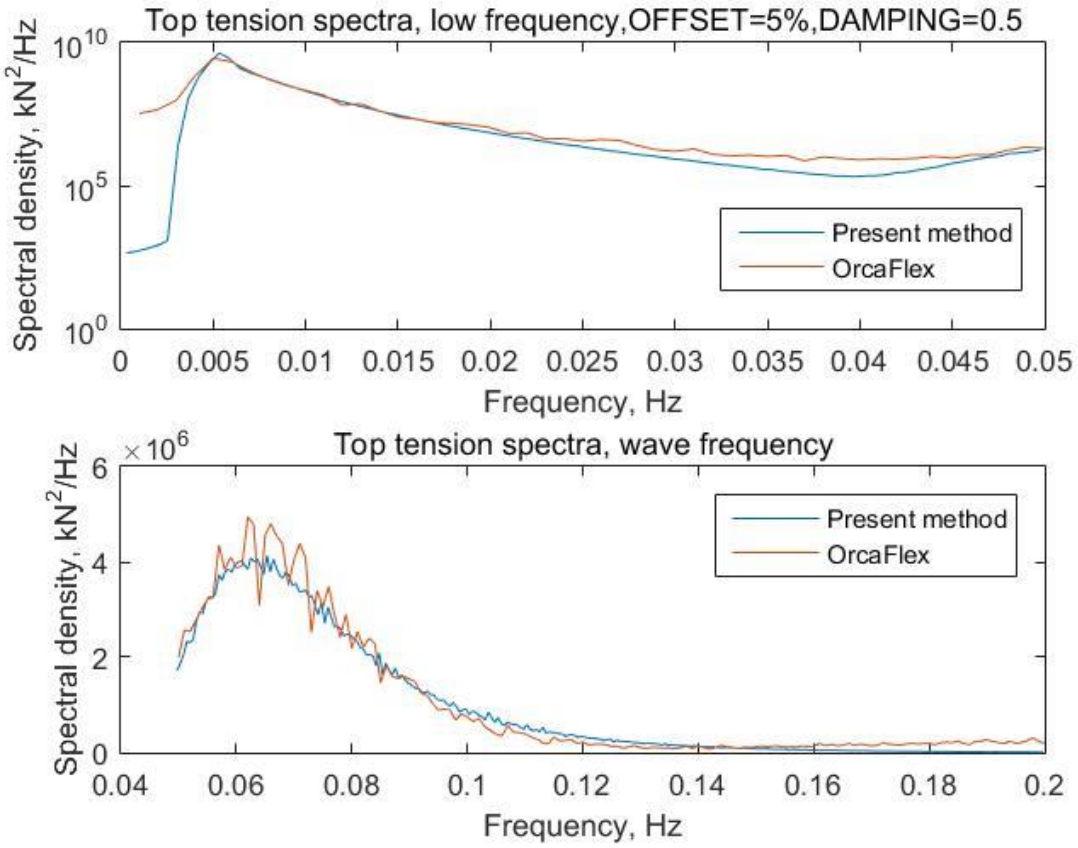

Figure 26. Spectra of the mooring line top tension for case (c)

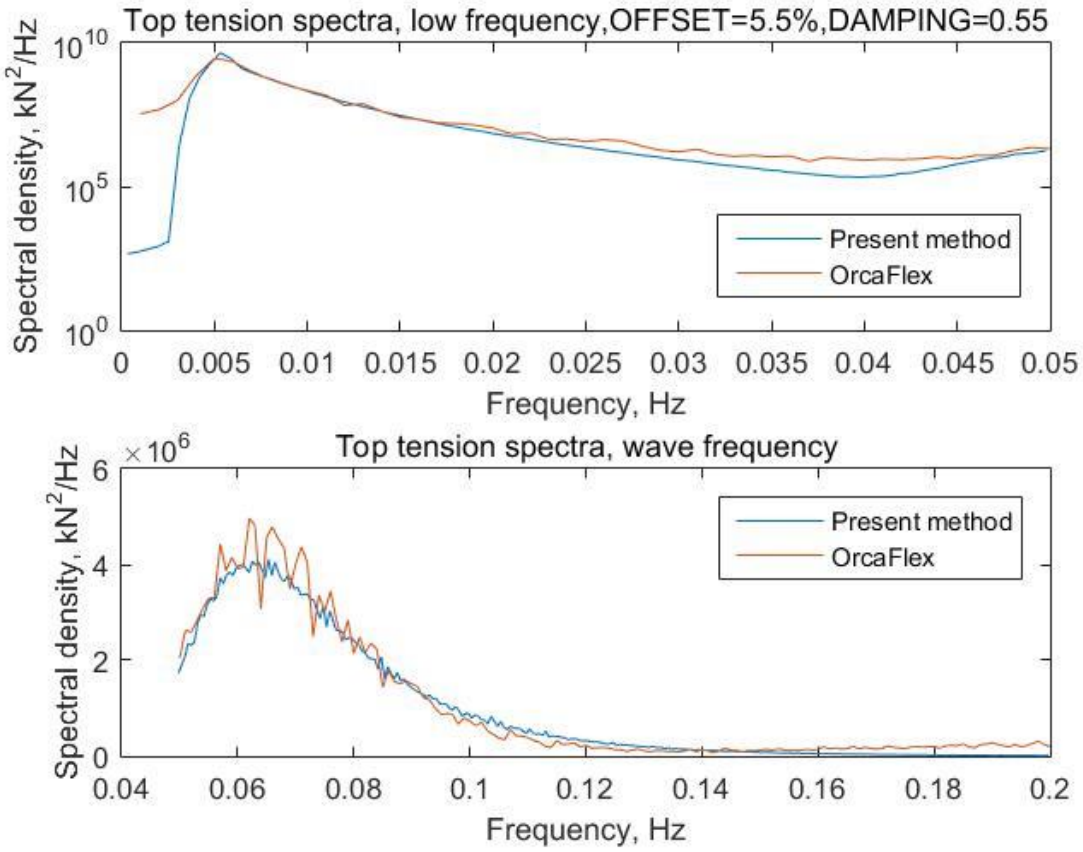

Figure 27. Spectra of the mooring line top tension for case (d)

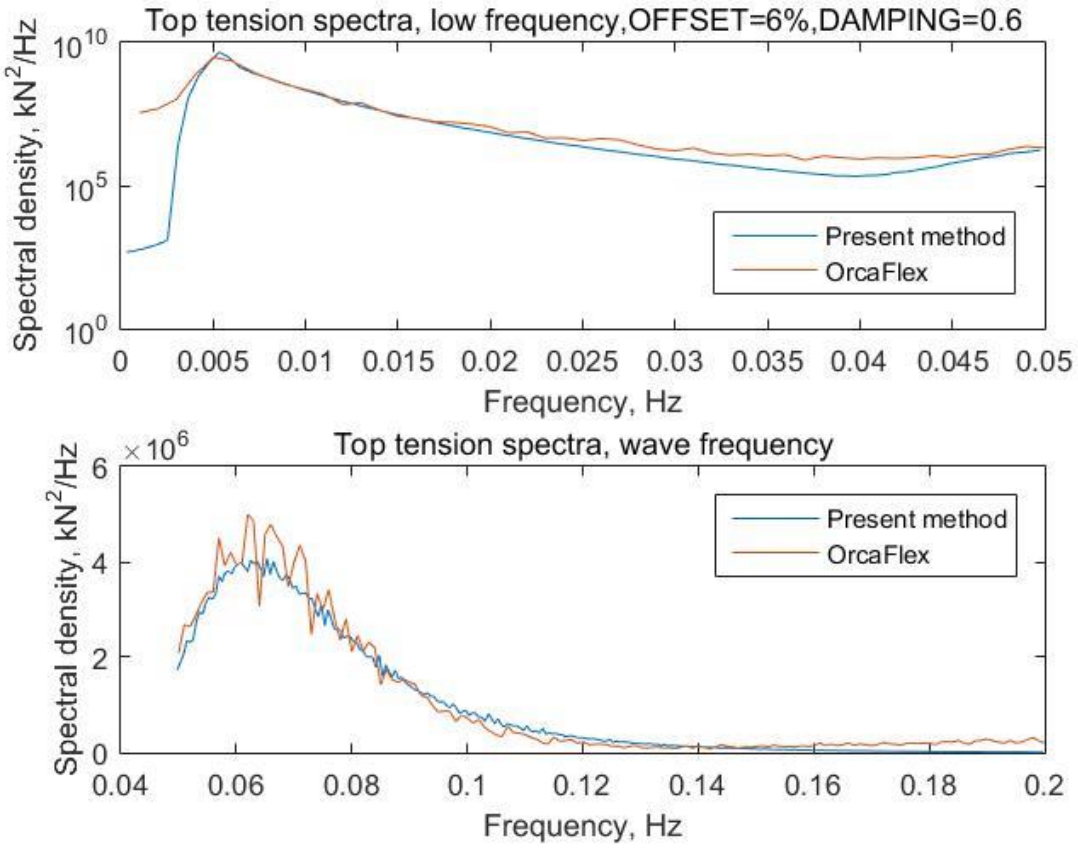

Figure 28. Spectra of the mooring line top tension for case (e)

In contrast, Figure 29 and Figure 30 display case (c) with uniform damping ratio 0.4 and 0.6, respectively. The results illustrate that small changes in damping ratio have a noticeable effect on the wave frequency top tension spectra, and 0.5 is an appropriate value for damping ratio for case (c) with five percent surge offset.

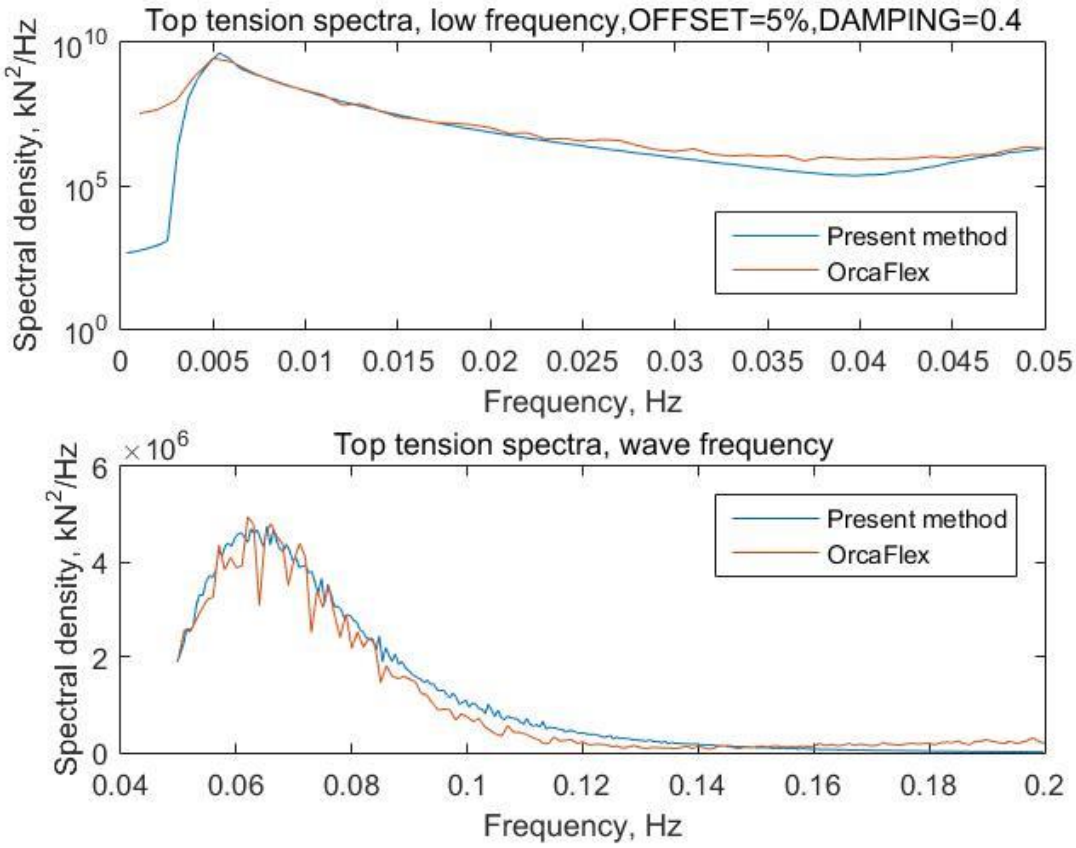

Figure 29. Spectra of the top tension for case (c) with damping ratio 0.4

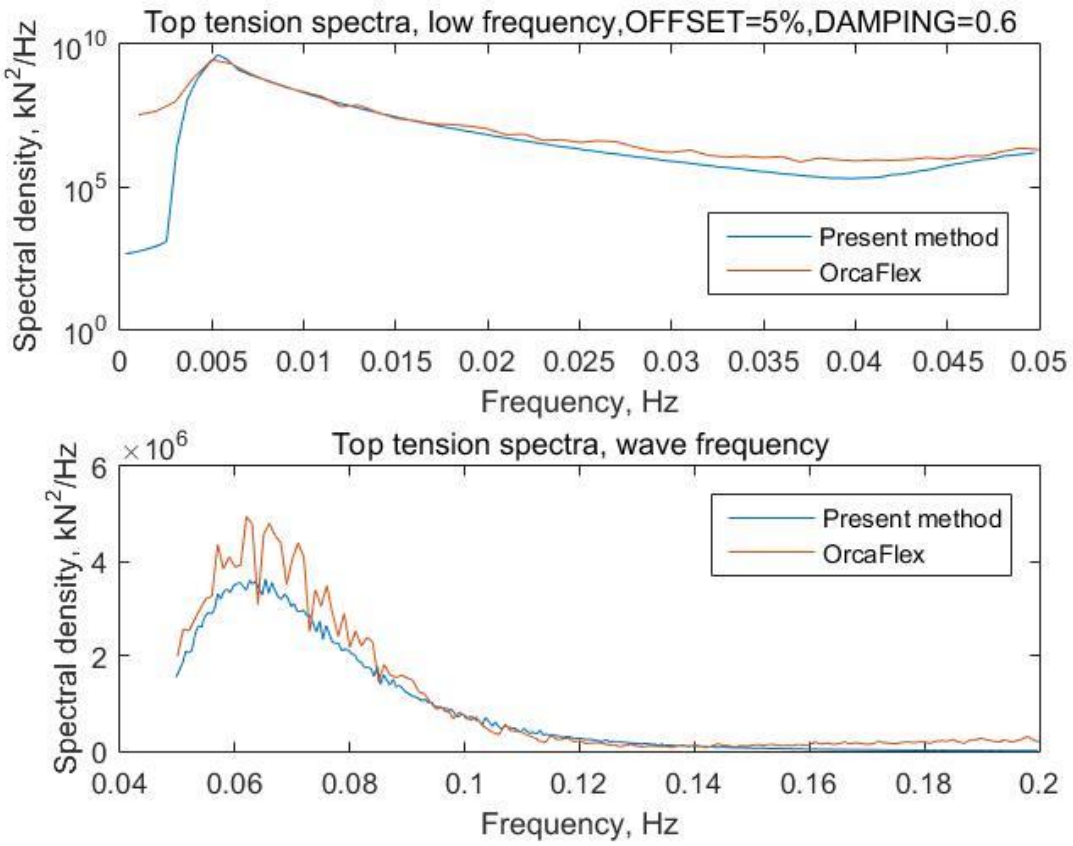

Figure 30. Spectra of the top tension for case (c) with damping ratio 0.6

Figure 31 displays the weighted harmonic response functions for all considered modes in case (c) as an example, while Figure 32 shows the corresponding summed harmonic response function. When the frequency is low, it can be observed that the value of the summed harmonic response function is nearly equal to one.

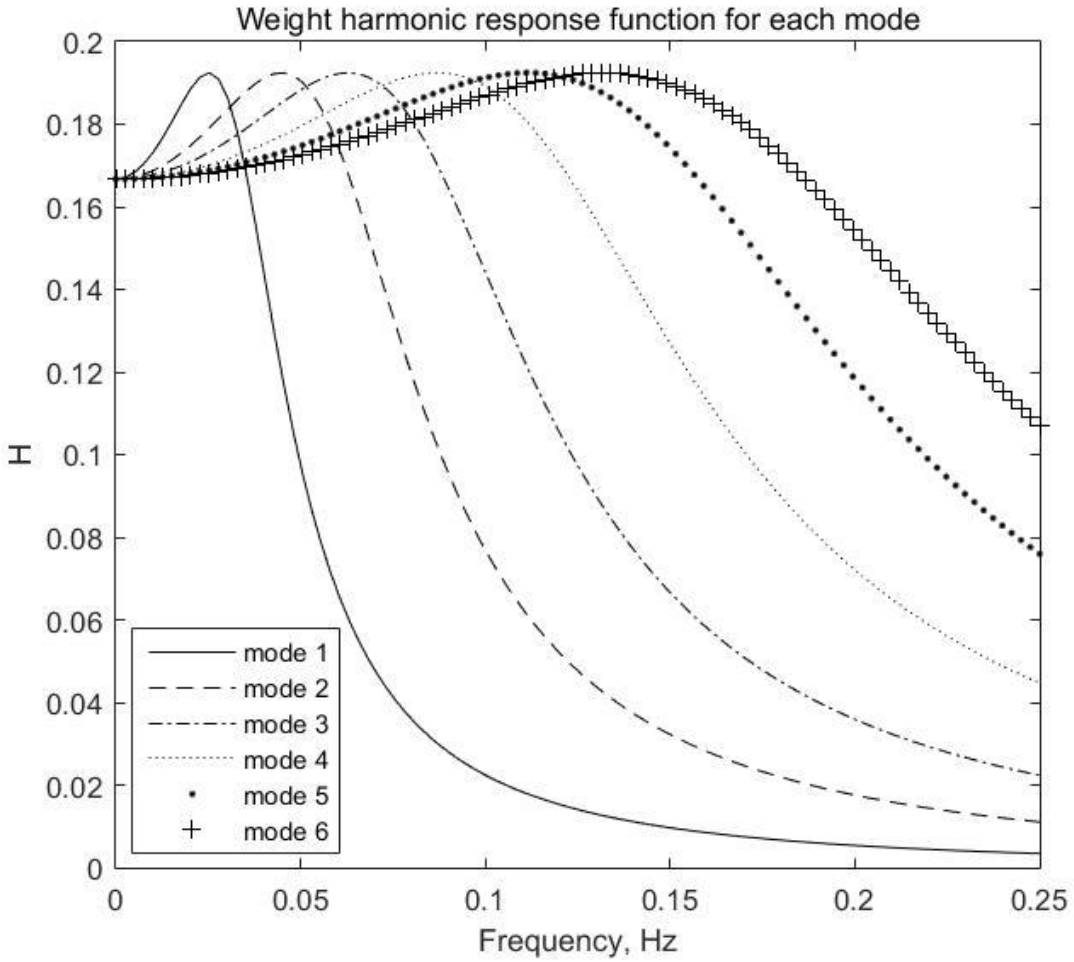

Figure 31. Weighted harmonic response functions for the first six modes for case (c)

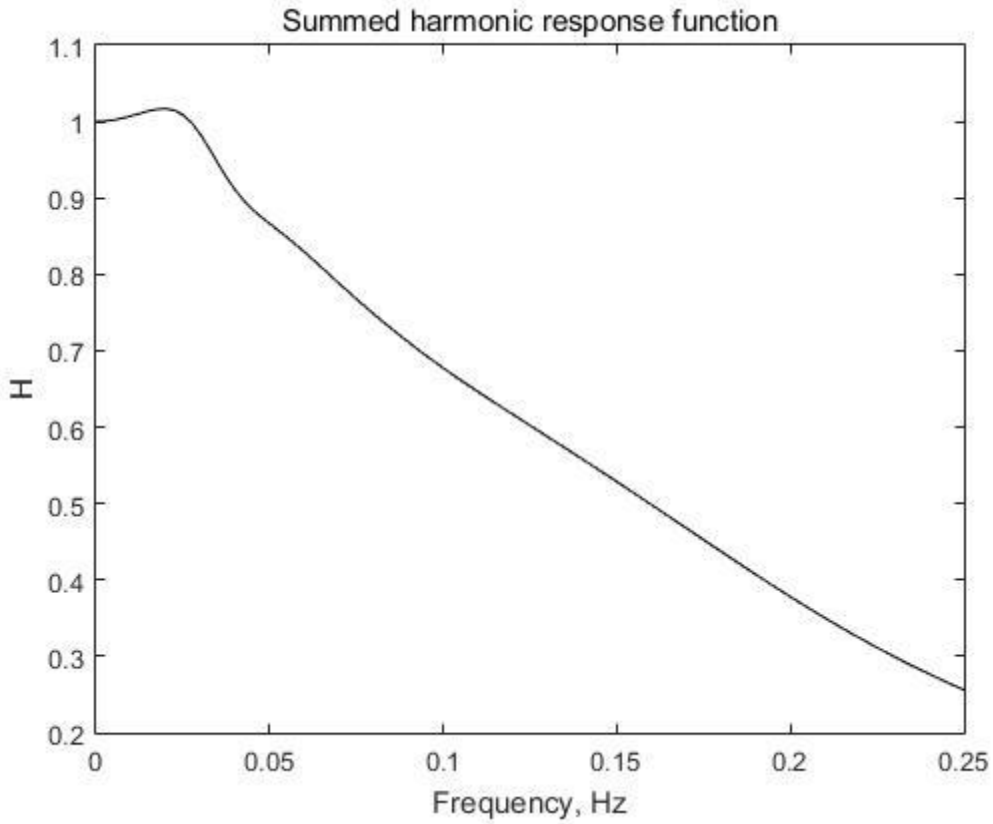

Figure 32. Summed harmonic response functions for case (c)

7.6.2 Estimation of mooring line top tension with different surge motion spectra

In order to investigate the practicability of the present method, spectra with different significant heights and peak periods are utilized, as shown in Table 17. The surge offset of the vessel is set to be five percent. Accordingly, the damping ratio for each case is assumed to be 0.5. Case (f), (g), (h) and (j) are modified from case (c) with different significant heights and peak periods. On one hand, various significant amplitudes of the

surge motion spectra lead to different scales of the mooring line top tension spectra. On the other hand, different peak periods for slow drift motion may not change the mooring line top tension spectra remarkably, since the value of summed harmonic response function near zero-frequency almost equals to one.

Table 17. Parameters of surge power spectrum used for the mooring line

Parameter		X_S, m		T_P, s		γ	
Case	Surge offset, %	Wave	Slow drift	Wave	Slow drift	Wave	Slow drift
(c)	5	9.14	50	15.5	188.68	1.0	3.3
(f)	5	13.72	75	15.5	188.68	1.0	3.3
(g)	5	4.57	25	15.5	188.68	1.0	3.3
(h)	5	9.14	50	20	283.02	1.0	3.3
(j)	5	9.14	50	14	141.51	1.0	3.3

The mooring line top tension spectra generated using the present method and OrcaFlex for case (f), (g), (h) and (j) are displayed in Figure 33 to Figure 36. The spectra using both methods for each case are in good agreement.

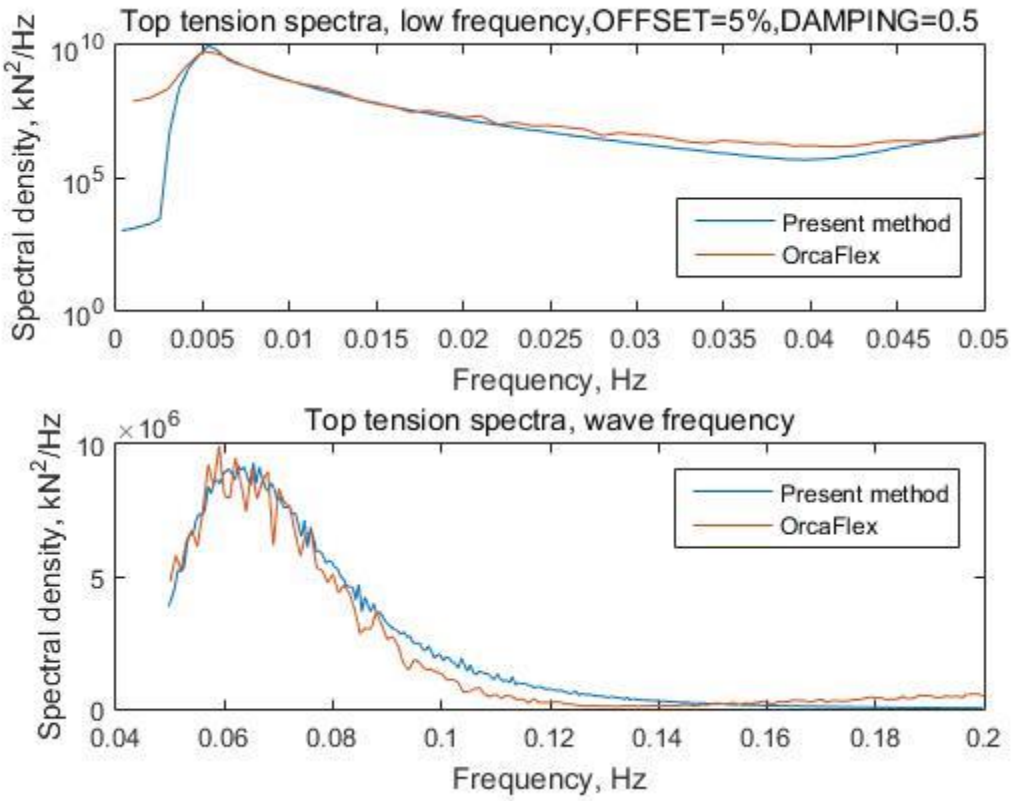

Figure 33. Spectra of the mooring line top tension for case (f)

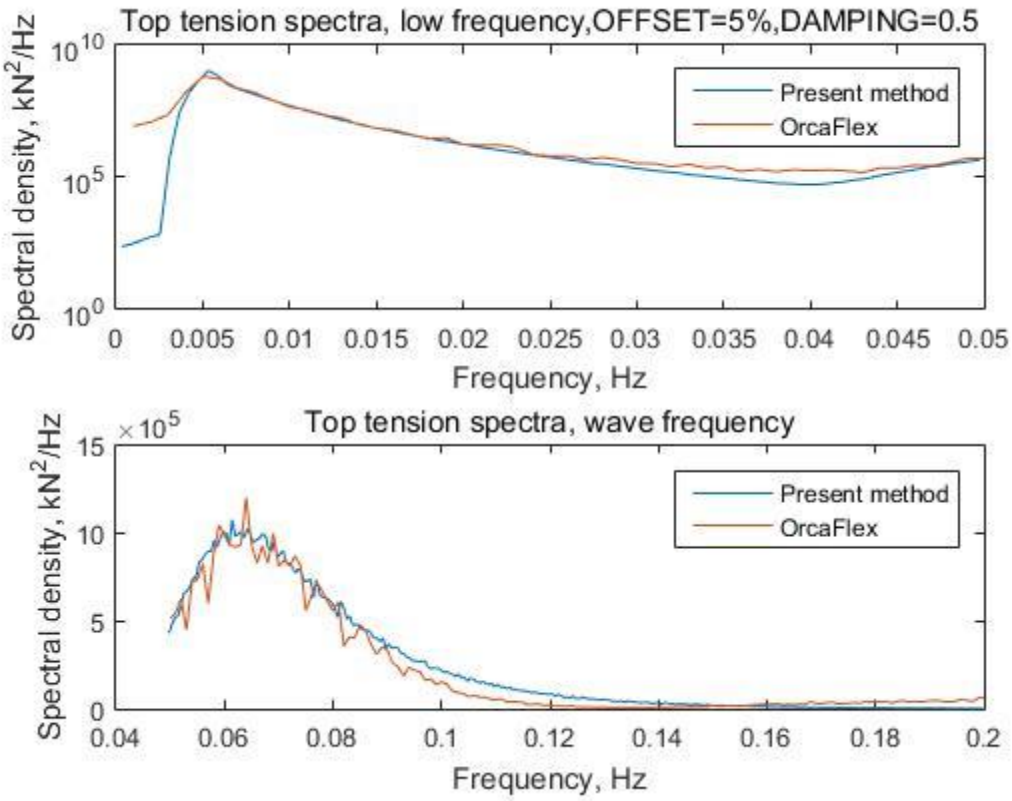

Figure 34. Spectra of the mooring line top tension for case (g)

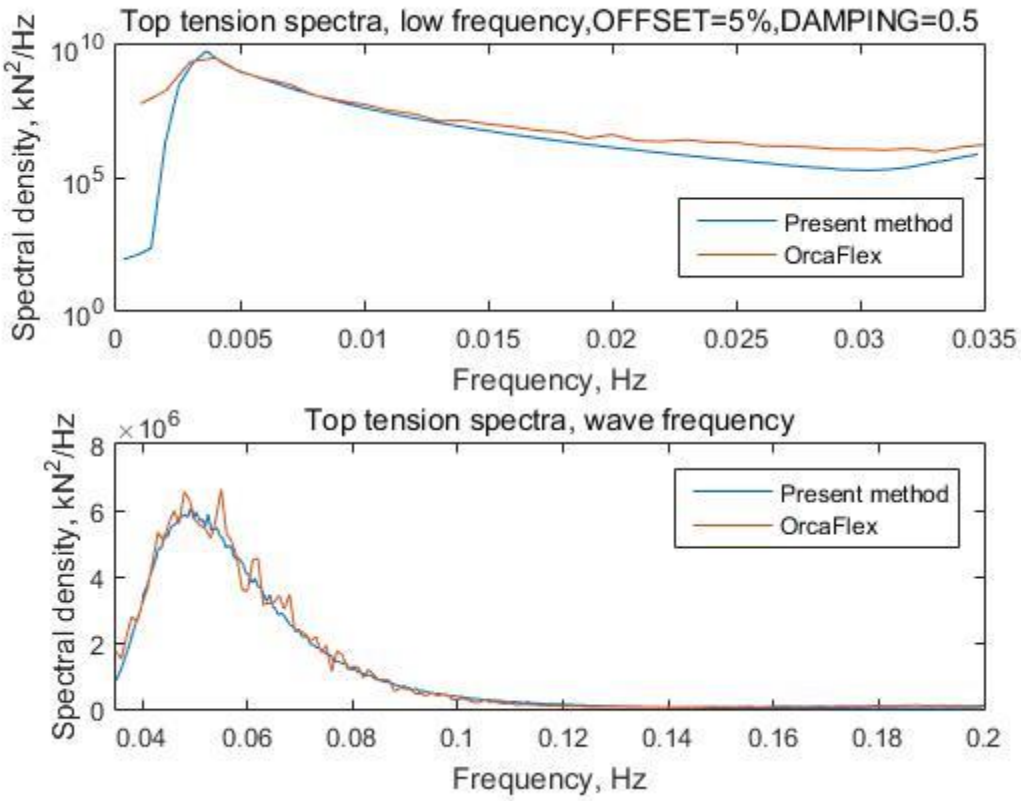

Figure 35. Spectra of the mooring line top tension for case (h)

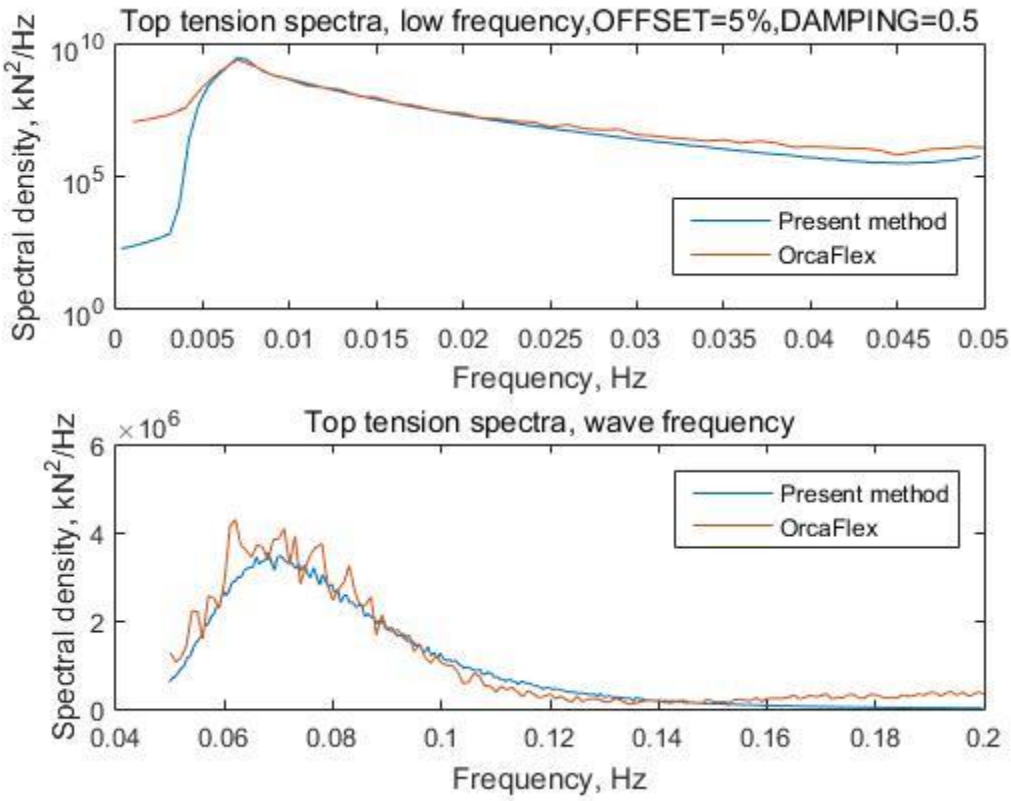

Figure 36. Spectra of the mooring line top tension for case (j)

7.7 Extreme value analysis of the mooring line top tension

The time series of the mooring line top tension can be obtained using frequency domain analysis as presented in Section 5.5. The corresponding time series from OrcaFlex simulations can be easily computed as well. For the case with five percent surge offset, four-hour time domain simulations were conducted using both the present method and OrcaFlex. Both simulations use the same time series of the vessel surge motion as input.

The resulting time series of mooring line top tension are shown in Figure 37. A visual comparison of a portion of the time series produced with both methods is provided in Figure 38. A positive conformity of the present method with OrcaFlex simulations can be observed.

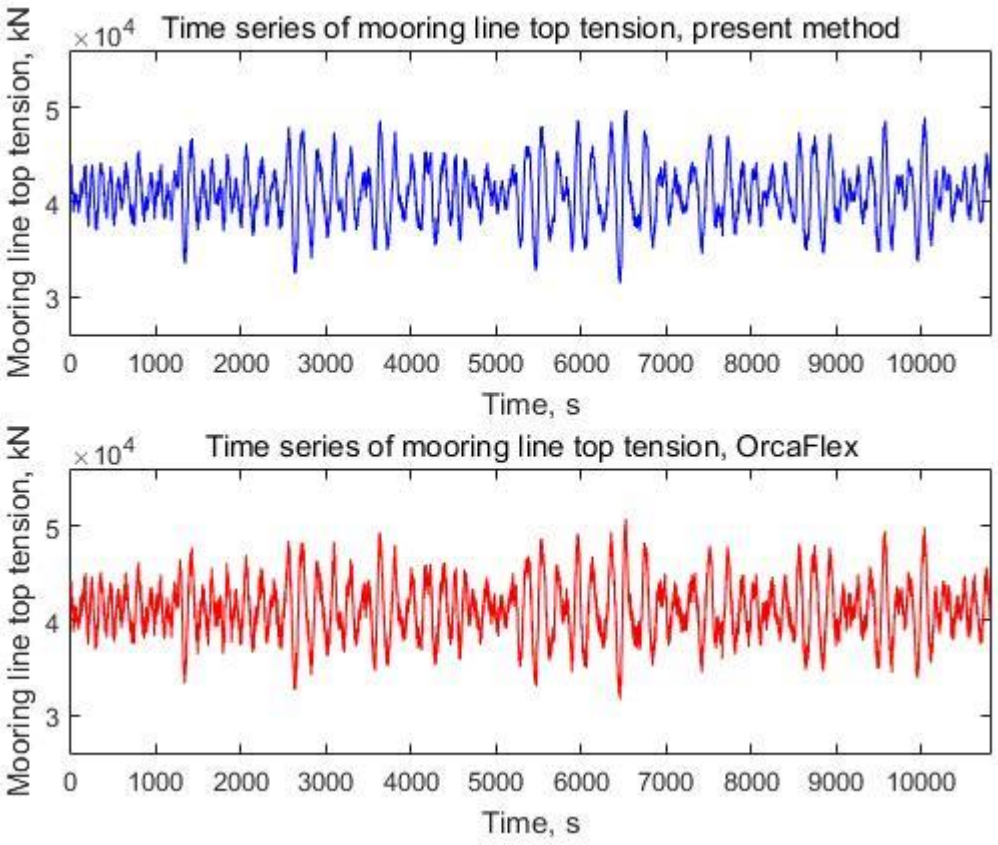

Figure 37. Time series of the mooring line top tension

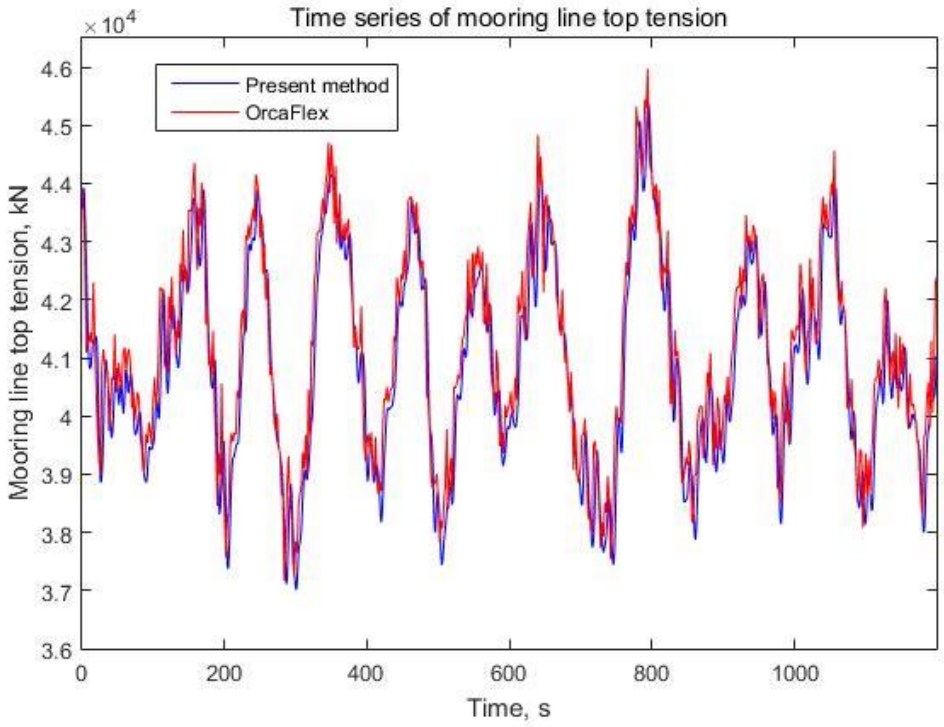

Figure 38. Comparison of time series of the mooring line top tension

7.7.1 Local maxima distribution of mooring line top tension

Given the time series of the mooring line top tension, the extreme value analysis can be conducted using Rice's theory. Local maxima of the mooring line top tension are used to fit the Rice distribution. For cases (a), (b), (c), (d) and (e) with different vessel surge offsets, three-hour time series are simulated using both the present method and OrcaFlex. The zeroth spectral moments of these processes are calculated and listed in Table 18, where the bandwidth parameters ε are also shown.

Table 18. Parameters of tension spectra for different surge offsets

Case	Surge offset	Method	m_0, kN^2	Bandwidth ε
a	4%	Present	7584588.83	0.987320
		OrcaFlex	7700645.12	0.999637
b	4.5%	Present	8020480.88	0.987324
		OrcaFlex	8144693.45	0.999657
c	5%	Present	8365031.99	0.987533
		OrcaFlex	8491077.92	0.999670
d	5.5%	Present	8668672.77	0.987718
		OrcaFlex	8797416.05	0.999680
e	6%	Present	8917018.32	0.987883
		OrcaFlex	9049378.28	0.999687

For the five cases with different surge offsets from four to six percent, the time series of the mooring line top tension are obtained using both present method and OrcaFlex simulation. Figure 39 display the PDF plots of Rice distribution of the mooring line top tension local maxima of case (c) using both methods. The results illustrates that local

tension maxima are positively correlated with surge offset. Meanwhile, the present method tends to estimate slightly higher local maxima than OrcaFlex simulation.

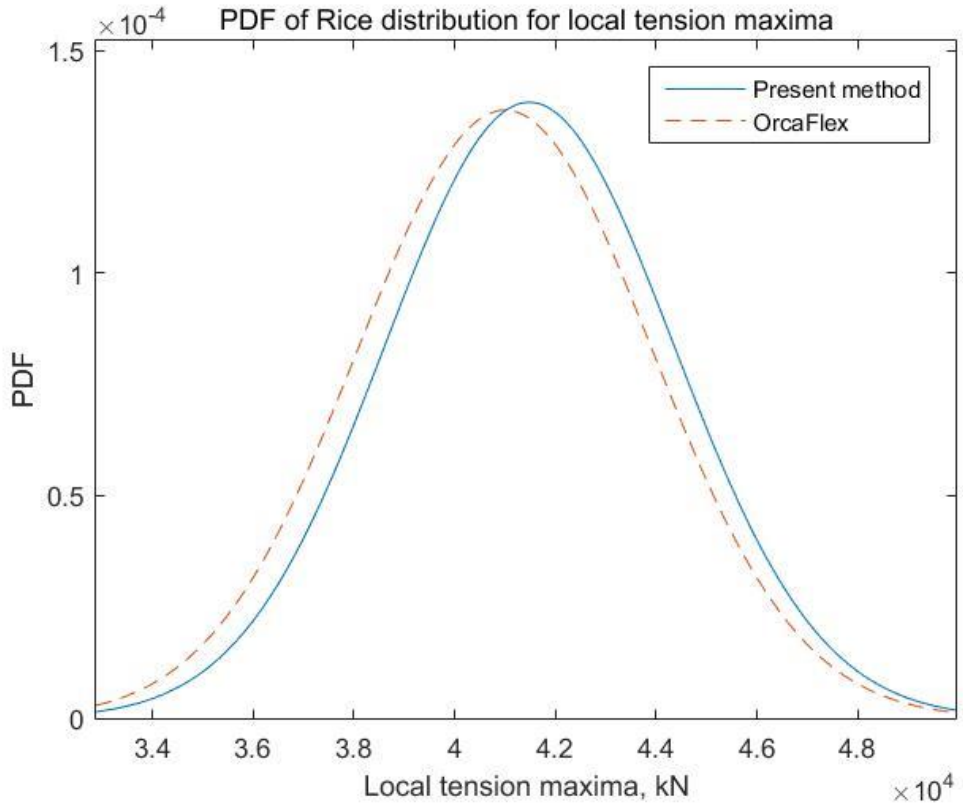

Figure 39. PDF of Rice distribution for local tension maxima of case (c)

The corresponding CDF plots of the fitted Rice distribution for case (c) are shown in Figure 40. Those plots prove a satisfying conformity between the present method and

OrcaFlex simulations. The CDF plots can be used to estimate the extreme values of top tension.

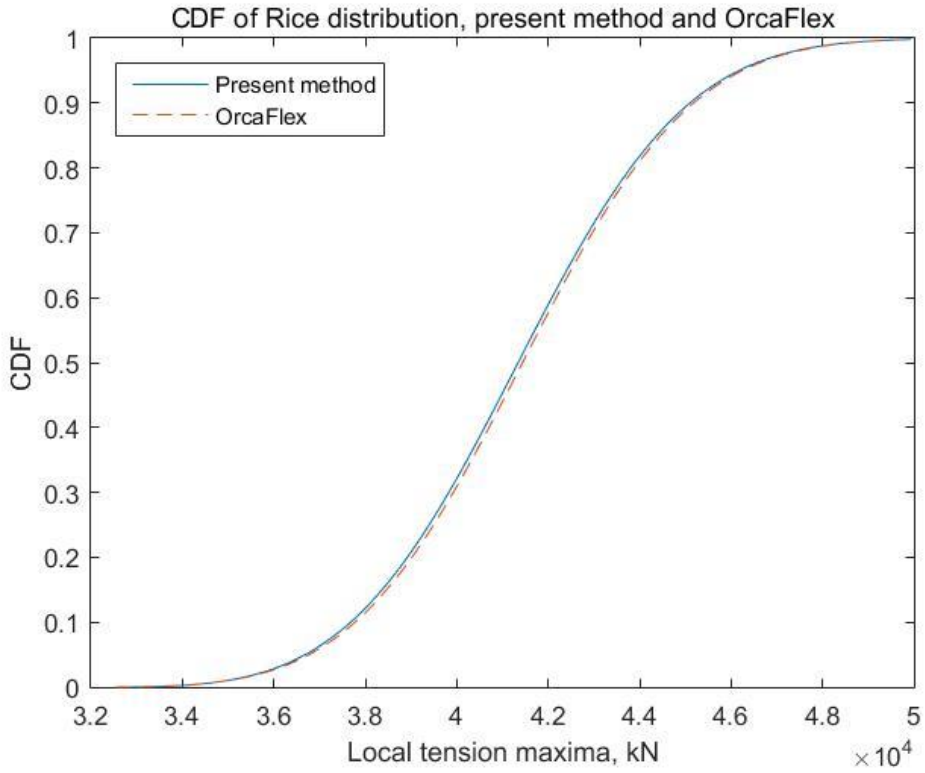

Figure 40. CDF of Rice distribution for local tension maxima of case (c)

7.7.2 Maximum among *N* maxima of the mooring line top tension

Table 18 shows that the bandwidth parameters of the Rice distribution for all cases are almost equal to one. Therefore, for those cases the Rice distribution can be simplified

to a Gaussian distribution because it is a broad-banded process. The probability density function and cumulative distribution function of the Gaussian distribution are given as

$$f\left(x_r\right)=\frac{1}{\sqrt{2\pi m_0}}e^{-\frac{x_r^2}{2m_0}} \tag{104}$$

$$F\left(x_r\right)=\frac{1}{2}\left[1+erf\left(\frac{x_r}{\sqrt{2m_0}}\right)\right] \tag{105}$$

The cumulative distribution and probability density of the maximum among N maxima for this process is written as follows

$$F_M\left(x_r\right)=\left[\frac{1}{2}+\frac{1}{2}erf\left(\frac{x_r}{\sqrt{2m_0}}\right)\right]^N \tag{106}$$

$$f_M\left(x_r\right)=N\left[\frac{1}{2}+\frac{1}{2}erf\left(\frac{x_r}{\sqrt{2m_0}}\right)\right]^{N-1}\frac{1}{\sqrt{2\pi m_0}}e^{-\frac{x_r^2}{2m_0}} \tag{107}$$

For the mooring line case with five percent offset, the CDF and PDF are plotted in Figure 41 and Figure 42, with a set of numbers of local maxima.

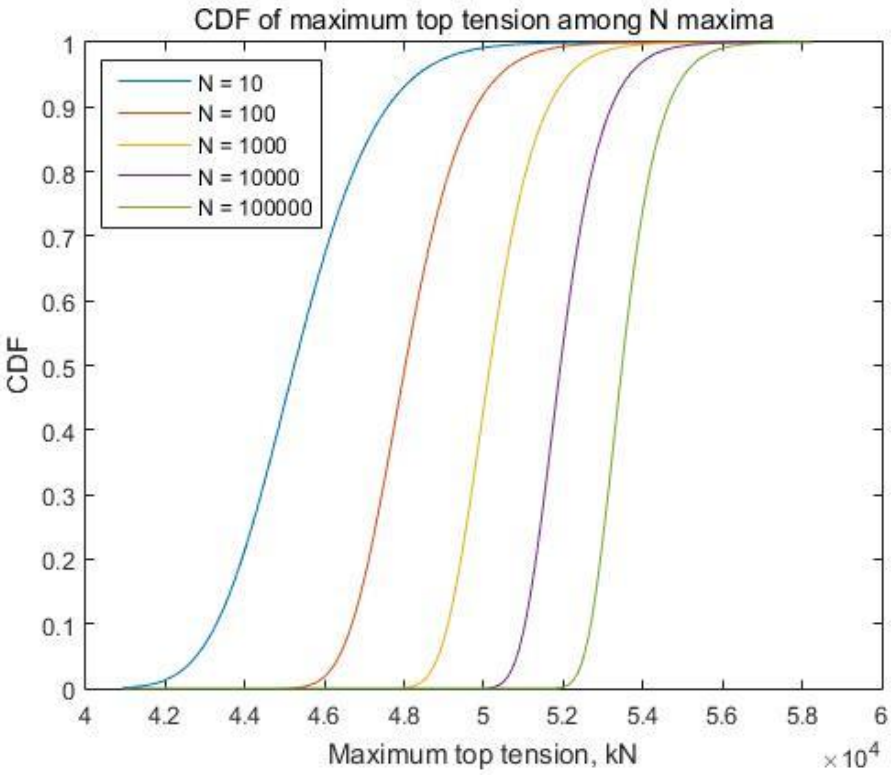

Figure 41. CDF of maximum top tension among *N* maxima

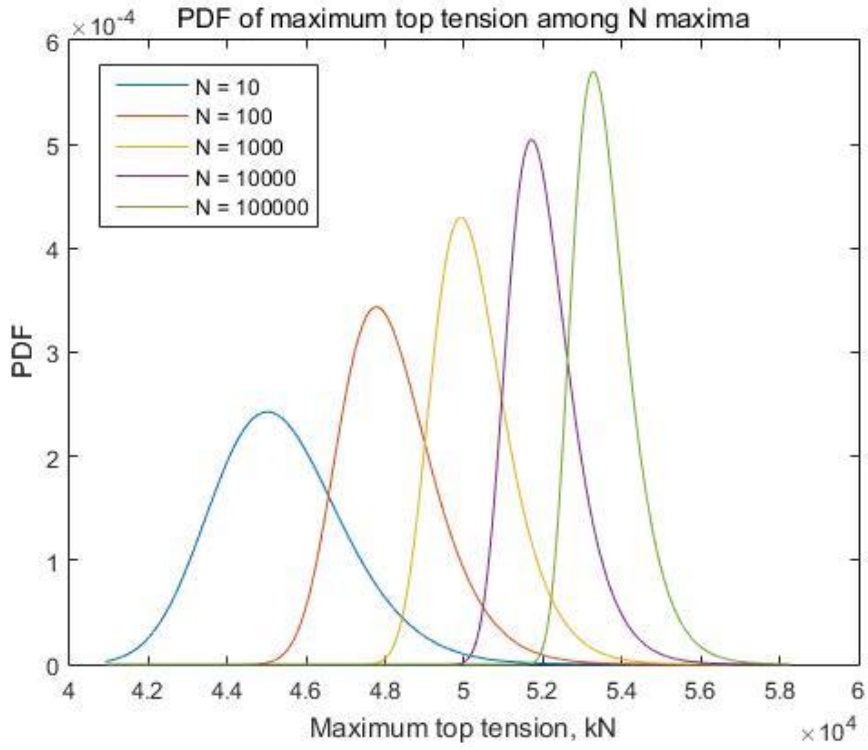

Figure 42. PDF of maximum top tension among *N* maxima

Figure 41 and Figure 42 illustrate that as the number of local maxima increases, the most likely maximum value among all local maxima will be larger; and the PDF curve tends to be narrower. Meanwhile, the expected maximum value among *N* maxima with various *N* can be estimated and shown as the red line in Figure 43.

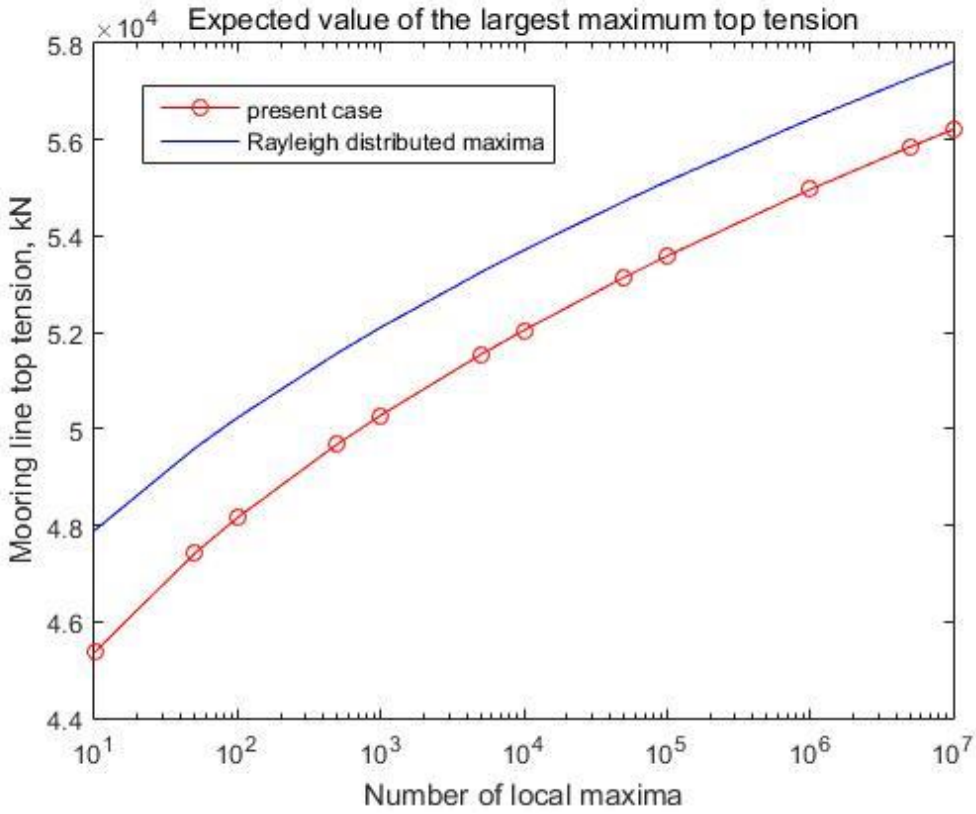

Figure 43. Expected value of the largest maximum top tension

The expected values of the largest maximum for a narrow-banded Gaussian process can be calculated by Eq. (100). With the spectral moments of the present case, the expected values for this narrow-banded process are plotted as the blue line in Figure 43. Therefore, the expected largest maximum of the present case is slightly smaller than that of a narrow-banded process. In addition, the expected maximum of a general Gaussian process is smaller than that of narrow-banded process and larger than that of a broad-

banded process; thus the corresponding values lie in the area between blue line and red line in Figure 43.

For a general Gaussian process, the expected maximum value can be estimated for design purposes. A simple example regarding the mooring line case with five percent offset is given in Table 19.

Table 19. Example of estimation of the expected largest maximum

Property	Duration, *s*	m_2, kN^2Hz^2	m_4, kN^2Hz^4	$E\left(t_{peak}\right)$, *s*	No. peaks	T_M, *kN*
Value	10800	1518.00	10.57	11.98	901.50	50193.84

Another quantity of particular interest for mooring line top tension, $T_P\left(t\right)$ can be calculated numerically with a given reasonable value of probability P. Table 20 shows the results for the mooring line case with five percent surge offset. The last row of this table displays the most probable maximum (*MPM*) value of the mooring line top tension.

Table 20. Top tension estimated with various *N* not exceeding a given probability

Top tension, *kN*	*N*=10	*N*=100	*N*=1000	*N*=10000	*N*=100000
$P = 0.37$	44701.95	47645.30	49848.37	51665.84	53244.11
$P = 0.5$	45240.10	48026.11	50153.50	51926.50	53475.04
$P = 0.9$	47582.56	49798.50	51623.42	53206.63	54622.79
$P = 0.95$	48332.22	50401.71	52139.91	53664.85	55038.55
$P = 0.99$	49839.12	51657.96	53237.15	54650.41	55940.33
$P = \frac{N-1}{N}$	47582.56	51657.96	54653.05	57136.52	59303.82

Based on the mean value $\bar{T}_{top}$, zeroth spectral moment m_0 and *MPM* value, the peak factor *PF* can be calculated using

$$PF = \frac{MPM - \bar{T}_{top}}{\sqrt{m_0}} \tag{108}$$

For case (a), (b), (c), (d) and (e), the most probable maximum values of the mooring line top tension for a 3-hour simulation are computed and listed in Table 21.

Table 21. 3-hr MPM values and peak factors for cases with different surge offsets

Surge offset	4%	4.5%	5%	5.5%	6%
MPM, kN	48967.27	51759.69	54531.30	57316.82	60100.98
PF	4.71	4.71	4.71	4.71	4.71

7.8 Application of present method in preliminary design

7.8.1 General procedure applying the present method

During the preliminary design of an offshore floating structure, the hull, risers and other components are designed first. Based on the buoyancy and payload of the design of those components, the required vertical downward force of the mooring system can be estimated. An initial design of the mooring system is generated by adjusting design parameters to provide a vertical top tension, which is almost equal to the required vertical force. The present method can be utilized to quickly examine the dynamic mooring line top tension of this design, especially the extreme value. In this process, the damping ratio is tuned to fit the design and can be re-tuned for different applications if necessary. Based on the results, the designs of mooring system and other components are adjusted in order to satisfy technical requirements and optimize the performance of the entire system. This

procedure will be conducted several times until a satisfactory preliminary design is achieved. As for the mooring system design, parameters such as number of lines, anchor radius, length and cross-section area of the segments and buoys or clump weights will be varied. The present method will improve the efficiency of this preliminary design process significantly by saving the time for estimating dynamic mooring line top tension.

To apply the present method in a design exercise, one would start with a given surge motion spectrum, a given set of mooring line parameters (i.e. a given initial design) and a given mean offset position (e.g. five percent of water depth). This information is determined using the project technical requirements and the initial design of other components. The steps for utilizing the present method are given as follows.

1) Calculate the static equilibrium configuration and the sag ratio of this mooring line at the given mean offset position.

2) Select the damping ratio for modal superposition based on a previously calibrated curve (such as Figure 23).

3) Calculate the rate of change of top tension with surge offset (e.g. Figure 6)

4) Conduct the modal analysis in the Lagrange local coordinates and estimate the natural frequencies lying in the frequency range of the given surge motion spectrum

5) With the theoretical harmonic response function for each mode and the uniform set of weighting factors, the modal superposition is performed to determine the spectrum of mooring line top tension.

6) Calculate the zeroth, second and fourth spectral moments using the spectrum of mooring line top tension for purposes of applying Rice distribution to estimate the 3-hour *MPM* value and 3-hour peak factor of the mooring line top tension.

After these six steps are performed for all individual mooring lines, all mooring line top tension statistics are available such as mean, standard deviation, spectrum, root mean square, 3-hour *MPM* and 3-hour peak factor. Based on this information, the design of the mooring system is assessed to determine whether it is adequate or needs to be modified, for example, by adjusting the design parameters such as the anchor radius or the length, size, or material quality of one or more segments of the mooring lines.

7.8.2 An example design exercise using the present method

An example design exercise is given as follows. The parameters of the 100-year surge power spectrum used are listed in Table 9. The initial design of the mooring line is slightly modified from Table 8 with different lengths of segments in order to give an example of adjusting the design parameters to improve the performance of the mooring system. The length of each segment for this design exercise is shown in Table 22. The mean offset

position is set to be five percent of the water depth, which is a reasonable value associated with the 100-year surge power spectrum. To simplify the problem, the design object is a lumped mooring line mentioned in Section 7.1. The initial anchor radius of the mooring line is change to 3955.22 m in order to maintain the same horizontal top tension (i.e. the horizontal restoring force for the vessel) at the mean offset position as the initial design in case (c). The procedure applying the present approach in this example design exercise is demonstrated by the subsequent six steps.

Table 22. Lengths of segments of a multi-segment mooring line

Segment property	Bottom chain	Polyester	Top chain
Length, *m*	400	3950	150

The top tension components of case (c) and this modified example design are given in Table 23. The horizontal top tension components of case (c) and this example design are almost equal to each other.

Table 23. Anchor radius and top tension components of case (c) and the example design

Variable	Anchor radius, *m*	Vertical, *kN*	Horizontal, *kN*	Top Tension, *kN*
Case (c)	3953.00	22778.98	33976.00	40905.39
Example	3955.22	22676.51	33976.03	40848.44

1) The static equilibrium configuration of this mooring line at given mean offset position is calculated and shown in Figure 44. The sag ratio of this mooring line is computed to be 0.0128.

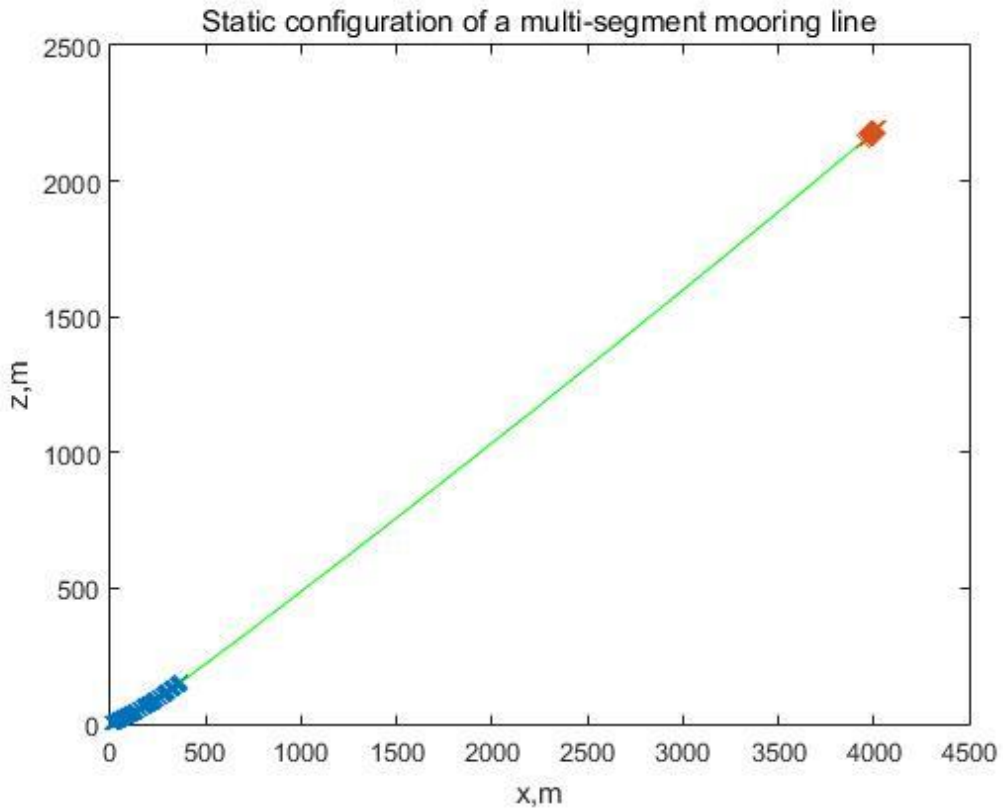

Figure 44. Static equilibrium configuration of a multi-segment mooring line

2) The damping ratio for modal superposition is selected to be 0.58 by interpolation with the sag ratio obtained in step (1) and the calibrated curve Figure 23.

3) The "slope" or the rate of change of mooring line top tension with surge offset is calculated to be 226.75241 *kN/m*.

4) The modal analysis is conducted in the Lagrange local coordinates and the natural frequencies lying in the frequency range of the given surge motion spectrum are calculated and listed in Table 24.

Table 24. First seven natural frequencies of a mooring line in normal direction

Mode	1	2	3	4	5	6
Natural frequency, *Hz*	0.0355	0.0666	0.0912	0.1231	0.1578	0.1900

5) With the theoretical harmonic response function for each mode and the uniform set of weighting factors, the modal superposition is performed to determine the spectrum of mooring line top tension. The spectra of mooring line top tension using the present method and OrcaFlex are shown in Figure 45.

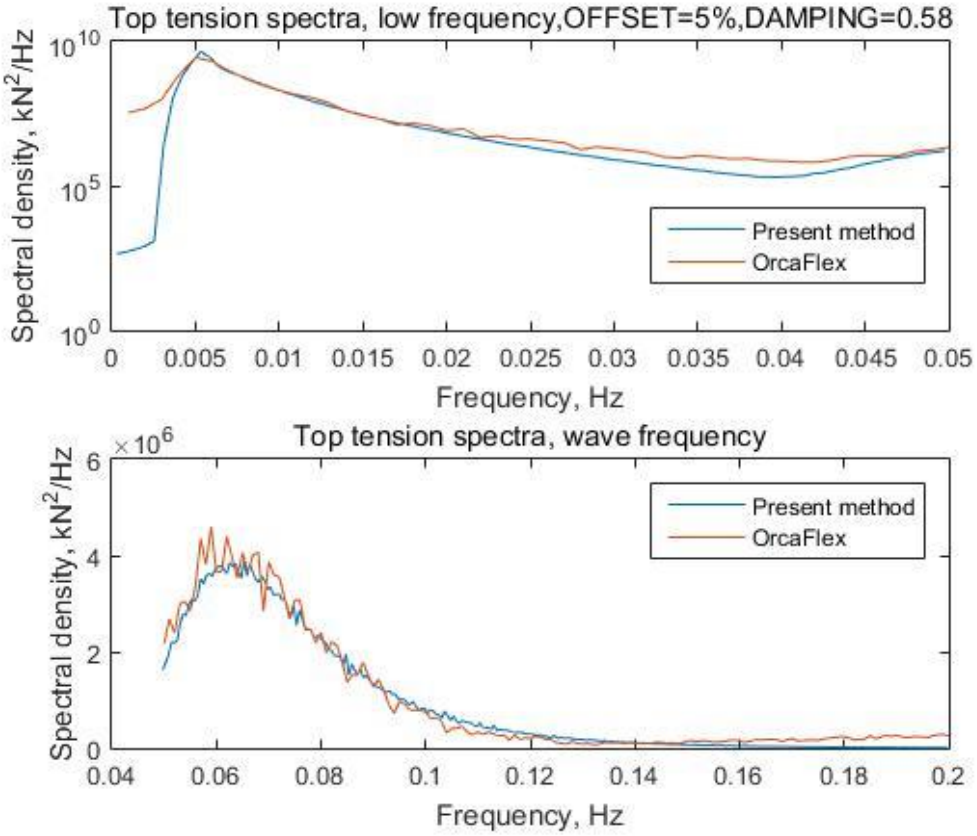

Figure 45. Spectra of the mooring line top tension using the present method and OrcaFlex

6) The zeroth, second and fourth spectral moments using the spectrum of mooring line top tension are calculated for purposes of applying the Rice distribution to estimate the 3-hour *MPM* value and 3-hour peak factor of mooring line top tension. The results are displayed in Table 25.

Table 25. Estimation of 3-hour MPM value of mooring line top tension

Property	m_0, kN^2	m_2, kN^2Hz^2	m_4, kN^2Hz^4	Bandwidth ε
Value	8396565.87	1257.06	7.71	0.99
Property	$E\left(t_{peak}\right), s$	No. peaks	3-hr *MPM*, *kN*	3-hr *PF*
Value	12.77	846	54424.57	4.67

This example design case uses longer polyester rope and shorter chain than case (c). As illustrated by the results listed in Table 25, the 3-hour *MPM* mooring line top tension and peak factor of this example design case are both reduced as compared with the results of case (c) listed in Table 21, as expected.

8. SUMMARY AND CONCLUSIONS

The equations of motion of mooring lines are derived using the work-energy variational method. It is found that the equations of motion for the three Lagrangian local directions are uncoupled. Based on this result, a finite element model of the dynamics of a multi-segment mooring line is presented. Modal analysis is conducted utilizing this model in order to obtain the natural frequencies and associated mode shapes. The accuracy of this approach is demonstrated through comparison with results from several previous works. In addition, the hydrodynamic damping is linearized and implemented in the present method in order to investigate the damped mooring lines.

Furthermore, the modal superposition approach is applied to investigate the mooring line top tension in the frequency domain. The extreme value statistics of mooring line top tension is also addressed. The results are compared with nonlinear time domain simulations using OrcaFlex and both are in good agreement.

A set of codes is developed to conduct static and dynamic analysis of multi-segment mooring lines, modal superposition and extreme value analysis. This code set is deemed to be a fast design tool for mooring lines, which is accurate and computationally efficient.

Several cases of a multi-segment mooring line are analyzed with the present method. Different environmental conditions are considered in order to illustrate the influences of those conditions.

First, it is determined that the natural periods for the tangential modes are far smaller than those for the normal and bi-normal modes. This is easy to understand since the equations of motion demonstrate that the tangential direction of a mooring line is much stiffer than the normal and bi-normal direction. Meanwhile, the slopes of mode shapes in all cases are discontinuous at the segment boundaries of the multi-segment mooring line, since the material properties of these segments are different.

Second, by comparing the cases with and without surrounding water and added mass, although the buoyancy will change the static equilibrium configuration of the mooring line, the buoyancy does not affect the dynamics in the tangential direction at all. Meanwhile, it increases the natural periods in the normal direction by a small amount. In contrast, the added mass effect will increase the natural periods in the normal direction more significantly.

Third, for damped mooring lines, as the drag damping coefficient increases, the natural periods of each mode will increase. However, only the natural periods of the several lowest modes in the normal direction change significantly. Furthermore, if the drag damping ratio is sufficiently large, several lowest modes will vanish.

Fourth, Poisson's effect slightly increases the natural period in the normal direction while it does not affect that in the tangential direction. It is illustrated by the equations of motion that the deeper the water depth, the more significant the Poisson's effect on the dynamics of the mooring line will be.

Fifth, the modal superposition approach is applied for cases with different mooring line configurations and vessel surge motion spectra. An assumed damping ratio in this approach is demonstrated to be positively proportional to the sag of the mooring line configuration.

Last, extreme value analysis of the mooring line top tension is performed. The local maxima of the top tension are deemed to be Rice distributed. Based on the results, the relevant statistical properties of the top tension process are determined, such as the CDF and PDF of the local maxima and the most probable maximum tension in given exposure duration. It is demonstrated that as the exposure duration increases, the expected value of the maximum tension will become larger and the PDF curve will become more narrow. Statistic quantities of particular interest in the design process of marine structures can be estimated easily utilizing the present method.

The present method can be straightforwardly extended to:

- accommodate specified top motion that is not in the plane of the mooring line

- calculate the tension response at any point in the mooring line, such as at the connections between the chain and polyester segments
- calculate not only tension response but any other dynamic responses of interest, such as displacement or vector components of tension

The last two bullet items involve simple linear transformation of the harmonic response functions used in the modal superposition.

In conclusion, a finite element model of multi-segment mooring lines is constructed and applied to perform modal analysis. Combining with modal superposition approach, a fast and accurate design tool for the estimation of the extreme values of multi-segment mooring line top tension is developed. Several cases of the mooring line are analyzed with the present method. Based on the results, the influences of multi-segment properties, environmental conditions, hydrodynamic damping and Poisson's effect are investigated and discussed.

REFERENCES

Broch, JT. "Effects of Spectrum Non-Linearities Upon the Peak Distribution of Random Signals." *B&K Techn. Journ* 3 (1963): 5-29.

Chen, Xiaohong. "Studies on Dynamic Interaction between Deep-Water Floating Structures and Their Mooring/Tendon Systems." Ph D, Texas A&M University, 2002.

Chucheepsakul, Somchai and Srinil, Narakorn. "Free Vibrations of Three-Dimensional Extensible Marine Cables with Specified Top Tension Via a Variational Method." *Ocean Engineering* 29, no. 9 (2002): 1067-1096.

Garrett, DL. "Dynamic Analysis of Slender Rods." *Journal of Energy Resources Technology* 104, no. 4 (1982): 302-306.

Henohold, WM and Russell, JJ. "Equilibrium and Natural Frequencies of Cable Structures (a Nonlinear Finite Element Approach)." *Computers & Structures* 6, no. 4 (1976): 267-271.

Irvine, H. Max. *Cable Structures* The MIT Press Series in Structural Mechanics, 1981.

Karimirad, Madjid. "Stochastic Analyses." In *Offshore Energy Structures*, 269-288: Springer International Publishing, 2014.

Morison, J. R. *The Force Exerted by Surface Waves on Piles* Report. Berkeley: University of California, Dept. of Engineering, Fluid Mechanics Laboratory, 1949.

Naess, Arvid and Moan, Torgeir. *Stochastic Dynamics of Marine Structures*: Cambridge University Press, 2012.

Reddy, J. N. *An Introduction to the Finite Element Method*. 3rd ed. Mcgraw-Hill Series in Mechanical Engineering, 2006.

Sparks, C. P. "The Influence of Tension, Pressure and Weight on Pipe and Riser Deformations and Stresses." *Journal of Energy Resources Technology* 106, no. 1 (1984): 46-54.

Triantafyllou, M. S. "The Dynamics of Taut Inclined Cables." *The Quarterly Journal of Mechanics and Applied Mathematics* 37, no. 3 (1984): 421-440.

Vassalos, D., Huang, S. "Dynamics of Small-Sagged Taut-Slack Marine Cables." *Computers and Structures* 58, no. 2 (1996): 557-562.